PATTERN COLLAPSE IN LITHOGRAPHIC NANOSTRUCTURES: QUANTIFYING PHOTORESIST NANOSTRUCTURE BEHAVIOR AND NOVEL METHODS FOR COLLAPSE MITIGATION

A Dissertation
Presented to
The Academic Faculty

by

Wei-Ming Yeh

In Partial Fulfillment
of the Requirements for the Degree
Doctor of Philosophy in the
School of Chemical and Biomolecular Engineering

Georgia Institute of Technology
May 2013

COPYRIGHT 2013 BY WEI-MING YEH

PATTERN COLLAPSE IN LITHOGRAPHIC NANOSTRUCTURES: QUANTIFYING PHOTORESIST NANOSTRUCTURE BEHAVIOR AND NOVEL METHODS FOR COLLAPSE MITIGATION

Approved by:

Dr. Clifford L. Henderson, Advisor
School of Chemical and Biomolecular Engineering
Georgia Institute of Technology

Dr. Dennis W. Hess
School of Chemical and Biomolecular Engineering
Georgia Institute of Technology

Dr. Elsa Reichmanis
School of Chemical and Biomolecular Engineering
Georgia Institute of Technology

Dr. Laren M. Tolbert
School of Chemistry
Georgia Institute of Technology

Dr. J. Carson Meredith
School of Chemical and Biomolecular Engineering
Georgia Institute of Technology

Date Approved: [May 03, 2013]

To my family

ACKNOWLEDGEMENTS

I would like to thank many people for their help and support to the completion of this thesis work. First, I would like to express my sincerest gratitude to my research advisor, Dr. Clifford L. Henderson, for taking me as his graduate student and giving me a chance to conduct this research project. He always offered valuable opinions and guided me to overcome problems in my research works. I will always be grateful to him for giving me the opportunity to conduct research under his guidance.

I would like to express my thanks to Dr. Dennis Hess, Dr. Elsa Reichmanis, Dr. Carson Meredith, and Dr. Laren Tolbert for serving on my thesis committee. Their suggestion and advice are very valuable and helpful for me in this thesis work. I would like to acknowledge Intel Corporation for funding support and thank Dr. Steve Putna, Dr. Todd Younkin, and Dr. Wang Yueh at Intel Corporation for their suggestion and discussion on my research works and projects.

I would like to thank all the previous and present members of my research group for their support. Many thanks to Dr. David Noga for transferring his cleanroom tool skills to me, Dr. Hua-Wei Chu for for transferring his AFM skills, Jose Baltazar for running some tools in the cleanroom, Jing Cheng for helping in organic synthesis, and Nathan Jarnagin for collaborating and studying on the directly self-assembling polymers. Special thanks to Dr. Richard A. Lawson for his useful discussion on my research and Devin Brown in Microeletronics Research Center of Georgia Institute Technology for his assistance and useful discussion on the operation of electron-beam lithography system.

I would also like to thank my wonderful friends: Pei Yoong Koh, Yanhui Yuan, Yi Ding, Yanto Yanto, Li-Wei Chou, Su-Chen Lai, Liren Xu, Ming-Chien Hsieh, Huayu Li, Boyi Fu, Chen Zhang, Zhenguan Tang, Lu Xu, Luye He, and other friends in Yuntao Association. They have provided me with the balance between work and life. These friendships will be my most valuable treasure in my life. In addition, I would like specially thank to my dear girl friend, Jiawen Xie for her unconditional support, understanding in my life, and standing with me while I was involved in my research works. Most of all, I would like to thank to my parents and my brothers for all their support and encouragement throughout my life.

TABLE OF CONTENTS

Page

ACKNOWLEDGEMENTS iv

LIST OF TABLES ix

LIST OF FIGURES x

SUMMARY xvi

CHAPTER

1 INTRODUCTION 1

1.1 Introduction to Microlithography 1

1.2 Background of Pattern Collapse 4

1.3 Organization of Thesis 8

1.4 References 12

2 DEVELOPMENT OF A NOVEL REACTIVE RINSE STRATEGY FOR PHENOLIC POLYMER RESISTS BASED ON AN ADIPIC ACID CROSSLINKER AND EDC-NHS COUPLING TO MITIGATE RESIST PATTERN COLLAPS 14

2.1 Introduction 15

2.2 Experimental 16

2.3 Results and Discussion 21

2.4 Conclusions 34

2.5 References 35

3 EFFECT OF CROSSLINKER STRUCTURE ON RESIST PATTERN COLLAPSE BEHAVIOR WHEN USING A REACTIVE RINSE PROCESS FOR PHENOLIC RESIST POLYMERS BASED ON EDC-NHS COUPLING 37

3.1 Introduction 38

3.2 Experimental 39

3.3 Results and Discussion 44

3.4 Conclusions 56

3.5 References 58

4 DEVELOPMENT OF REACTIVE RINSES FOR CARBOXYLIC ACID FUNCTIONALIZED RESIST POLYMERS BASED ON POLYAMINE CROSSLINKERS AND EDC-NHS COUPLING 60

4.1 Introduction 60

4.2 Experimental 62

4.3 Results and Discussion 66

4.4 Conclusions 77

4.5 References 78

5 DEVELOPMENT OF A GENERAL REACTIVE RINSE PROCESS FOR RESIST PATTERN COLLAPSE MITIGATION BASED ON ION EXCHANGE OF POLYIONIC CROSSLINKERS TO THE DEVELOPED RESIST FEATURE SURFACE 80

5.1 Introduction 80

5.2 Experimental 83

5.3 Results and Discussion 87

5.4 Conclusions 99

5.5 References 100

6 THE USE OF REACTIVE ADHESION PROMOTERS TO MITIGATE PATTERN COLLAPSE IN THIN-FILM LITHOGRAPHY 102

6.1 Introduction 103

6.2 Experimental 105

6.3 Results and Discussion 107

6.4 Conclusions 121

6.5 References 122

7 EFFECT OF DRYING RATE ON PATTERN COLLAPSE BEHAVIOR IN THIN FILM LITHOGRAPHY 124

7.1 Introduction 124

7.2 Experimental 126

7.3 Results and Discussion 130

7.4 Conclusions 139

7.5 References 140

8 A COMPREHENSIVE MODEL AND METHOD FOR MODEL PARAMETERIZATION FOR PREDICTING PATTERN COLLAPSE BEHAVIOR IN PHOTORESIST NANOSTRUCTURES 141

8.1 Introduction 142

8.2 Experimental 143

8.3 Pattern Collapse Modeling 148

8.4 Results and Discussion 154

8.5 Conclusions 165

8.6 References 166

9 CONCLUSIONS AND RECOMMENDATIONS 168

9.1 Conclusions 168

9.2 Recommendations for Future Works 171

9.3 References 173

LIST OF TABLES

Page

Table 1.1: Summary of QCM results on the study of the effect of film thickness during AA reactive rinse process 32

Table 1.2: Summary of QCM results on the study of the effect of rinse time at first step of AA reactive rinse process 32

LIST OF FIGURES

Page

Figure 1.1: Illustration of the microlithography and pattern formation processes 2

Figure 1.2: Two primary failure modes of pattern collapse: (A) photoresist line bending or breakage, and (B) photoresist line adhesion failure. θ is the contact angle on the resist wall 8

Figure 1.3: The flowchart of this work 11

Figure 2.1: (A) Top view and (B) side view of pattern design used in this work for determining the critical stress at the point of pattern collapse; (C) An example for determining the position (S_{1c}) of critical stress (σ_c): SEM image of nominal 70 nm feature width line pair arrays used to identify the critical S_{1c} space. 20

Figure 2.2: Schematic illustration of reactive rinse process: (A) adipic acid reactive rinse; (B) propanoic acid reactive rinse 22

Figure 2.3: Surface contact angles during the reactive rinses. Polystyrene (squares) or ESCAP-1 films were performed one minute AA/EDC/NHS (triangles) or one minute PA/EDC/NHS rinses (circles), followed by one minute EDC/NHS rinse, and dried with a nitrogen stream. 23

Figure 2.4: Grazing angle IR spectra of control PHOST film, PHOST film treated by PA reactive rinse, and PHOST film treated by AA reactive rinse. The inset plot shows the zoom-in spectra of carbonyl stretching vibration region. 24

Figure 2.5: (A) Schematic presentation of the side of ESCAP-1 film treated by reactive rinse. ESCAP represents the ESCAP-1 film without reactive rinse. R/ESCAP and ESCAP/R represent the samples treated by reactive rinse on one side of ESCAP-1 films. R/ESCAP/R represents the sample treated by reactive rinse on two sides of ESCAP-1 film. (B) Effective moduli of ESCAP-1 films treated with PA control rinse or AA reactive rinse. (C) Effect of crosslinked surfaces of ESCAP-1 films using AA reactive rinse on the resulting modulus relative to an unmodified film. Data are shown in 95% confidence and all film thicknesses are 24 nm. 26

Figure 2.6: SEM images of nominal 80nm and 90 line widths on (A) the sample without AA reactive rinse, and (B) the sample with AA reactive rinse. The numbers on the left of arrays represent the nominal widths of all small parallel lines. The numbers on the top of arrays represent the nominal S_1 space between two small lines. The arrows in the figure indicate the critical space (S_{1c}) which is the position in the pattern array with the smallest spacing between adjacent lines where resist lines can withstand the largest capillary stress before collapse. 28

Figure 2.7: Critical stresses at the point of pattern collapse as a function of feature width in different samples: ESCAP-1 control samples (squares); samples treated by AA reactive rinse (circles); and samples treated by PA reactive rinse (triangles). 30

Figure 2.8: Estimated crosslink thickness as a function of (A) film thicknesses and (B) the rinse time at the first step of AA reactive rinse. 33

Figure 3.1: Chemical structure of ESCAP-1 photoresist 40

Figure 3.2: (A) Chemical structures of crosslinkers for studying the effect of linker functionality and the core structure, and (B) chemical structures of crosslinkers for studying the effect of linker length 43

Figure 3.3: Schematic illustrations of reactive rinse processes: (A) one-step reactive rinse for the crosslinkers without solubility issue; (B) two-step reactive rinse for the crosslinkers with ester precipitates or the solubility limit at the first step solution. 44

Figure 3.4: Grazing angle IR spectra of control PHOST film, PHOST film treated by PA control rinse, and PHOST film treated by AA reactive rinse. 46

Figure 3.5: Effective moduli of ESCAP-1 films treated with PEG3 reactive rinse solution in various concentrations. Data are shown in 95% confidence and all film thicknesses are 24 nm 48

Figure 3.6: (A) Top view and (B) side view of pattern design used in this work for determining the critical stress at the point of pattern collapse; (C) An example for determining the critical position: SEM image of nominal 70 nm feature width line pair arrays used to identify the critical S_{1c} space 50

Figure 3.7: SEM images of nominal 70nm line widths on (A) the samples without reactive rinse, and (B) the samples with TMA reactive rinse. The numbers on the top of arrays represent the nominal S_1 space between two small lines. The arrows in the figure indicate the critical spaces (S_{1c}) which are the position in the pattern array with the smallest spacing between adjacent lines where resist lines can withstand the largest capillary stress before collapse. 51

Figure 3.8: Critical stresses at the point of pattern collapse as a function of feature width in different rinse samples: ESCAP-1 control samples (solid squares); samples treated by AA reactive rinse (solid circles); samples treated by PEG3 reactive rinse (blank circles); samples treated by THA reactive rinse (half filled pentangles); samples treated by TCA reactive rinse (solid triangles); samples treated by TMA reactive rinse (blank triangles); samples treated by BTCA reactive rinse (solid stars); and samples treated by PMA reactive rinse (blank stars). All films are 252 nm thick. 55

Figure 3.9: Critical stresses as a function of feature width in different samples: ESCAP-1 control samples (solid squares); samples treated by AA reactive rinse (solid circles); samples treated by MA reactive rinse (blank diamonds); samples treated by PA reactive rinse (solid triangles); samples treated by SuA reactive rinse (solid pentangles); and samples treated by SeA reactive rinse (blank stars). All films are 252 nm thick. 57

Figure 4.1: Chemical structure of DUP-A02 photoresist we used in this work 64

Figure 4.2: (A) Top view and (B) side view of pattern design used in this work for determining the critical stress at the point of pattern collapse; (C) An example for determining the position of critical stress: SEM image of nominal 70 nm feature width line pair arrays used to identify the critical S_{1c} space. The number on the top of array represents the space between two small lines (S_1). 66

Figure 4.3: Schematic illustration of the process for making pedant COOR groups on the resist surface. 67

Figure 4.4: Resist surface conditions as a function of exposure dose. All samples were developed by AZ300MIF and rinsed by DI water. Solid squares on the top plot represent the water contact angle. Circles on the top plot represent the normalized thickness. (A) AFM image of unformulated DUP-A02 resist surface before exposure; (B) AFM image of resist surface exposed by 10 mJ/cm^2. 69

Figure 4.5: Schematic illustration of amine reactive rinse process. 70

Figure 4.6: XPS survey spectra of the A02-COOR film (bottom) and A02-COOR film treated by amine reactive rinse (top). 71

Figure 4.7: SEM images of nominal 70 nm and 80 nm line widths on (A) pattern sample which did not receive amine reactive rinse, and (B) pattern sample treated by amine reactive rinse. The numbers on the left of arrays represent the nominal widths of all small parallel lines. The numbers on the top of the arrays represent the nominal S_1 space widths between two small lines. The arrows in the figure indicate the critical spaces (S_{1c}) which are the position in the pattern array with the smallest spacing between two small lines where resist lines can withstand the largest capillary stress before collapse. 73

Figure 4.8: Critical stresses at the point of pattern collapse as a function of feature width in different rinse samples: DUP-A02 control samples (solid squares); samples treated by1,6-hexanediol reactive rinse (solid circles); samples treated by 1,6-hexanediamine reactive rinse (solid triangles); samples treated by T-403 triamine reactive rinse (solid stars). Film thicknesses are 252 nm. 77

Figure 5.1: Chemical structure of the DUP-A02 photoresist we used in this work. 84

Figure 5.2: (A) Top view and (B) side view of pattern design used in this work for determining the critical stress at the point of pattern collapse; (C) An example for determining the position of critical stress: SEM image of nominal 70 nm feature width line pair arrays used to identify the critical S_{1c} space. The number on the top of array represents the space between two small lines (S_1). 87

Figure 5.3: Schematic illustration of the process for making the resist surface that mimics the surface condition after development. 88

Figure 5.4: Schematic illustration of HMBr ionic rinse process 90

Figure 5.5: (A) High resolution N_{1s} spectra of the A02-COOR control film and films rinsed by HMBr for 30sec, 1min, 2min, and 5min. (B) The area ratio of N_{1s} and Si_{2p} as a function of HMBr rinse time. 91

Figure 5.6: Effective moduli of PMMA/PMAA and PS film after HMBr reactive rinse.93

Figure 5.7: SEM images of nominal 70 nm and 80 nm line widths on (A) pattern samples which did not receive HMBr rinse, and (B) pattern samples treated by HMBr rinse. The numbers on the left of arrays represent the nominal widths of all small parallel lines. The numbers on the top of arrays represent the nominal S_1 space widths between two small lines. The arrows in the figure indicate the critical spaces (S_{1c}) which are the position in the pattern array with the smallest spacing between two small lines where resist lines can withstand the largest capillary stress before collapse. 95

Figure 5.8: (A) Critical stresses at the point of pattern collapse as a function of feature width in different rinse samples: DUP-A02 control samples (squares), samples treated with diol reactive rinse (circles), samples treated with diamine reactive rinse (triangles), and samples treated with HMBr rinse (diamonds). All samples thicknesses are 252 nm. (B) Chemical structures of the linkers in this work. 99

Figure 6.1: (top left) Structure of the model resist used in this work, referred to here as ESCAP-1, which is a copolymer of hydroxystyrene, styrene, and t-butyl acrylate. (bottom) Schematic of the surface modification technique investigated in this work to enhance photoresist adhesion using a reactive vinyl ether silane. 105

Figure 6.2: Synthetic procedure used to prepare of vinyl ether silane **1** 107

Figure 6.3: (A) Water contact angles, (B) thicknesses, and for different VE modification time. The dash line in (B) represents the thickness obtained from molecular modeling. 110

Figure 6.4: S_{2p} high resolution XPS spectra for different VE modification time. 111

Figure 6.5: SEM images for different substrate treatments. Images of nominal 50 nm line width: (A) Bare Si_xN_y, (B) HMDS primed Si_xN_y, and (C) VE modified Si_xN_y; Images of nominal 60 nm line width: (D) Bare Si_xN_y, (E) HMDS primed Si_xN_y, and (F) VE modified Si_xN_y. 114

Figure 6.6: SEM images of nominal 50nm line widths on VE samples using different soft-bake conditions: (A) 140°C for 20 min, (B) 130°C for 10 min, and (C) 120°C for 10 min. 117

Figure 6.7: Critical stresses at the point of pattern collapse as a function of feature width in different substrates and baking conditions. 118

Figure 6.8: Critical spaces of experimental data and modeling results for HMDS and VE samples. 119

Figure 7.1: The model resist used in this work: ESCAP-1 (mole fractions n:m:p = 0.6:0.2:0.2). 126

Figure 7.2: (A) Top view and (B) side view of one parallel line test pattern element in the large test pattern array design used for studying pattern collapse in this work. 128

Figure 7.3: A flow chart of experimental process 130

Figure 7.4: SEM images for different drying methods. Nominal 70 nm wide line pairs dried (A) in stagnant room air, (B) in a vacuum oven, (C) under flowing dry nitrogen gas, and (D) by spin drying at 4500rpm for 3mins. 131

Figure 7.5: Tilted SEM images for different drying methods. Nominal 90 nm line width dried (A) in atmosphere, (B) in the vacuum oven, (C) by nitrogen blow, and (D) by the spinner with 4500rpm for 3mins. 132

Figure 7.6: Critical stresses as a function of feature width for different drying methods. 133

Figure 7.7: (A) Schematic of 6 x 7 SiN window array used for patterning of high resolution pattern collapse test structures with e-beam lithography in this work. Also shown are line orientations in those patterns with respect to the sample radius during spin drying. (B) Pattern design in the top-row windows used for calculating critical stress, (C) Pattern design in the bottom-row windows used for tilted images. 136

Figure 7.8: Critical stresses as a function of feature width under different pattern orientations. 137

Figure 8.1: (A) Top view and (B) side view of pattern design used in this work for determining the critical stress at the point of pattern collapse; (C) An example for determining the position of critical stress: SEM image of nominal 70 nm feature width line pair arrays used to identify the critical S_{1c} space. The numbers on the top of array represent the space widths between two small lines (S_1). 146

Figure 8.2: Schematic of the two important moments involved in the adhesion failure of a resist line from the substrate. 148

Figure 8.3: Schematic of the elastoplastic stress-strain curve assumed for the mechanical behavior of the polymeric photoresists studied in this work. 152

Figure 8.4: Effective moduli as a function of feature width measured by buckling metrology. Solid line represents the result of the simplified two-layer model. 155

Figure 8.5: Comparison of critical spaces for adhesion model, elastic model, elastoplastic model using constant resist modulus, elastoplastic model considering resist modulus as a function of feature size. (A) 97 nm thick and (B) 130nm thick resist films. 158

Figure 8.6: Comparison of critical spaces for adhesion model, elastic model, elastoplastic model using constant resist modulus, elastoplastic model considering resist modulus as a function of feature size. (A) 187nm thick and (B) 266nm thick resist films. 159

Figure 8.7: Resist collapse diagram predicted by our adhesion failure and elastoplastic failure model. 161

Figure 8.8: Predicted critical height as a function of feature width for 1:5 space/width ratio. 162

Figure 8.9: Predicted Critical aspect ratios as a function of feature width for various line/space ratios. Dashed lines represent behavior expected if resist maintained bulk modulus. 163

Figure 9.1: Schematic illustration of the HMBr rinse process. 170

Figure 9.2: Schematic representation of the photoreactive surface modification technique for increasing adhesion strength using benzophenone dimethylchlorosilane. 171

SUMMARY

The Microelectronics industry has continuously pushed the limit of critical dimensions to sub-20 nm. One of the challenges is pattern collapse, caused by unbalanced capillary forces during the final rinse and drying process. The use of surfactants offers a convenient method to reduce capillary forces but causes another deformation issue. This thesis work focuses on alternative approaches that are compatible with lithographic processes to mitigate pattern collapse. First, an e-beam lithography pattern with a series of varying line and space widths has been specifically designed in order to quantitatively study pattern collapse behavior. This pattern generates increasing stress in the pairs of resist lines as one moves across the pattern array and eventually a sufficiently small space value (critical space, S_{1c}) is reached in each array such that the stress applied to the resist exceeds the critical stress (σ_c) required for pattern bending and subsequently feature deformation and collapse occurrs. The patterns we designed allow us to qualitatively and quantitatively study pattern collapse and obtain consistent, reproducible results.

In the first part of the thesis work, a quick surface crosslink (called a reactive rinse) that involves the strengthening of the resist using crosslinking via carbodiimide chemistry while the resist structures are still in their wet state, has been developed and demonstrated. This technique provides efficient and significant improvement on the pattern collapse issue. In the second part of the thesis work, a triethoxysilane compound, vinyl ether silane (VE), has been successfully synthesized. It can be used to modify the silicon or silicon nitride substrates and form a covalent bond with the resist film instead of

manipulating the surface energies using common HMDS. Compared to traditional Hexamethyldisilazane (HMDS) vapor primed surfaces, the implementation of the VE adhesion promoter resulted in a significant improvement in the adhesion and resistance to adhesion based pattern collapse failure in small sub-60 nm resist features. In the third part of the thesis work, the effect of drying rates and drying methods has been systematically studied. SEM analysis and critical stress results showed that fast drying appear to reduce the resist collapse. The line pair orientations in each pattern array with respect to the wafer radius reveal an apparent effect of fluid flow and centrifugal forces on collapse. Finally, a comprehensive pattern collapse model that incorporates adhesion based pattern failure and elastoplastic deformation-based failure, and dimensionally dependent resist modulus properties has been developed. This model provides such an excellent prediction of the experimental data and supports the idea that this level of combined adhesion-failure and elastoplastic-failure based pattern collapse modeling, where one explicitly considers the dimensionally dependent mechanical properties of the resist can be quantitatively predictive and useful for understanding the pattern collapse behavior of polymeric nanostructures.

CHAPTER 1

INTRODUCTION

1.1 Introduction to Microlithography

An integrated circuit (IC) is an electronic circuit on a small chip of semiconductor material. Such a circuit can be made very compact and contains several billion transistors and other electronic components. Today, devices are commercially available which integrate more than billion transistors in a single chip, quite an improvement over the first single isolated transistor developed in the early 1950s at Bell Labs. The fabrication of high density IC devices requires manufacturing methods that possess nanometer-scale resolutions. This ability to manufacture the ever smaller transistor circuit elements that are critical to this IC technology progression has been enabled by advancements in the microlithography methods and materials used to produce the patterned material layers which make up each IC device.

Microlithography refers to the processes involved in transferring the desired micro- or nano-scale patterns from an IC design into the actual semiconductor device, and it involves a variety of steps ranging from mask making to the final development of relief images in a photoresist film. The process steps in microlithography are conceptually very simple, as shown in Figure 1.1. The substrate is first spin-coated with a photosensitive polymer thin film material called a photoresist. The photoresist is designed such that pattern-wise exposure to radiation can enable the selective removal of regions of the photoresist film, with the remaining regions serving as a protective mask during subsequent wafer processing steps. The desired device pattern, which has been previously made on a photomask, is then transferred to the resist film via the exposure of the resist film through the photomask using a radiation source (e.g. UV exposure from an excimer

laser or electron beam) and exposure tool (e.g. projection stepper or projection scanner). This radiation exposure creates a physiochemical change in the photoresist properties which ultimately modifies the solubility of the exposed regions of the film, thus allowing for development of relief images in the photoresist by exposure of the resist film to an appropriate developing solvents or aqueous-base solutions called developers. For the case of positive-tone photoresists, the region of the photoresist that is exposed to a radiation source changes the chemical structures so that it becomes soluble to the developer solution. The exposed resist is then washed away by the developer solution, leaving windows of the bare underlying material. Negative resists behave in just the opposite manner. Exposure to a radiation source causes the negative resist to polymerize, and more difficult to dissolve in the developer solution. Therefore, the negative resist remains on the surface wherever it is exposed, and the developer solution removes only the unexposed portions.

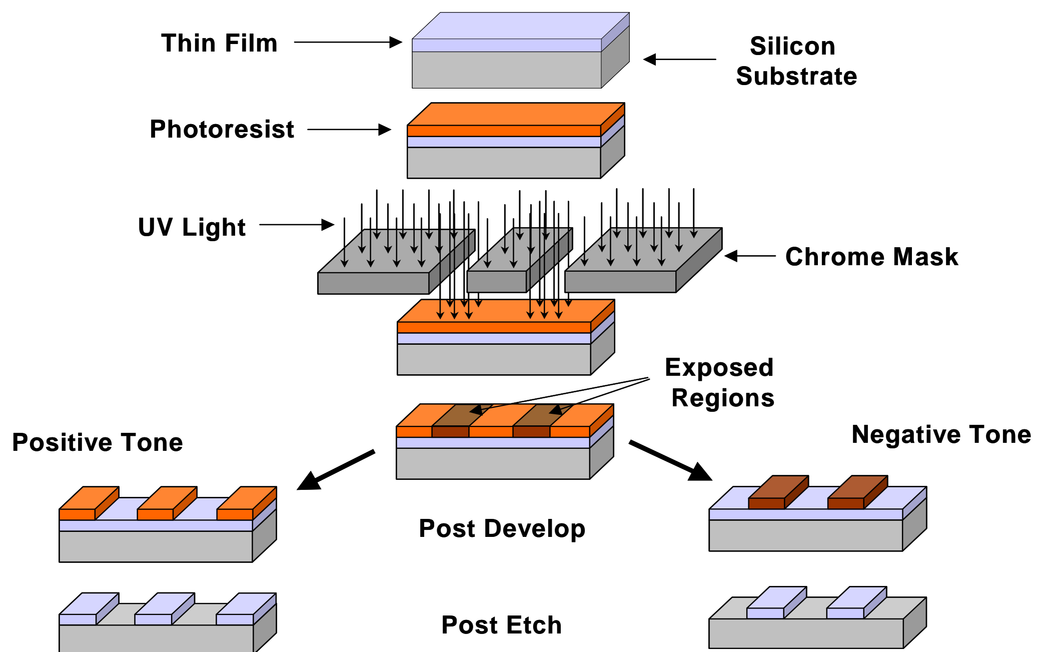

Figure 1.1 Illustration of the microlithography and pattern formation processes

Optional post-exposure processes, depending on the properties and requirements of the resist material, are then applied to the thin film. For example, in a chemically amplified resist (CAR) a post-exposure bake (PEB) at elevated temperature is performed to initiate the catalytic reaction responsible for changing the solubility of the photoresist in the exposed regions. A development process which selectively removes the unwanted regions of the resist film is then performed by soaking or spraying the resist film with an appropriate developing solvent. Today, almost all modern photoresists utilize tetramethyl ammonium hydroxide (TMAH) as the developer due to its relatively low environmental impact and its minimal health hazard. Once this patterned polymer film is formed, it is used as a masking layer to protect and isolate the covered regions of the substrate from processes such as plasma etching, metal deposition and ion implantation. Finally the rest resist layer is stripped away and the lithographic process is repeated for the next layer of the device[1].

Microlithography technology has been developed over many years. The theoretical resolution R can be simply described using a diffraction-limited model similar to Rayleigh criterion as shown in the following equations.

$$R = k_1 \frac{\lambda}{NA} \tag{1.1}$$

$$DOF = \pm k_2 \frac{\lambda}{NA^2} \tag{1.2}$$

Here k_1 and k_2 are primarily parameters that represent for capability, such as chemical and development contrasts, of a photoresist material to resolve a particular aerial image pattern (generally in the range from 0.3 to 0.8). λ is the wavelength of exposure radiation. NA is the numerical aperture of optical projection lens. NA is a

dimension less number that characterize the range of angles over which the optical lens can accept or emit light and is defined as equation (1.3)[2].

$$NA = n \times \sin\theta \qquad (1.3)$$

Here n is the refraction index of the medium where the lens is working (i.e. 1.0 for air and 1.44 for pure water). θ is the half-angle of the maximum cone of light that can enter or exit the lens. In the equation (1.1), approaches for increasing the resolution (R) and depth of field of optical projection exposure tools (DOF) allow use of shorter wavelength of exposure radiation, or to improve the photoresist properties to increase k_1 and k_2. These approaches have been used in practice: radiation wavelength decreases from 436 nm (G-line) and 365 nm (I-line) to currently optical systems operating at 193 nm or even shorter wavelengths, i.e. extreme ultraviolet (EUV)[3,4] , X-ray[5,6], and electron beam[7]. Furthermore, decreasing the numerical aperture of the optical projection lens (NA) is also a effective method for enhancing the resolution, such as in the immersion lithography technology. Previously, the medium was air (n = 1.00). If the refractive index is 1.0, theoretically NA is less than 1.0 at most, and realistically, it is no higher than 0.9 or so (θ = 65°). In immersion lithography, the medium through which the exposure light passes has been changed to purified water (n =1.44) instead of air (n=1.00). Therefore, the NA can be theoretically increased up to 1.44 times to achieve better resolution.

1.2 Background of Pattern Collapse

Integrated circuit (IC) technology and IC manufacturing technology have seen rapid and dramatic advancements over the past fifty years that have led to the ability to manufacture an incredibly complex and powerful array of electronic devices that touch all aspects of daily life. However, a potential roadblock for future lithographic processes

is pattern collapse caused by unbalanced capillary forces present during the drying step of the development process (the step in which photoresists are removed by solvents/developers in Fig1.1). The capillary stresses (σ) experienced by the resist can be described as shown in equation (1.4)[8].

$$\sigma = 6\gamma \cos\theta \left[\frac{H}{W}\right]^2 \left[\frac{1}{S_1}\right] \tag{1.4}$$

Here γ is surface tension, H/W is aspect ratio (height to width), S_1 is space between resist patterns. As it can be seen in equation (1.4), the smaller feature size, the higher the capillary stress resist patterns experience. Therefore, for the next generation lithography, pattern collapse is a critical issue for fabricating nano-scale features on chips.

Typically resist pattern collapse can be categorized by two failure modes as shown in Fig. 1.2. The first failure mode, related to the mechanical properties of resist, is photoresist pattern bending or breakage, shown in Fig. 1.2(A). Figure 1.2(B) shows another failure mode in which resist patterns lose adhesion on the substrate. Main factors affecting pattern collapse can be classified into three groups: (1) pattern geometry; (2) capillary forces/stresses induced by unbalanced liquid level during drying in the development process; (3) photoresist physical properties. The particular pattern geometry of interest can generally be characterized by a resist line height (H), resist line width (W) and a space between the resist line and adjacent features (S), whereby all these properties are strictly determined by a combination of the device layer design being patterned and the etch requirements for subsequent processing of the resist layer. Based on this fact, we are allowed to change the pattern dimensions to reduce pattern collapse. The capillary forces or stresses are governed by surface tension of rinse liquid in equation (1.4). Several research groups studied the use of surfactant in the rinse to improve the pattern collapse behavior. Huang and coworkers reported that they improved not only line width

roughness and collapse margin of line-space patterns, but also the contact-edge roughness (CER) and the depth of focus (DOF) of hole patterns by using their surfactants[9]. Drechsler et al. found that a rinse with cationic surfactants yields a reduction of the pattern collapse of test photoresist structures[10,11]. Although an appropriate surfactant in development step can reduce the surface tension of rinse solvent and the contact angle of rinse liquid on the resist wall, the patterns rinsed with surfactant appeared to shrink, which was also discussed by Huang[9] and Drechsler[12]. Zhang and coworkers also reported that the use of surfactant rinse in the development step provides significant improvement of pattern behavior, including reduced pattern collapse and line width roughness. However, they also observed that if the surfactant penetrates too deep into the resist, it may cause the resist deformation, leading to further pattern collapse[13]. Therefore, the use of surfactants to reduce capillary stress may not be an appropriate method in lithography process. The physical properties of the photoresist material that are important in the context of such collapse behavior include Young's modulus, yield stress, and strength of interaction with the substrate. One approach to improve the collapse caused by mechanical failure is to design new resist materials by introducing bulky and robust groups (i.e. benzyl or alicylic groups) on the resist structures in order to increase the mechanical restoring forces of resist features. However, such modification of resist physical properties for pattern collapse purposes is complicated and difficult to achieve through modified formulation of the resist itself due to the complex set of requirements that a resist must satisfy, as well as the complex set of physical and chemical phenomena that underlie the imaging processing itself. To achieve a procedure that is simple, suitable in the lithographic process, and able to enhance the photoresist mechanical properties, we have developed an alternative strategy of improving the resist mechanical properties after features are developed in the film, but before they are dried and are subjected to significant capillary forces.

Another major collapse mode is adhesion failure, in which resist patterns loss the adhesion strength at the resist and substrate interface. Much of the previous work on the interface interactions for improving the pattern adhesion failure has involved the use of an underlayer[14] or a bottom anti-reflective coating (BARC), which often have the added benefit of increasing the resist adhesion in addition to their primary benefits such as reflectivity control[15,16,17]. The industry standard method for improving resist adhesion is to make a surface more organophilic by treatment with hexamethyldisilazane (HMDS)[18]. However, HMDS treatments only modify adhesion by manipulating Van der Waals forces and interaction energies between resist molecules and functional groups on the surface, and such interactions are relatively weak compared to covalent bond energies. One potential approach towards addressing adhesion related defects and the resulting failure is to design a surface modifier that can covalently attach to both the substrate and the resist and prevent failure through chemical bonds.

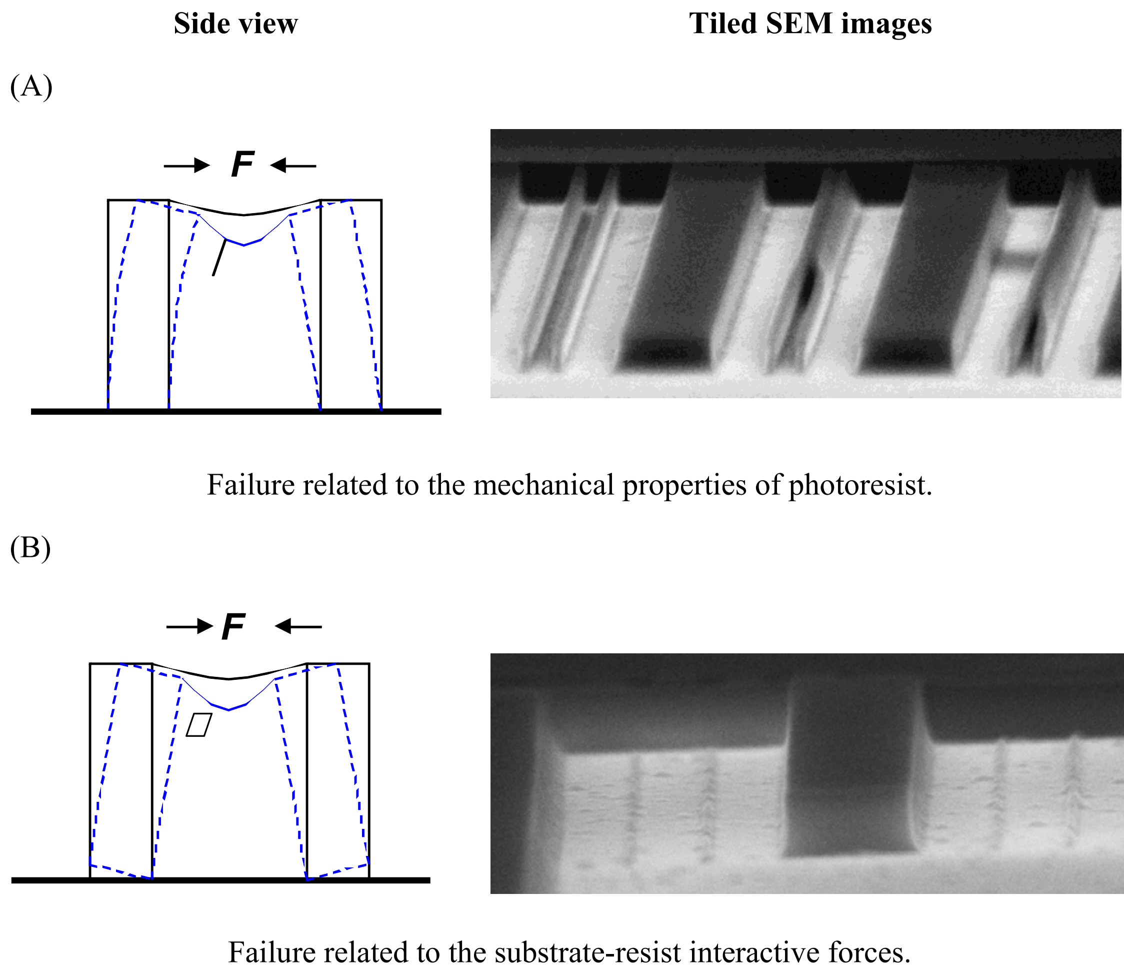

Figure 1.2 Two primary failure modes of pattern collapse: (A) photoresist line bending or breakage, and (B) photoresist line adhesion failure. θ is the contact angle on the resist wall.

1.3 Organization of Thesis

As depicted in the title of this thesis, the flowchart of this study is shown in figure 1.3. Since the use of surfactants to reduce the capillary stress may cause resist deformation, leading to further pattern collapse[13] (the dash area in our flowchart), we attempted to develop methods compatible with lithographic processes that can mitigate such pattern collapse in high resolution structures. Our study can divided into four major

categories: (1) enhancement of restoring force to mitigate pattern collapse caused by weak mechanical properties of photoresists; (2) adhesion promoters to increase the adhesion strength for pattern collapse caused by adhesion failure; (3) examination of some factors related to the lithography process such as effect of drying rate and different drying methods; (4) a compressive model development to predict and understand the photoresist behaviors. Resist materials we used in this work contained 248 nm resists, 193 nm resists, and PMMA-co-PMAA e-beam resists. There are three approaches in the category of restoring force enhancement. Our methodology involves the actual strengthening of the resist using a post-development crosslink reaction while the resist structures are still in their wet state. The crosslink reactive rinse methodology stems from the observation that negative tone photoresists which operate by crosslinking result in a covalently bonded network and often exhibit superior patterning capabilities which can be attributed to the fact that the resist has adopted a networked macromolecular structure after exposure and most likely inherited superior mechanical properties relative to the unexposed polymeric structure. Our idea sought to capitalize on the notion of using crosslinking combined with the high surface to volume ratios present in high resolution resist features, and therefore a reactive rinse procedure was developed which could potentially crosslink the phenolic groups or carboxylate groups on the surface of a photoresist. Buckling metrology is used to qualify the mechanical properties of resists and verify our surface crosslink reactions.

For adhesion enhancement, we synthesized a functional vinyl ether silane which is able to modify the Si_xN_y surface of substrates used for high resolution patterning tests of a model resist system. The primary innovation tested in this work is the inclusion of a reactive moiety in the surface modifier that can form a covalent bond with the resist film coated on top of it. For the discussion on process-dependent factors, our goal was to probe the extent to which the time during which a resist structure is subjected to capillary force-induced loads affects the pattern collapse behavior of such structures. This focus is

on modulating the drying time of the final rinse liquid (water) and quantifying the observed changes in pattern collapse. From the fundamental studies in pattern collapse, we gained basic knowledge in pattern behavior. In the meantime, a comprehensive pattern collapse model that accounts for both adhesion based pattern failure and elastoplastic deformation-based failure was developed and compared to our experimental data. The required model parameters (i.e. film modulus) were extracted from basic experiments on the resist materials and substrates themselves without the need for actual patterning experiments. Patterning experiments on our designed structures were performed to validate the work. Due to the speciality of each project, an introduction and background for each topic will be provided separately in each chapter.

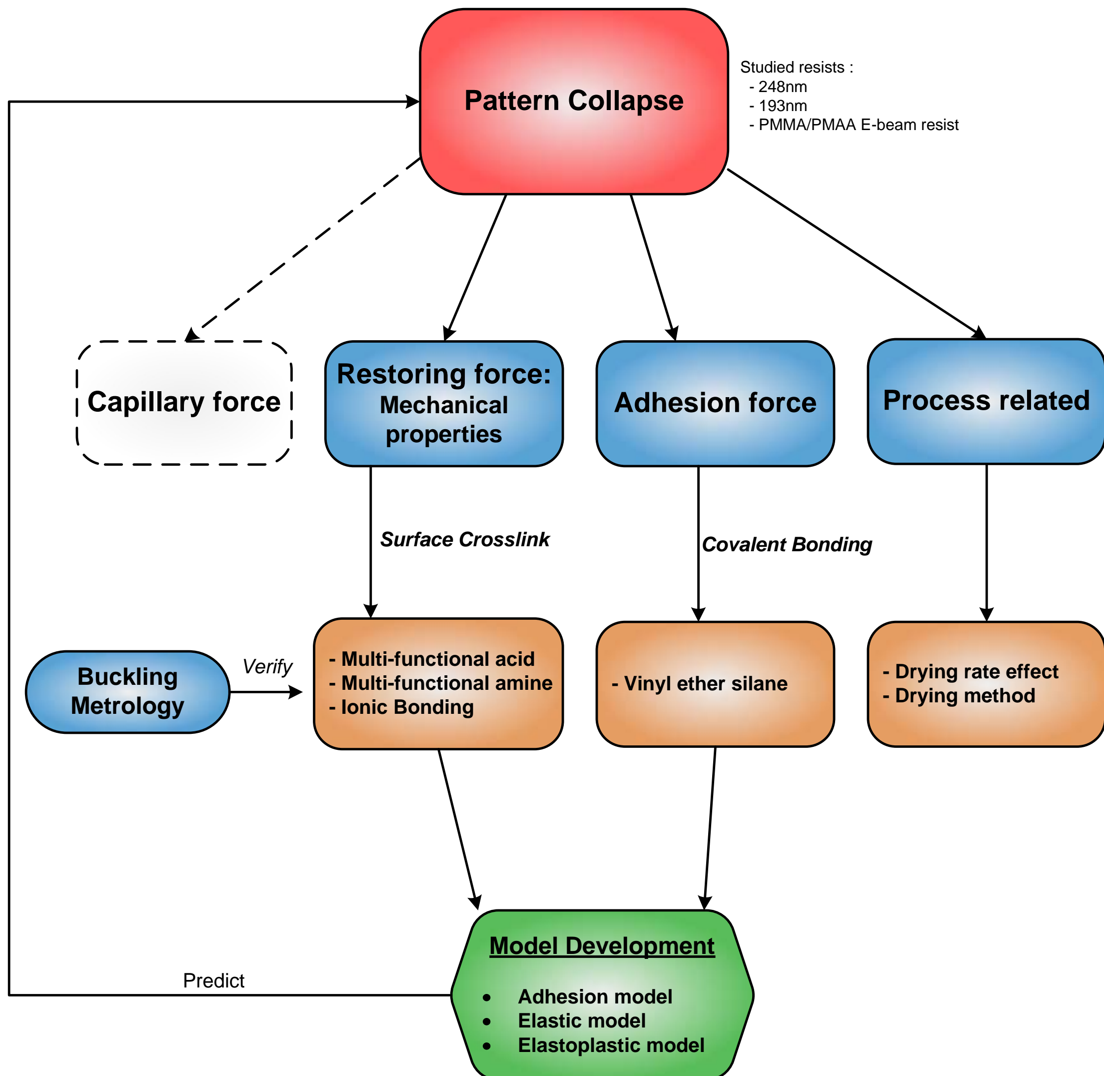

Figure 1.3 The flowchart of this work

1.4 References

1. Lee, C.-T. Development and Advanced Characterization of Novel Chemically Amplified Resists for Next Generation Lithography. Georgia Insitute of Technology, Atlanta, Georgia, USA, 2008.

2. Levinson, H. J., *Optical pattern formation, in principle of lithography*. 2nd ed.; SPIE Optical Engineering Press: Bellingham, Washington, USA, 2004.

3. Itani, T., A Comprehensive Review of EUV Resist Materials and Pro cessing at Selete. *J Photopolym Sci Tec* **2011,** *24* (2), 111-118.

4. Pollentier, I.; Lokasani, R.; Gronheid, R., Assessment of Challenges in EUV Resist Outgassing and Contamination Characterization. *J Photopolym Sci Tec* **2012,** *25* (5), 609-616.

5. Malek, C. K.; Das, S., Swelling behaviour of poly(methylmethacrylate) thick resist layers in deep X-ray lithography. *J Synchrotron Radiat* **2003,** *10*, 272-279.

6. Shew, B. Y.; Li, H. C.; Pan, C. L.; Ko, C. H., X-ray micromachining SU-8 resist for a terahertz photonic filter. *J Phys D Appl Phys* **2005,** *38* (7), 1097-1103.

7. Ballav, N.; Chen, C. H.; Zharnikov, M., Electron beam and soft X-ray lithography with a monomolecular resist. *J Photopolym Sci Tec* **2008,** *21* (4), 511-517.

8. Namatsu, H.; Kurihara, K.; Nagase, M.; Iwadate, K.; Murase, K., Dimensional Limitations of Silicon Nanolines Resulting from Pattern Distortion Due to Surface-Tension of Rinse Water. *Appl Phys Lett* **1995,** *66* (20), 2655-2657.

9. Huang, V.; Chiu, C. C.; Lin, C. A.; Chang, C. Y.; Gau, T. S.; Lin, B. J., Effect of novel rinsing material and surfactant treatment on the resist pattern performance. *Proc. SPIE* **2007,** *6519*, 65193C-9.

10. Drechsler, A.; Petong, N.; Bellmann, C.; Synytska, A.; Busch, P.; Stamm, M.; Grundke, K.; Wunnicke, O., Adsorption of cationic surfactants onto photoresist surfaces - A way to reduce pattern collapse in high aspect ratio patterning. *Can J Chem Eng* **2006,** *84* (1), 3-9.

11. Drechsler, A.; Belmann, C.; Synytska, A.; Petong, N.; Grundke, K.; Stamm, M.; Reichelt, J.; Wunnicke, O., The adsorption of cationic surfactants on photoresist surfaces and its effect on the pattern collapse in high aspect ratio patterning. *Colloid Surface A* **2007,** *311* (1-3), 83-92.

12. Drechsler, A.; Petong, N.; Bellmann, C.; Busch, P.; Stamm, M.; Grundke, K.; Wunnicke, O.; Reichelt, J., The effect of adsorbed cationic surfactant on the pattern collapse of photoresist lines in photolithographic processes. *Prog Coll Pol Sci S* **2006,** *132*, 82-94.

13. Zhang, P.; Rao, M. B.; Jaramillo, J. M.; Horvath, B. t.; Ross, B.; Paxton, T.; Davis, T.; Cook, P. t.; Witko, D., Pattern collapse and line width roughness reduction by surface conditioner solutions for 248-nm lithography. *Proc. SPIE* **2005,** *5753*, 252-260.

14. Guerrero, D. J.; Xu, H.; Mercado, R.; Blackwell, J., Underlayer Designs to Enhance EUV Resist Performance. *J Photopolym Sci Tec* **2009,** *22* (1), 117-122.

15. Kawai, A.; Moriuchi, T.; Niiyama, T.; Kishioka, T.; Maruyama, D.; Sakaida, Y.; Matsumoto, T., Adhesion improvement of ArF resist pattern depending on BARC material. *Microelectron Eng* **2006,** *83* (4-9), 659-662.

16. Kurano, K.; Kishioka, T.; Hiroi, Y.; Ohashi, T.; Kawai, A., Peeling analysis of ArF resist pattern on BARC by using AFM. *J Photopolym Sci Tec* **2007,** *20* (6), 825-826.

17. Park, E. M.; Choi, J.; Kang, B. H.; Dong, K. Y.; Park, Y.; Song, I. S.; Ju, B. K., Investigation of the effects of bottom anti-reflective coating on nanoscale patterns by laser interference lithography. *Thin Solid Films* **2011,** *519* (13), 4220-4224.

18. Helbert, J. N.; Saha, N., Application of Silanes for Promoting Resist Patterning Layer Adhesion in Semiconductor Manufacturing. *J Adhes Sci Technol* **1991,** *5* (10), 905-925.

CHAPTER 2

DEVELOPMENT OF A NOVEL REACTIVE RINSE STRATEGY FOR PHENOLIC POLYMER RESISTS BASED ON AN ADIPIC ACID CROSSLINKER AND EDC-NHS COUPLING TO MITIGATE RESIST PATTERN COLLAPSE

The semiconductor industry is constantly pushing the limits of the lithography processes used to fabricate integrated circuits. One of the important issues is pattern collapse during drying after development. One of the primary modes of pattern collapse at small feature sizes is pattern bending or deforming due to a weak mechanical restoring force of the resist features. The main forces which govern such pattern deformation are related to the mechanical properties of the resist. One approach to improve this pattern problem is to enhance the mechanical properties of resist features. Instead of changing the chemical formulation of the resist, the simple way for achieving the mechanical enhancement is to crosslink the resist surface. In this chapter, an adipic acid carbodiimide reactive rinse was applied on resist patterns to crosslink hydroxyl groups on resist surface in the post-development process. Pattern collapse test structures were fabricated and analyzed to quantify the impact of the use of adipic acid reactive rinse treatment. The results of critical stress analysis and SEM studies of the resulting patterns confirm that the use of a reactive rinse can significantly enhance the mechanical properties of the resist and dramatically mitigate pattern collapse.

2.1 Introduction

As the semiconductor industry continues to push to smaller critical dimensions, pattern collapse caused by unbalanced capillary forces during the final rinse and drying process has become an important problem that can practically limit the resolution of a resist material long before its intrinsic resolution limit is reached. The capillary forces experienced by the resist are dependent upon a number of factors including the dimension of the pattern, the resist material, the surface tension of the final rinse solvent, and the contact angle of the final rinse liquid on the resist line side wall. The dimension of the pattern and the resist material are dictated by design requirements for the lithographic process. Therefore, changing the pattern geometry and material may not be an option to reduce the capillary forces. Several research groups have studied the use of surfactant in the rinse to improve the pattern behavior. One research group reported that they improved not only line width roughness and collapse margin of line-space patterns, but also the contact-edge roughness (CER) and the depth of focus (DOF) of hole patterns by using their own surfactants[1]. Although an appropriate surfactant in development step can reduce the surface tension of rinse solvent and the contact angle of rinse liquid on the resist wall, the patterns rinsed with a surfactant appeared to cause shrinkage[2]. Moreover, it was observed that if the surfactant penetrates too deep into the resist structures, it may cause resist deformation, leading to further pattern collapse[3]. Therefore, rather than attempt to modify the rinse solvent by adding a surfactant, our method involves the actual strengthening of the resist using a post-development crosslinking reaction while the resist structures are still in their wet state.

The crosslinking reactive rinse methodology stems from the observation that negative tone photoresists which operate by crosslinking result in a covalently bonded network and often exhibit superior patterning capabilities which can be attributed to the fact that the resist has adopted a networked macromolecular structure after exposure and

most likely inherited superior mechanical properties relative to the unexposed polymeric structure. Our idea sought to capitalize on this notion of using crosslinking combined with the high surface to volume ratios present in high resolution resist features, and therefore a reactive rinse procedure was developed which could potentially crosslink the phenolic groups on the surface of a photoresist.

Water soluble carbodiimides have been frequently applied as crosslinking agents for biological materials like the collagen[4,5]. The carboxyl groups of amino acid residues are activated with *N*-ethyl-*N'*-(3-dimethylaminopropyl)carbodiimide hydrochloride (EDC) in the presence of *N*-hydroxysuccinimide (NHS) to form NHS esters. The NHS esters then can react with nucleophiles, such as primary amine groups to form stable amide bonds[6,7] or hydroxyl groups to form ester bonds[8]. In this work, adipic acid with two carboxylic groups, was applied to crosslink poly(hydroxystyrene)-based positive tone copolymer (referred to here as ESCAP-1) using such carbodiimide chemistry. One advantage of this reactive rinse is that it is an aqueous process that should be easily compatible with high volume, track-based lithographic processes. Contact angle studies and grazing IR were used to characterize the surface crosslinking reaction after reactive rinse treatment. Thin-film buckling experiments were performed on ESCAP-1 resist thin films before and after application of the reactive rinse, and this data was used to calculate the effective modulus of the resist films before and after treatment. Adipic acid reactive rinse treatment was found to result in a clear improvement in the resistance of the resists to pattern collapse as observed by SEM. A comparison of critical stress at the point of pattern collapse as a function of resist feature size also clearly showed significantly improvement in the mechanical resilience of resist samples processed with the reactive rinse treatment. Quartz crystal microbalance (QCM) studies suggested that the crosslink reaction was confined near the surface of resist structure and the estimated penetration depth was about 6 nm.

2.2 Experimental

Materials A model photoresist, consisting of a resist resin supplied by JSR and Intel (referred to here as ESCAP-1, composed of a poly(hydroxystyrene-co-styrene-co-t-butyl methylmethacrylate) terpolymer with a molar ratio of 0.6:0.2:0.2), a triphenylsulfonium nonaflate (TPS-Nf) photoacid generator (PAG), and a trioctyl amine (TOA) base quencher, was created by dissolving all the components in propylene glycol methyl ether acetate (PGMEA) at loadings of 7.4 wt% total solids in PGMEA with 5 wt% TPS-Nf relative to ESCAP-1 and 10 mol% TOA relative to the TPS-Nf PAG. The developer, used in this study, AZ300MIF was supplied by AZ Electronic Materials Company. All other reagents were purchased from Sigma-Aldrich, VWR, or Alfa-Aesar.

Substrate Preparation Silicon nitride windowed (Si_xN_y) substrates were used as substrates for high-resolution electron beam imaging of resist materials. The preparation of Si_xN_y substrates have been described in our previous work[9]. The purpose of Si_xN_y windowed substrates is to eliminate electron backscattering from the substrate and thus produce extremely sharp aerial images and essentially vertical sidewalls in the final resist patterns. Substrates were primed with 1,1,3,3,3-hexamethyldisilazane (HMDS) vapor at 70 torr and 110°C to enhance the adhesion of resist patterns before the resist was coated.

Reactive Rinse Process The resist processing consisted of spin coating the resist films at various spin speeds for 60 seconds to obtain films of varying thickness. The control films were soft-baked at 110 °C for 2 min, exposed and patterned via e-beam, post-exposure baked at 110 °C for 1 min, developed by AZ300MIF for 30 sec, rinsed by deionized water for 30 sec and finally dried with a stream of nitrogen. E-beam lithography was carried out using a JEOL JBX-9300FS e-beam lithography system with an accelerating voltage of 100 kV, a beam diameter of 8 nm, a 2 nA current, and a 10 nm shot pitch. SEM images were taken using a Zeiss Ultra 60 scanning electron microscope and used to calculate the actual spaces and line widths.

0.1 M Adipic acid (AA), 0.1M EDC, and 0.1M NHS reactive rinse solutions (denoted as 0.1M AA/EDC/NHS) were prepared in deionized water. The samples which underwent the reactive rinse were taken through the same procedure up through the development step. After development, the samples were placed in a 0.1 M solution of AA/EDC/NHS for 1 minute, then in 0.1M EDC/NHS solution for additional 1 minute. After two step rinses, samples were rinsed with deionized water and dried with a stream of nitrogen in a manner identical to the control samples. Water contact angle measurements were used to monitor the surface conditions at each step of the reactive rinse. Grazing angle FTIR spectra were collected to identify the surface reaction on poly(4-hydroxystyrene) (PHOST) coated on gold substrates using an FTIR microscope (IRscope II microscope, Bruker AXS Inc.).

Pattern Performance Analysis The pattern used to study the collapse of the formulated ESCAP-1 resist has been described previously[10]. An e-beam lithography pattern with a series of varying line and space widths was specifically designed in order to quantitatively study pattern collapse (Fig. 2.1A and B). The pattern structure used in this work was designed so that the spacing (S) between two small parallel lines decreased from left to right starting from 200 nm down to 10 nm for a constant line width. This pattern generates increasing capillary stress in the pairs of resist lines as one moves across the pattern array from left to right and eventually a sufficiently small space value (critical space, S_{1c}) was reached in each array such that the stress applied to the resist exceeded the critical stress (σ_c) required for pattern bending and subsequently feature deformation and collapse occurred as shown in Fig. 2.1C. Critical space, S_{1c} is indicated as the last position where the pattern pair lines can stand as the capillary stress increases from left to right. Critical space (S_{1c}) and line widths (W) were measured precisely from high resolution SEM images using custom written MALAB software designed for high resolution SEM feature analysis. The patterns we designed allowed us to qualitatively and quantitatively study pattern collapse and obtain consistent, reproducible results.

Mechanical Property Measurement The buckling measurements used to study the moduli of the ESCAP-1 resist has been described in our previous work[11]. A homemade buckling stage was designed to stretch poly(dimethylsiloxane) (PDMS) and release the pre-strain on PDMS. The resist film was transferred in DI water from the wafer which was treated by oxygen plasma for 30 minutes before resist film spincoating. Since the interface between resist film and silicon wafer is highly hydrophilic, the water easily penetrates into the interface. Resist film can be easily transferred on the pre-strain PDMS substrate. After the strain on the PDMS was released on the homemade stage, ESCAP-1 film underwent periodic buckling at a wavelength that minimized the total strain energy in the system[12]. The wavelength of the buckling patterns of the polymer films were measured by using atomic force microscopy (AFM, Agilent Picoplus system). The average wavelengths on the film surface were calculated by FFT analysis of the AFM images of the surface by using MATLAB software.

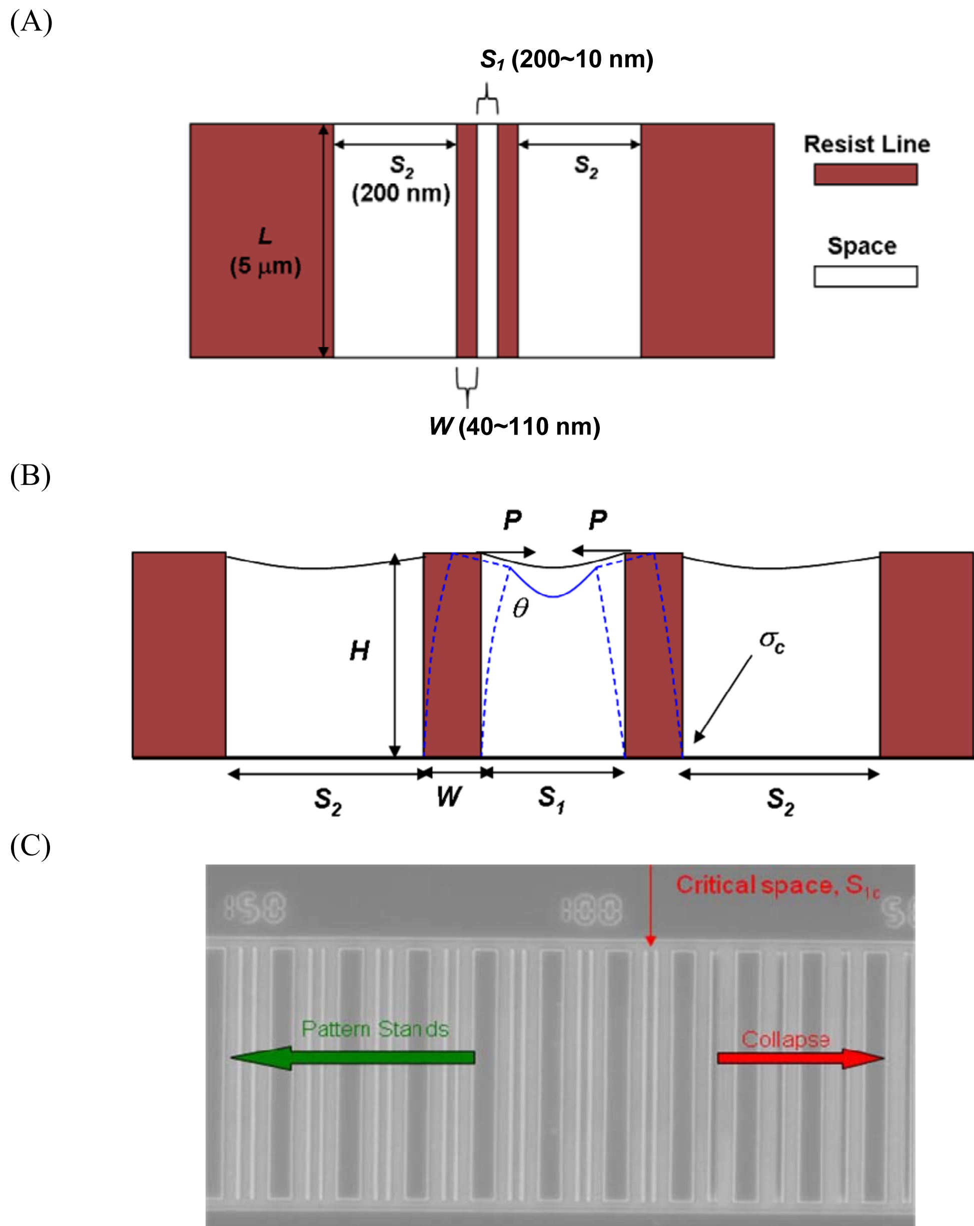

Figure 2.1 (A) Top view and (B) side view of pattern design used in this work for determining the critical stress at the point of pattern collapse; (C) An example for determining the position (S_{1c}) of critical stress (σ_c): SEM image of nominal 70 nm feature width line pair arrays used to identify the critical S_{1c} space.

2.3 Results and Discussion

ESCAP-1 photoresist is a terpolymer composed of hydroxystyrene, styrene, t-butyl methylmethacrylate with a molar ratio of 0.6:0.2:0.2. The 60% molar ratio of hydroxystryrene provides mostly hydroxyl groups on the resist surface, which can be used as reactive groups in conjunction with rinse additives to cross-link the surface of the patterns and films with functional carboxylic acids. The concept of reactive rinse is shown in Fig. 2.2A. ESCAP-1 films and polystyrene films (PS) were treated with 0.1M AA/EDC/NHS solution for 1min, followed by additional 1min rinse of 0.1M EDC/NHS solution to crosslink the unreacted phenolic groups on the pattern surface. Propanoic acid (PA) was used as a control agent and followed the same procedure for comparison of di-acid crosslinkers, shown in Fig. 2.2B.

The surface contact angle was used to monitor the surface conditions of ESCAP-1 films for each step on the reactive rinse process, and the results are plotted in Fig. 2.3. The surface contact angle of polystyrene films without reactive phenolic groups for carbodiimide reaction stayed the same surface contact angle after reactive rinse. For the AA reactive rinse samples, as shown in Fig. 2.2A, surface contact angle increased by approximately 10 degree after one minute of AA/EDC/NHS treatment. The contact angle increased again after the second EDC/NHS treatment. Statistically, after first step of reactive rinse, some of acid groups were crosslinked with two phenolic groups of ESCAP-1 and some acids are only reacted with one side on the ESCAP-1 surface, resulting in the hydrophobic surface due to the decrease of the amount of phenolic groups and the increase of the amount of hydrocarbon on the film surface. On the second step of reactive rinse, EDC/NHS was applied for the acids which were not completely crosslinked to enhance the crosslinking efficiency. Because more crosslinked surface led to fewer amounts of phenolic and unreacted carboxylic acid groups, the film surface became more hydrophobic than the surface which was only treated once. For PA rinse samples, as shown in Fig. 2.2B, surface contact angle of ESCAP-1 films increased after

the first minute treatment due to the decrease of phenolic groups on the film surface. After the second EDC/NHS rinse, surface contact angle remained the same contact angle (~80 degree). This also suggests that the second step in AA reactive rinse is useful for increasing the amount of surface crosslink.

(A)

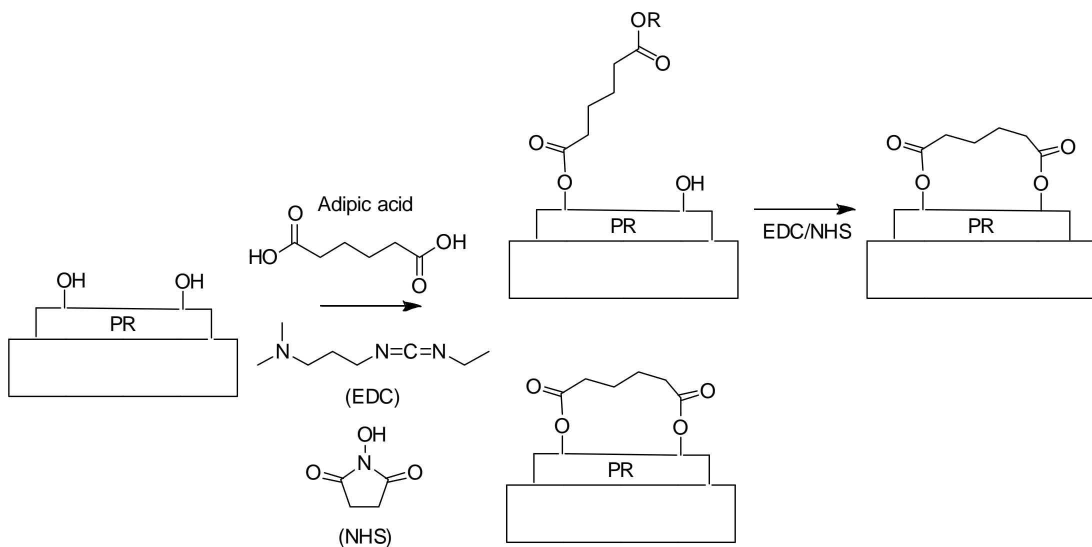

(B)

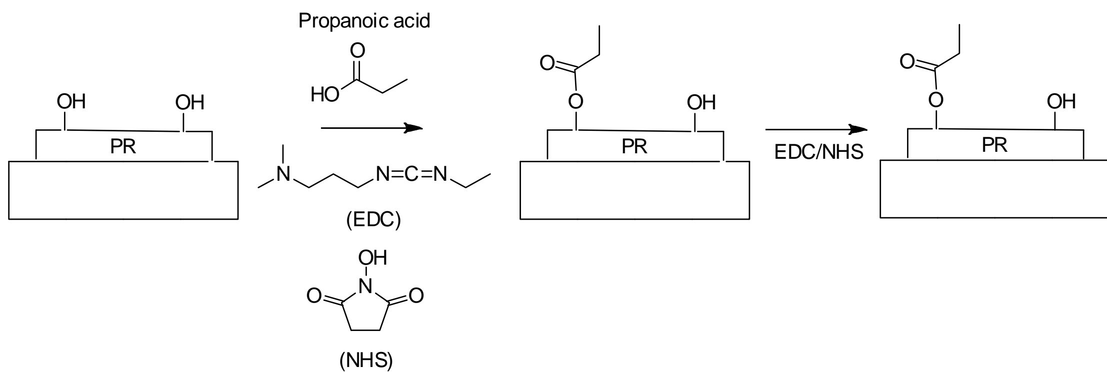

Figure 2.2 Schematic illustration of reactive rinse process: (A) adipic acid reactive rinse; (B) propanoic acid reactive rinse.

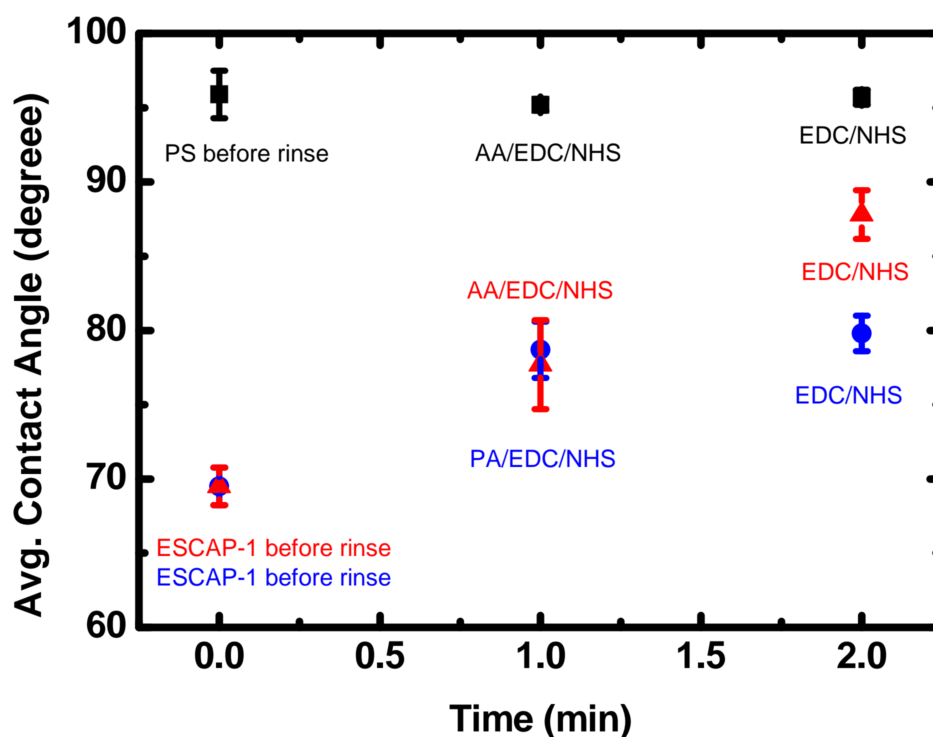

Figure 2.3 Surface contact angles during the reactive rinses. Polystyrene (squares) or ESCAP-1 films were performed one minute AA/EDC/NHS (triangles) or one minute PA/EDC/NHS rinses (circles), followed by one minute EDC/NHS rinse, and dried with a nitrogen stream.

Poly(4-hydroxystyrene) (PHOST) films, 25 nm thick, were coated on gold substrates for increasing the grazing angle IR signal intensity. Figure 2.4 shows the grazing angle infrared spectra for the samples before and after AA reactive rinse. A new peak was observed in the carbonyl stretching vibration region at 1730 cm^{-1} on the samples that had been treated with PA control rinse and AA reactive rinse. From the inset plot in Fig. 2.4, the transmittance of AA rinse sample showed the deeper peak at carbonyl stretching vibration region due to more acid groups on adipic acid. These results are also consistent with the contact angle results that AA reactive rinse is capable of crosslinking the phenolic groups and form ester covalent bonds on the resist surface.

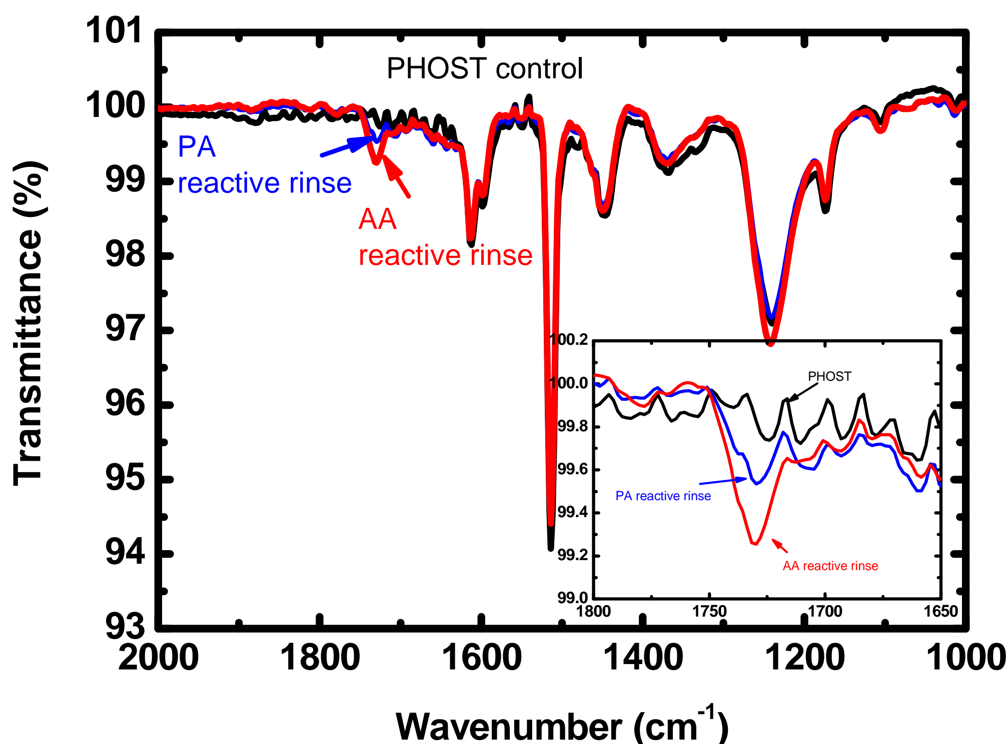

Figure 2.4 Grazing angle IR spectra of control PHOST film, PHOST film treated by PA reactive rinse, and PHOST film treated by AA reactive rinse. The inset plot shows the zoom-in spectra of carbonyl stretching vibration region.

The sample denoted as ESCAP/R is the ESCAP-1 film treated by AA reactive rinse process before transferred to PDMS. Because the rinse treated film on silicon is faced down on the PDMS, the crosslinked surface layer is located at the bottom of ESCAP-1 film, shown in Fig. 2.5A. The sample denoted as R/ESCAP is the ESCAP-1 film treated by AA reactive rinse after the film is transferred on PDMS so the crosslinked layer is located on the top of ESCAP-1 film. The R/ESCAP/R sample is the ESCAP-1 treated by AA reactive rinse on both sides of the resist film. After one side treatment on ESCAP-1 films (ESCAP/R) with AA and PA reactive rinses, the moduli of the

crosslinked ESCAP-1 film were measured by thin film buckling, as shown in Fig. 2.5B. After treating one side of the thin ESCAP-1 film with AA reactive rinse, the effective modulus of ESCAP-1 film significantly increased to almost twice that of the unmodified ESCAP-1 film. The modulus of the film treated by PA reactive rinse and unmodified ESCAP-1 film were almost identical, which also support the idea that AA reactive rinse is capable of crosslinking the phenolic groups on the film surface and enhancing the modulus of the resist film. Fig. 2.5C shows the effect of crosslink surface of ESCAP-1 film applying AA reactive rinse on the one side or two sides of resist films. The effective moduli of films treated on one side (R/ESCAP and ESCAP/R) increased significantly compared to the unmodified film. Treating both sides of the film returned the modulus essentially to its bulk value. The increase of the effective modulus confirmed that modifying the surface of a resist with AA cross-linker leads to a significant enhancement of the mechanical properties and suggested that the same approach could be used to improve the mechanical properties of nanoscale resist structures.

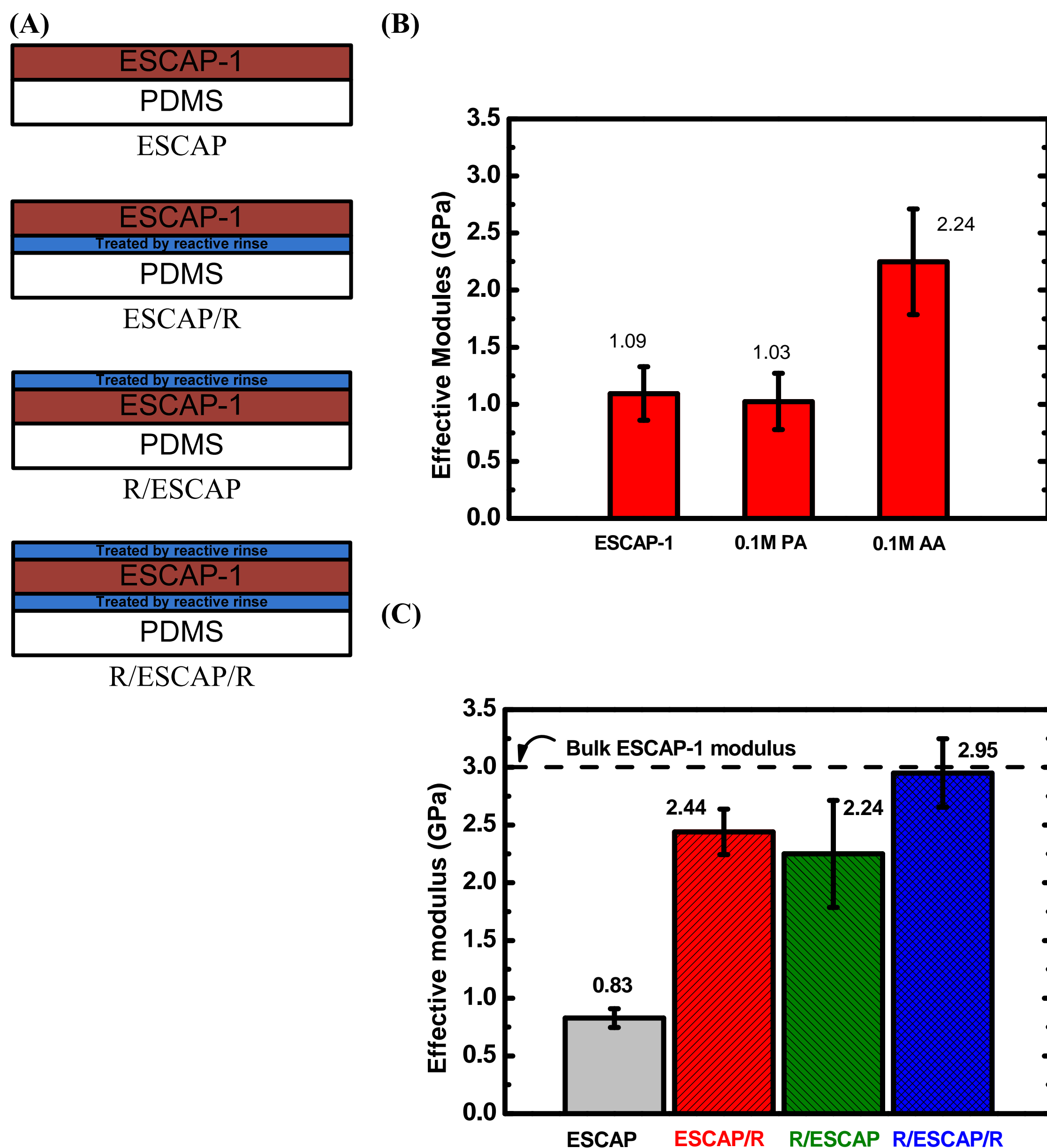

Figure 2.5 (A) Schematic presentation of the side of ESCAP-1 film treated by reactive rinse. ESCAP represents the ESCAP-1 film without reactive rinse. R/ESCAP and ESCAP/R represent the samples treated by reactive rinse on one side of ESCAP-1 films. R/ESCAP/R represents the sample treated by reactive rinse on two sides of ESCAP-1 film. (B) Effective moduli of ESCAP-1 films treated with PA control rinse or AA reactive rinse. (C) Effect of crosslinked surfaces of ESCAP-1 films using AA reactive rinse on the resulting modulus relative to an unmodified film. Data are shown in 95% confidence and all film thicknesses are 24 nm.

An e-beam lithography pattern with a series of varying line and space widths was specifically designed to quantitatively study pattern collapse[10]. The pattern structure used in this work was designed so that the spacing (S) between two small parallel lines decreased from left to right ranging from 200 nm to 10 nm for a constant line width. This pattern generated increasing stress in the pairs of resist lines as one moves across the pattern array and eventually a sufficiently small space value (critical space, S_{1c}) was reached in each array such that the stress applied to the resist exceeded the critical stress (σ_c) required for pattern bending, subsequently causing feature deformation and collapse. Smaller spacing resulted in higher capillary stress on the pair of resist lines.

The SEM images after AZ300MIF development and after additional reactive rinse are shown in Figure 2.6. The numbers on the left of arrays represent the nominal widths (W) of all small parallel lines. The arrows in the figure indicate the critical space (S_{1c}) which is the position in the pattern array with the smallest spacing between adjacent lines where resist lines can withstand the largest capillary stress before collapse. SEM images of samples which did not receive AA reactive rinse (see Figure 2.6A) showed that patterns collapsed at 110 nm space S_1 (S_{1c}) with nominal 80 nm line width and collapsed at 60 nm space S_1 (S_{1c}) with nominal 90 nm line width. SEM images of samples where the AA reactive rinse was applied showed patterned line pairs collapsing at 20 nm space S_1 (S_{1c}) with both nominal 80 nm and 90 nm line widths (see Figure 2.6B). Smaller critical spaces represented the cases where the resist lines could endure higher capillary force without collapsing. The use of the adipic acid reactive rinse resulted in the smallest critical space and enhanced pattern resistance to the capillary force relative to the samples without AA reactive rinse treatment.

(A)

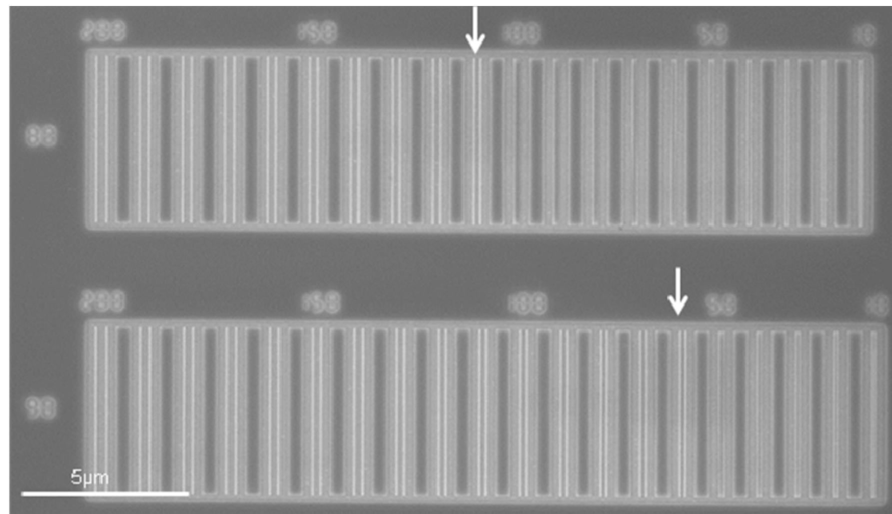

(B)

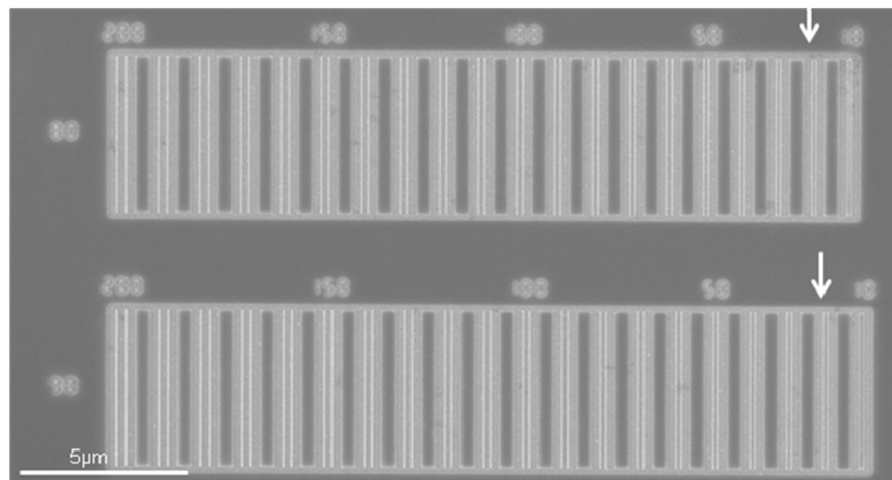

Figure 2.6 SEM images of nominal 80nm and 90 line widths on (A) the sample without AA reactive rinse, and (B) the sample with AA reactive rinse. The numbers on the left of arrays represent the nominal widths of all small parallel lines. The numbers on the top of arrays represent the nominal S_1 space between two small lines. The arrows in the figure indicate the critical space (S_{1c}) which is the position in the pattern array with the smallest spacing between adjacent lines where resist lines can withstand the largest capillary stress before collapse.

In order to ensure that crosslinking was the critical issue, a propionic acid rinse was also examined. Figure 2.7 shows the critical stresses for the samples treated by adipic acid reactive rinse and propionic acid rinse. The critical stress (σ_c) is defined as the maximum stress that can be applied to the photoresist lines prior to pattern collapse and occurs in critical space, the last space before the pair of resist lines collapse on the pattern structure we designed. The equation used to calculate the critical stress is expressed in equation (2.1), where γ is surface tension of rinse liquid (i.e. deionized water with γ=0.073 N/m in ESCAP-1 case), θ is the contact angle of the rinse liquid on the photoresist (i.e. deionized water with θ=77° in ESCAP-1 case), height H is the thickness of the photoresist film, S_2 is the respective outside space width between the lines of the pattern we designed, and S_{1c} is the critical pattern center space width where collapse is first indicated[10].

$$\sigma_C = 6\gamma \cos\theta \left(\frac{H}{W}\right)^2 \left(\frac{1}{S_{1c}} - \frac{1}{S_2}\right) \tag{2.1}$$

Critical stress is measured at the final stress point before the resist lines collapses and allows direct comparisons that are independent of pattern size and film thickness. The higher critical stress represents resist lines that have stronger resistance to the capillary stress. Without the adipic acid reactive rinse (squares in Fig. 2.7), pattern lines display a lower critical stress and pattern line that can't stand at higher stress. For the PA rinse samples (triangles in Fig. 2.7), the critical stress shows the similar critical stress as the samples which did not receive AA reactive rinse. After AA reactive rinse treatment (circles in Fig. 2.7), the pattern lines are able to withstand higher capillary stress than the sample without reactive rinse treatment or the sample treated by PA reactive rinse. These results also confirm our idea of carboiimide chemistry, reactive rinse that the AA reactive rinse is presumed to form covalent crosslink with the phenolic groups on the surface of

ESCAP-1 resist wall and improve the pattern resistance to capillary stress with the enhancement of mechanical properties due to surface crosslink.

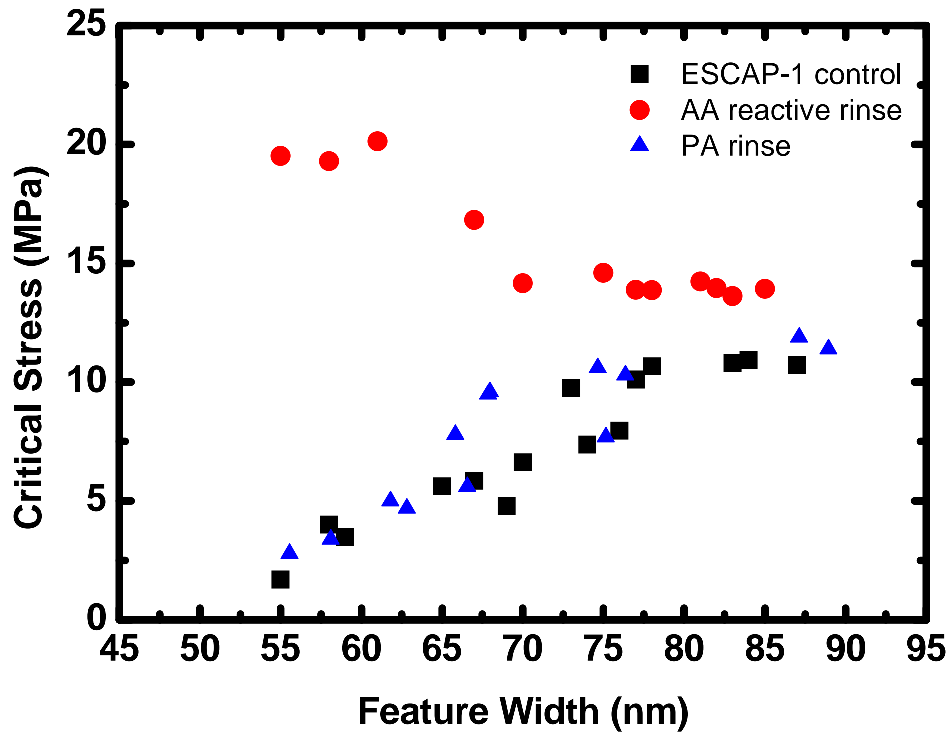

Figure 2.7 Critical stresses at the point of pattern collapse as a function of feature width in different samples: ESCAP-1 control samples (squares); samples treated by AA reactive rinse (circles); and samples treated by PA reactive rinse (triangles).

Critical stress data reach a plateau at larger feature widths. The transition in critical stress occurs for feature widths less than ~80 nm with decreasing (ESCAP-1 and PA samples) or increasing (AA reactive rinse samples) for thinner feature widths. In the case of 252 nm resist lines, the resist lines fail by weak mechanical properties of the resist structures, so the critical stress is highly correlated to the mechanical properties at higher resist lines[13]. Previous studies on ultra-thin polymer films have suggested that the

effective modulus of such films can be divided into two modulus combination: robust bulk layer modulus, and surface layer modulus which has smaller modulus and is responsible for many of the abnormal interfacial/confinement trends observed with thin films, and a bulk modulus[14],[15]. In the control case (solid squares in Fig. 2.7), without any reactive rinse treatment, for the larger feature width, the surface layer is only a small part of whole film. Therefore, the effect of surface layer on total film modulus is negligible, and the effective modulus of the pattern is dominated by the bulk modulus. For smaller feature widths however, the depth of the soft surface layer becomes comparable to that of the bulk layer and strongly affects the overall properties of the film[15]. The effective modulus is very sensitive to the dimension of feature size. Because the AA reactive rinse is applied to crosslink the surface layer, for the smaller feature width, the benefit of total film modulus from the surface crosslink becomes more significant and results in the dramatic increase as the feature width decreases.

A quartz crystal microbalance was also used to characterize the reaction of the cross-linked surface by measuring the mass uptakes that occur on the film during the reactive rinse process. Table 2.1 is summarized the QCM results after AA reactive rinse for three different film thicknesses. After AA reactive rinses on various thickness films, the increases in film mass are essentially identical. This suggests that the adipic acid crosslinking reaction is confined to near the surface of the resist film. Furthermore, based on the assumption that each adipic acid reacts with two -OH groups on ESCAP-1 surface, the amount of reacted -OH groups (colunm D) can be estimated from column C. Since the ratio of hydroxyl styrene is 60 mol percent of the total ESCAP-1 film, theoretically the total amount of -OH groups can be calculated from the amount of ESCAP-1 film. The ratio of reacted -OH groups (column E) is defined as the amount of reacted -OH groups divided by the total amount of -OH groups in the ESCAP-1 film. Assuming that the density of -OH groups is uniform throughout the ESCAP-1 film, the crosslink thickness (column F) can be estimated by multiplying the film thickness by the reacted -OH group

ratio. For the three different thicknesses studied, the thickness of surface crosslink layer was estimated by QCM is to be about 6 nm and shown in Fig. 2.8A. Another QCM study of effect of varying the rinse time at the first step on reactive rinse is summarized in Tab. 2.2. It also shown that for different rinse time, the increases in film mass are again virtually identical, which also supports the idea that the surface reactions are very fast and the process is self-limiting. Fig. 2.8B shows the estimated crosslink thickness as a function of rinse time at first step. The estimated thickness of crosslink depth is also 6 nm.

Table 1.1 Summary of QCM results on the study of the effect of film thickness during AA reactive rinse process.

(A) ESCAP Thickness (nm)	(B) ESCAP (μg/cm2)	(C) Δm after reactive rinse (μg/cm2)	(D) Reacted –OH (nmole/cm2)	(E) Reacted OH ratio (%)	(F) Crosslink Thickness estimate (nm)
20.6	2.31±0.27	0.25±0.20	3.46±2.81	29.9±1.5	6.2±0.3
65.1	6.86±0.39	0.37±0.11	3.15±0.64	9.2±1.9	6.0±1.2
183.9	20.65±0.12	0.28±0.13	3.92±1.82	3.8±0.9	7.0±1.7

Table 1.2 Summary of QCM results on the study of the effect of rinse time at first step of AA reactive rinse process.

(A) ESCAP Thickness (nm)	(B) ESCAP (μg/cm2)	(C) Δm after reactive rinse (μg/cm2)	(D) Reacted –OH (nmole/cm2)	(E) Reacted OH ratio (%)	(F) Crosslink Thickness estimate (nm)
65.1	6.86±0.39	0.37±0.11 (1min)	3.15±0.64	9.2±1.9	6.0±1.3
64.6	6.86±0.16	0.26±0.16 (2min)	3.00±1.32	8.7±0.9	5.6±0.6
74.9	8.46±0.20	0.25±0.18 (3min)	3.52±2.44	8.3±1.4	6.3±1.0
73.1	8.37±0.20	0.23±0.22 (4min)	3.25±3.03	7.7±1.8	5.7±1.3
73.2	8.40±0.18	0.20±0.21 (5min)	2.80±2.95	6.7±2.1	4.9±1.5

(A)

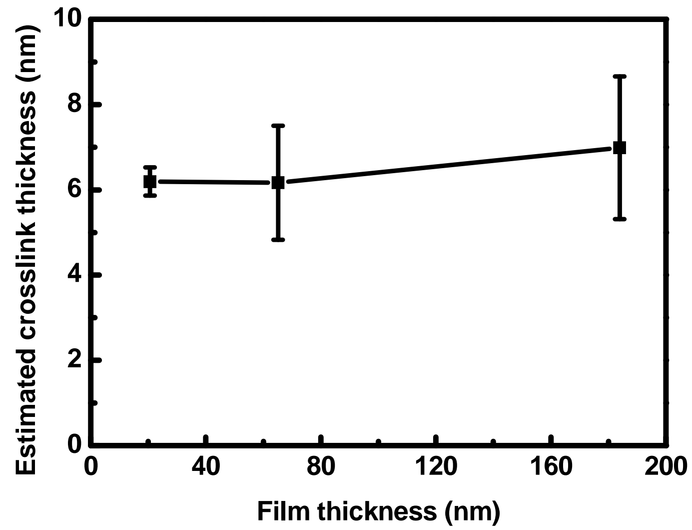

(B)

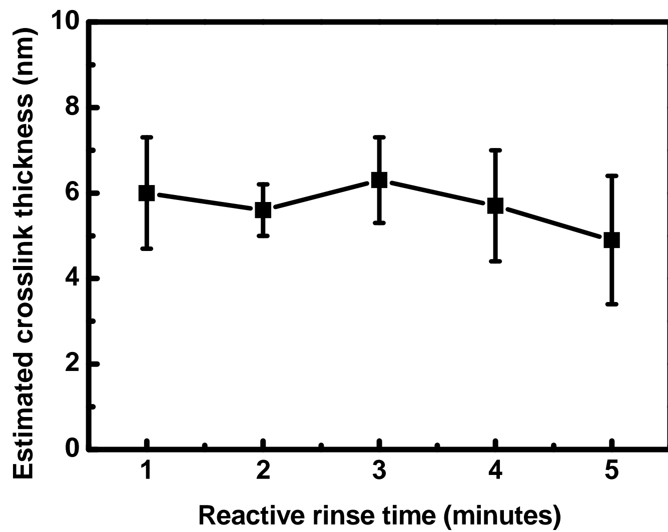

Figure 2.8 Estimated crosslink thickness as a function of (A) film thicknesses and (B) the rinse time at the first step of AA reactive rinse.

2.4 Conclusions

An adipic acid reactive rinse was applied in a post-development process to crosslink resist surfaces and to enhance the mechanical modulus of resist structures to mitigate pattern collapse. The surface contact angle and grazing angle IR results indicated that adipic acid covalently crosslinked the phenolic groups and formed esters on the resist surface. The buckling metrology also confirmed that the use of adipic acid reactive rinse in post-development process resulted in significant enhancement of the mechanical properties of ESCAP-1 films. SEM images showed that resist lines after adipic acid reactive rinse treatment were able to withstand at higher capillary stress than samples without the reactive rinse. Furthermore, QCM studies indicated that the adipic acid crosslink reaction was very fast and confined to near the surface of the resist film, and that the estimated crosslink thickness was about 6 nm.

2.5 References

1. Huang, V.; Chiu, C. C.; Lin, C. A.; Chang, C. Y.; Gau, T. S.; Lin, B. J., Effect of novel rinsing material and surfactant treatment on the resist pattern performance. *Proc. SPIE* **2007,** *6519*, 65193C-9.

2. Drechsler, A.; Belmann, C.; Synytska, A.; Petong, N.; Grundke, K.; Stamm, M.; Reichelt, J.; Wunnicke, O., The adsorption of cationic surfactants on photoresist surfaces and its effect on the pattern collapse in high aspect ratio patterning. *Colloid Surface A* **2007,** *311* (1-3), 83-92.

3. Zhang, P.; Rao, M. B.; Jaramillo, J. M.; Horvath, B. t.; Ross, B.; Paxton, T.; Davis, T.; Cook, P. t.; Witko, D., Pattern collapse and line width roughness reduction by surface conditioner solutions for 248-nm lithography. *Proc. SPIE* **2005,** *5753*, 252-260.

4. Damink, L. H. H. O.; Dijkstra, P. J.; vanLuyn, M. J. A.; vanWachem, P. B.; Nieuwenhuis, P.; Feijen, J., Cross-linking of dermal sheep collagen using a water-soluble carbodiimide. *Biomaterials* **1996,** *17* (8), 765-773.

5. Damink, L. H. H. O.; Dijkstra, P. J.; vanLuyn, M. J. A.; vanWachem, P. B.; Nieuwenhuis, P.; Feijen, J., In vitro degradation of dermal sheep collagen cross-linked using a water-soluble carbodiimide. *Biomaterials* **1996,** *17* (7), 679-684.

6. Powell, H. M.; Boyce, S. T., EDC cross-linking improves skin substitute strength and stability. *Biomaterials* **2006,** *27* (34), 5821-5827.

7. Updegrove, T. B.; Correia, J. J.; Chen, Y. F.; Terry, C.; Wartell, R. M., The stoichiometry of the Escherichia coli Hfq protein bound to RNA. *Rna* **2011,** *17* (3), 489-500.

8. Everaerts, F.; Torrianni, M.; Hendriks, M.; Feijen, J., Biomechanical properties of carbodiimide crosslinked collagen: Influence of the formation of ester crosslinks. *J Biomed Mater Res A* **2008,** *85A* (2), 547-555.

9. Lee, C.-T.; Wang, M.; Jarnagin, N. D.; Gonsalves, K. E.; Roberts, J. M.; Yueh, W.; Henderson, C. L., Photosensitivity and line-edge roughness of novel polymer-bound PAG photoresists. *Proc. SPIE* **2007,** *6519*, 65191E-9.

10. Yeh, W. M.; Noga, D. E.; Lawson, R. A.; Tolbert, L. M.; Henderson, C. L., Comparison of positive tone versus negative tone resist pattern collapse bahavior. *J Vac Sci Technol B* **2010,** *28* (6), C6s6-C6s11.

11. Yeh, W.-M.; Noga, D. E.; Lawson, R. A.; Tolbert, L. M.; Henderson, C. L., Thin film buckling as a method to explore the effect of reactive rinse treatments on the mechanical properties of resist thin films. *Proc. SPIE* **2010,** *7639*, 76391I-6.

12. Chung, J. Y.; Nolte, A. J.; Stafford, C. M., Surface Wrinkling: A Versatile Platform for Measuring Thin-Film Properties. *Adv Mater* **2011,** *23* (3), 349-368.

13. Yeh, W. M.; Lawson, R. A.; Henderson, C. L., A comprehensive model and method for model parameterization for predicting pattern collapse behavior in photoresist nanostructures. *Proc. SPIE* **2011,** *7972* (1), 79721X.

14. Stafford, C. M.; Harrison, C.; Beers, K. L.; Karim, A.; Amis, E. J.; Vanlandingham, M. R.; Kim, H. C.; Volksen, W.; Miller, R. D.; Simonyi, E. E., A buckling-based metrology for measuring the elastic moduli of polymeric thin films. *Nat Mater* **2004,** *3* (8), 545-550.

15. Singh, L.; Ludovice, P. J.; Henderson, C. L., Influence of molecular weight and film thickness on the glass transition temperature and coefficient of thermal expansion of supported ultrathin polymer films. Thin Solid Films 2004, 449 (1-2), 231-241.

CHAPTER 3

EFFECT OF CROSSLINKER STRUCTURE ON RESIST PATTERN COLLAPSE BEHAVIOR WHEN USING A REACTIVE RINSE PROCESS FOR PHENOLIC RESIST POLYMERS BASED ON EDC-NHS COUPLING

A potential roadblock for future lithographic processes is pattern collapse caused by unbalanced capillary forces experienced by the photoresist pattern during final rinse and drying. To mitigate the pattern collapse, we developed a post-development strategy which involved the actual strengthening of the resist using a post-development crosslinking reaction while the resist structures were still in their wet state. A post-development strategy to reduce pattern collapse was developed whereby the phenolic functional groups of the resist were cross-linked via a multi-carboxylic acid, using carbodiimide chemistry. Application of this reactive rinse on resist patterns of comparable thickness clearly resulted in an improvement in resistance to collapse as observed by SEM. A comparison of critical stress as a function of feature size for samples with and without the reactive rinse treatment also clearly showed the improvement on the pattern collapse issue. The results of studies which compared the number of crosslinkable carboxylic acid functionalities in the crosslinker, the crosslinker core, and the link length on the reactive rinse process were shown. The ability to significantly reduce pattern collapse in small resist nanostructures has been demonstrated.

3.1 Introduction

The semiconductor industry is constantly pushing the limits of the lithography process used to fabricate integrated circuits. However, a potential roadblock for future lithographic processes is pattern collapse caused by unbalanced capillary forces present during the drying step of the lithographic process. The capillary forces experienced by the resist are dependent upon a number of factors including the surface tension of the final rinse solvent, the contact angle of the final rinse liquid on the resist line side wall, and the dimensions of the pattern. Since the dimension of the pattern is restricted by the requirement of etching or other processes, many research groups have focused on other methods to reduce the surface tension and contact angle on the resist. Several research groups have studied the use of surfactants in the rinse to improve the pattern behavior. Huang and coworkers reported that they improved not only line width roughness and collapse margin of line-space patterns, but also contact-edge roughness (CER) and the depth of focus (DOF) of hole patterns by using their developed surfactants[1]. Drechsler et al. found that a rinse with cationic surfactants yields a reduction of the pattern collapse of test photoresist structures[2]. Although an appropriate surfactant in development step can reduce the surface tension of rinse solvent and the contact angle of rinse liquid on the resist wall, the patterns rinsed with a surfactant were found to have the shrinkage issue, which was also discussed by Huang and Drechsler. Zhang and coworkers also reported that the use of surfactant rinse in the development step provided significantly improvement of pattern behavior including reduced pattern collapse and line width roughness[3]. However, they also observed that if the surfactant penetrated too deep into the resist structures, it may cause the resist further deformation, leading to further pattern collapse[3]. Therefore, rather than attempt to modify the rinse solvent by adding a surfactant or using a super critical fluid[4], our methodology involved the actual

strengthening of the resist using a post-development crosslinking reaction while the resist structures are still in their wet state.

The crosslink reactive rinse methodology stems from the observation that negative tone photoresists which operate by crosslinking result in a covalently bonded network and often exhibit superior patterning capabilities which can be attributed to the fact that the resist has adopted a networked macromolecular structure after exposure and most likely inherited superior mechanical properties relative to the unexposed polymeric structure. Our idea sought to capitalize on this notion of using crosslinking combined with the high surface to volume ratios present in high resolution resist features, and therefore a reactive rinse procedure was developed which could potentially crosslink the phenolic groups on the surface of a photoresist.

The pattern collapse of a hydroxystyrene-based positive tone copolymer (referred to here as ESCAP-1) using an e-beam lithography pattern with a predetermined series of line/space widths has been investigated. The calculation of the critical stress allowed us to study and quantify the performance at the point of collapse of the photoresist. In this work, the pattern performances before and after reactive rinse were observed by SEM. A comparison of critical stress as a function of feature size for samples with and without the reactive rinse treatment was also studied using our designed pattern arrays[5]. The results of studies which compare the number of crosslinkable carboxylic acid functionalities in the crosslinker, the hydrophilicity of the crosslinker chain and linker length on the reactive rinse process will also be discussed.

3.2 Experimental

Materials A model photoresist, consisting of a resist resin supplied by JSR and Intel (referred to here as ESCAP-1, composed of a poly(hydroxystyrene-co-styrene-co-t-

butyl methylmethacrylate) terpolymer with a molar ratio of 0.6:0.2:0.2, shown in Fig. 3.1), a triphenylsulfonium nonaflate (TPS-Nf) photoacid generator (PAG), and a trioctyl amine (TOA) base quencher, was made by dissolving all the components in propylene glycol methyl ether acetate (PGMEA) at loadings of 7.4 wt% total solids in PGMEA with 5 wt% TPS-Nf relative to ESCAP-1 and 10 mol% TOA relative to the TPS-Nf PAG. The developer, AZ300MIF was supplied by AZ Electronic Materials Company. All other reagents used in this study were purchased from Sigma-Aldrich, VWR, or Alfa-Aesar. E-beam lithography was carried out using a JEOL JBX-9300FS e-beam lithography system with an accelerating voltage of 100 kV, a beam diameter of 8 nm, a 2 nA current, and a 10 nm shot pitch. SEM images were taken using a Zeiss Ultra 60 scanning electron microscope.

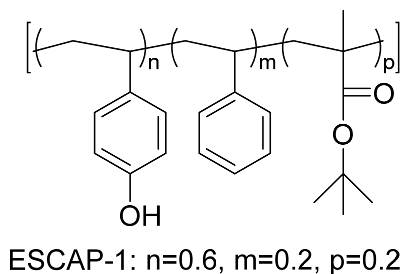

Figure 3.1 Chemical structure of ESCAP-1 photoresist.

Substrate Preparation Silicon nitride windowed (Si_xN_y) substrates were used as substrates for high-resolution electron beam imaging of resist materials. The preparation of Si_xN_y substrates have been described in our previous work[6]. The purpose of Si_xN_y windowed substrates is to eliminate electron backscattering from the substrate and thus produce extremely sharp aerial images and essentially vertical sidewalls in the final resist patterns. Substrates were primed with 1,1,3,3,3-hexamethyldisilazane (HMDS) vapor at 70 torr and 110°C to enhance the adhesion of resist patterns before the resist was coated.

Reactive Rinse Process The resist processing consisted of spin coating the resist films from 7.4wt% ESCAP-1 formulated solution at various spin speeds for 60 seconds to obtain films of varying thickness. The control films were soft-baked at 110 °C for 2 min, exposed and patterned via e-beam, post-exposure baked at 110 °C for 1 min, developed by AZ300MIF for 30 sec, rinsed by deionized water for 30 sec and finally dried with a stream of nitrogen. The chemical structures of various acid linkers in this study are shown in Figure 3.2. Solutions of 0.1 M reactive rinse with an equivalent of EDC/NHS (0.1M crosslinker/EDC/NHS) were prepared in deionized water, i.e. for the four carboxyl groups in pyromellitic acid (PMA), 0.1M PMA rinse solution (PMA/EDC/NHS) was made by dissolving 0.1 mole PMA, 0.4 mole EDC and 0.4 mole NHS in 1 liter deionized water. The same terminology is used with reference to the 0.1 M EDC/NHS solution. The schematic process of reactive rinse is shown in Figure 3.3. The samples which underwent the reactive rinse were taken through the same procedure up through the development step. After development, the samples were placed in a 0.1 M solution of crosslinker/EDC/NHS for two minutes and followed by DI water rinse for 30 seconds, schematically presented in Figure 3.3A. For some crosslinkers (AA, TMA, SuA, and SeA), solid precipitates were observed after making 0.1M solutions due to the solubility limit of the ester intermediate in DI water or solubility of crosslinker itself in DI water. After filtering the 0.1M crosslinker/EDC/NHS solution, an additional rinse step (0.1M EDC/NHS) is applied to activate the unreacted acid functional groups to increase the degree of crosslink. The effect of crosslinker concentration issue is discussed in the following section. After the development step, the samples were placed in a 0.1 M solution of crosslinker/EDC/NHS that filtered with 0.2μm syringe filter for one minute, then in 0.1M EDC/NHS solution for additional one minute, as presented in Fig. 3.3B. After two-step rinses, samples were rinsed with deionized water and dried under a stream of nitrogen in a manner identical to the control samples. The grazing angle FTIR spectra were collected to identify the surface reaction on poly(4-hydroxystyrene) (PHOST)

coated on gold substrates using an FTIR microscope (IRscope II microscope, Bruker AXS Inc.).

(A)

Difunctional Acid Crosslinkers: | Trifunctional Acid Crosslinkers: | Multifunctional Acid Crosslinkers:

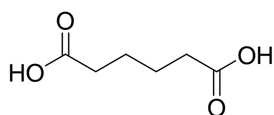

Adipic acid (AA)

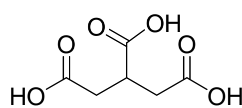

Tricarballylic acid (TCA)

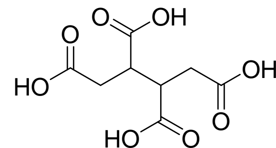

1,2,3,4-Butanetetracarboxylic acid (BTCA)

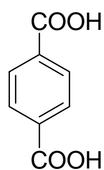

Terephthalic acid (THA)

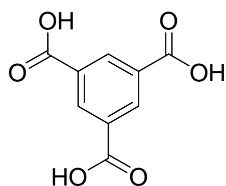

Trimesic acid (TMA)

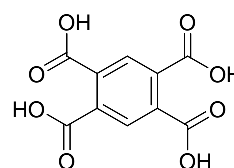

Pyromellitic acid (PMA)

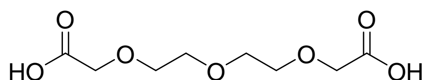

3,6,9-Trioxaundecanedioic acid (PEG3)

(B)

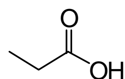

Propanic acid (PA, C3')

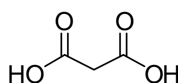

Malonic acid (MA, C3)

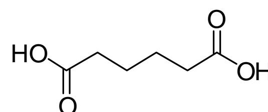

Adipic acid (AA, C6)

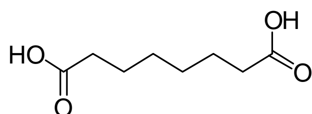

Suberic acid (SuA, C8)

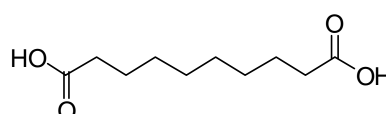

Sebacic acid (SeA, C10)

Figure 3.2 (A) Chemical structures of crosslinkers for studying the effect of linker functionality and the core structure, and (B) chemical structures of crosslinkers for studying the effect of linker length.

(A)

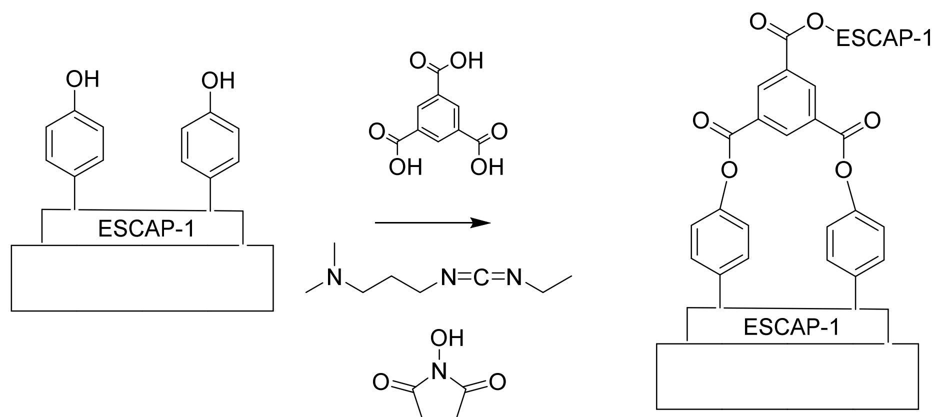

(B)

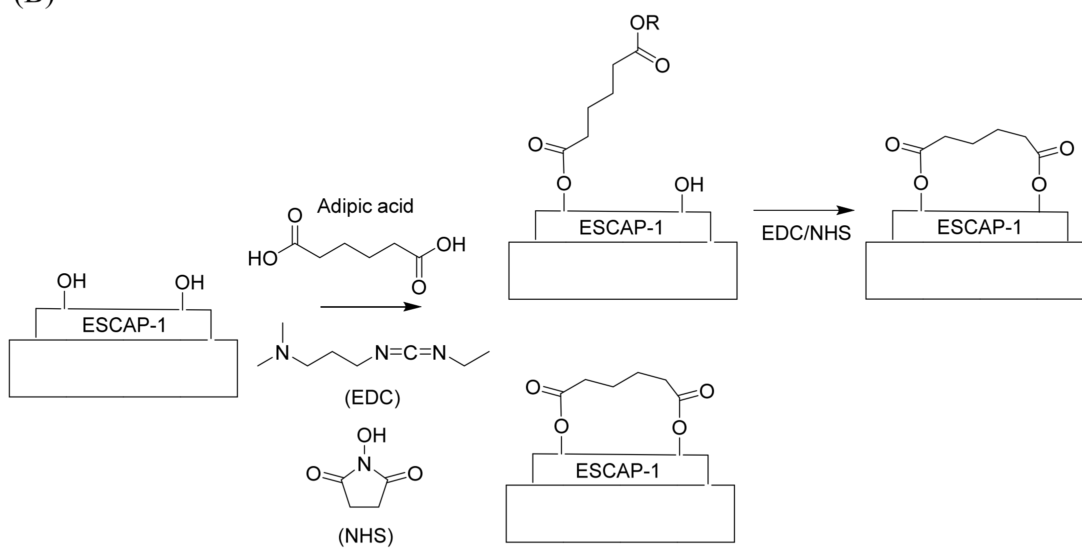

Figure 3.3 Schematic illustrations of reactive rinse processes: (A) one-step reactive rinse for the crosslinkers without solubility issue; (B) two-step reactive rinse for the crosslinkers with ester precipitates or the solubility limit at the first step solution.

3.3 Results and Discussions

ESCAP-1 photoresist is a terpolymer composed of hydroxystyrene, styrene, t-butyl methylmethacrylate with a molar ratio of 0.6:0.2:0.2. 60% molar ratio of hydroxystryrene provides most phenolic groups on the resist surface. Such amount of phenolic groups on ESCAP-1 polymer chain is capable of being used as reactive groups in conjunction with rinse additives to cross-link the surface of the patterns and films with functional carboxylic acids. The reactive rinse mechanism is shown in Figure 3.3. Carboxyl groups of acid linkers are activated with EDC in the presence of *N*-Hydroxysuccinimide (NHS) and form NHS esters. The NHS esters then can react with necleophiles, such as primary amine groups to form stable amide bonds[7],[8] or hydroxyl groups to form ester bonds[9]. In our case, the EDC reacts with a carboxyl to form an ureaester intermediate. In the presence of NHS, EDC can be used to convert carboxyl groups to amine-reactive NHS esters. The NHS esters then can attack the phenolic groups on the ESCAP-1 surface and form a crosslink structure. Among the crosslinkers we used in Figure 3.1, the precipitate occurred in 0.1M AA/EDC/NHS, and 0.1M TMA/EDC/NHS rinse solutions. The NMR spectra suggested that the precipitates in both solutions are di-NHS esters and multi-functional NHS esters. 0.2μm size of syringe filter was used to filter the NHS esters. Furthermore, the second step, 0.1 M EDC/NHS reactive rinse is necessary to activate the unreacted carboxyl groups of crosslinkers.

Poly(4-hydroxystyrene) (PHOST) films, 25 nm thick, were coated on gold substrates for increasing the grazing angle IR signal intensity. Figure 3.4 shows the grazing angle infrared spectra of the samples treated by PA control rinse and the samples treated by AA reactive rinse. A new peak is observed in region at 1730cm^{-1} corresponding to the carbonyl stretch. The peak at 1730cm^{-1} confirms the idea that acid groups are able to react with the hydroxyl functional groups and form ester covalent bonds on the resist surface using EDC/NHS chemistry.

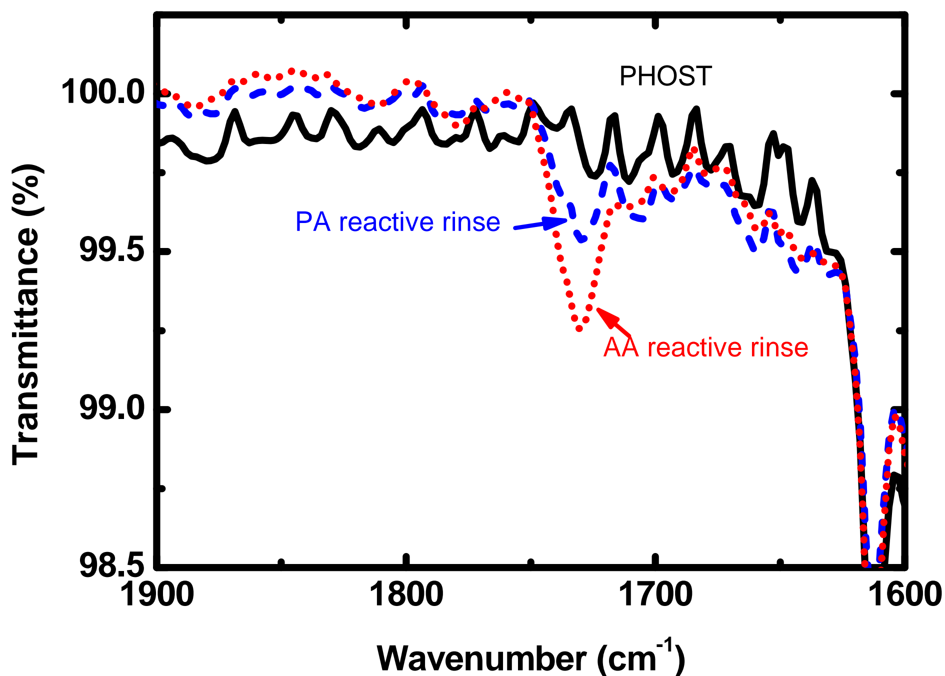

Figure 3.4 Grazing angle IR spectra of control PHOST film, PHOST film treated by PA control rinse, and PHOST film treated by AA reactive rinse.

EDC reacts with a carboxyl group on crosslinker, forming an amine-reactive O-acylisourea intermediate. However, the intermediate is also susceptible to hydrolysis, making it unstable and short-lived in aqueous solution. The addition of NHS stabilizes the amine-reactive intermediate by converting it to an amine-reactive NHS ester, thus increasing the efficiency of EDC-mediated coupling reactions[8, 10]. The amine-reactive NHS ester intermediate has sufficient stability to permit crosslinking procedures. But different acid structures result in different NHS ester intermediates, some of which are partially soluble in DI water and also some of diacid linkers only partially dissolved in DI water (i.e. AA, SuA, and SuA). So we removed the ester precipitate or un-dissolved solids with 0.2μm syringe filters to avoid particle contamination. Since the concentration of filtered reactive rinse solution is smaller than 0.1M crosslinker/EDC/NHS, the effect

of crosslinker concentration on the crosslink degree should be considered. Because surface crosslink has been demonstrated the improvement of mechanical properties[11,12], the increase of mechanical properties (i.e. modulus) is one method for us to determine the crosslink degree and investigate the effect of linker concentration on the surface crosslink reaction. Currently there are several methods available to measure the mechanical properties of polymer films, including indentation[13,14], beam curvature[15] and surface acoustic waves[16]. However, using these techniques to measure the mechanical properties of extra-thin polymer films is a challenge. so a custom-built strain stage was developed in order to probe the mechanical properties of thin films[17]. Figure 3.5 shows the effective moduli of polymer films rinsed by different PEG3 concentrations on the polymer surface. Film modulus increases from 1.09 GPa to ~3.54 GPa after 0.1M PEG3 reactive rinse. This indicates that the reactive rinse is able to crosslink the surface phenolic groups and enhances the film mechanical property. The effective moduli of polymer films rinsed with three various concentrations showed similar mechanical enhancement from EDC/NHS reaction. All solubilities of crosslinkers in DI water for this study are larger than 1mM (even for the filtered solutions) so the crosslinker concentration we used in this study has no strong effect on the surface crosslink reaction.

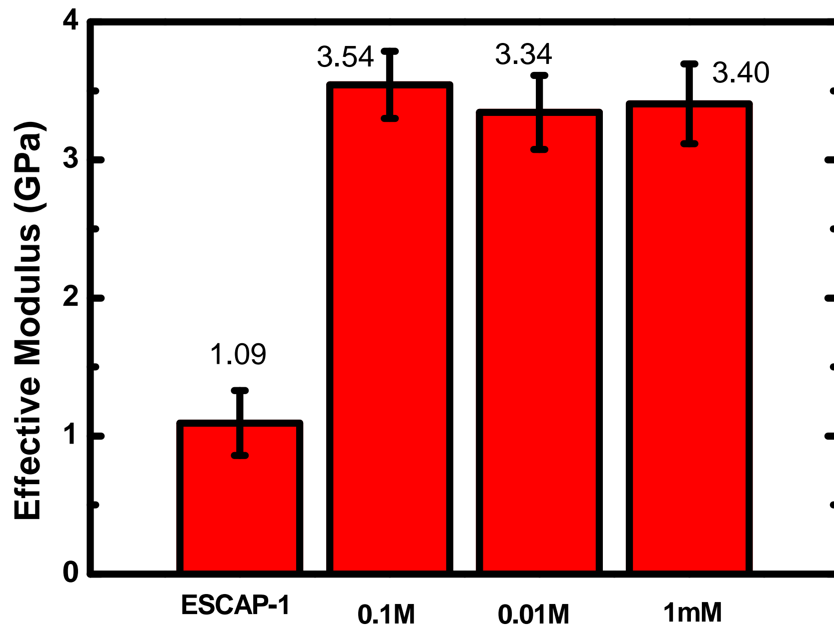

Figure 3.5 Effective moduli of ESCAP-1 films treated with PEG3 reactive rinse solution in various concentrations. Data are shown in 95% confidence and all film thicknesses are 24 nm.

Critical stress (σ_c) is defined as the maximum stress that can be applied to the photoresist lines prior to pattern collapse. The pattern used in this work was designed so that the S_1 space width decreased from left to right starting from 200 nm down to 10 nm for a constant line width W, shown in Figure 3.6. This pattern generates increasing stress in the pairs of resist lines as one moves across the pattern array and eventually a sufficiently small S_l value was reached in each array such that the stress applied to the resist exceeded the critical stress required for pattern bending and subsequently feature deformation and collapse occurred. Figure 3.6C is an example of SEM image of nominal 70 nm feature width line pair arrays for determining the position of critical stress. The numbers on the top of arrays are the space widths between two small parallel lines. The

space width increases from left to right so capillary stress increases from left to right as well. The last position (i.e. 90nm in this case) where pattern lines can stand for increasing capillary stress is defined as critical space (S_{1c}) and the capillary stress resulted in pattern collapse at critical position is regarded as critical stress (σ_c).

Figure 3.7 shows SEM images of nominal 70 nm line width for samples without reactive rinse treatment and for the samples which underwent TMA reactive rinse. The numbers on the top of arrays represent the nominal space widths (S_1) between two small parallel lines. The arrows in the figure indicate the critical space (S_{1c}) which is the position in the pattern array with the smallest spacing between adjacent lines where resist lines can withstand the largest capillary stress before collapse. SEM images of such which did not receive reactive rinse (see Figure 3.7A) showed that patterns collapsed at 130 nm space width (S_{1c}). SEM images of samples where the AA reactive rinse was applied showed patterned line pairs collapsed at 40nm space width (S_{1c}) (see Figure 3.7B). Smaller critical space represents the case where the resist lines could endure higher capillary force without collapse. The use of the TMA reactive rinse resulted in smaller critical space and enhanced pattern resistance to the capillary force relative to the samples without reactive rinse treatment.

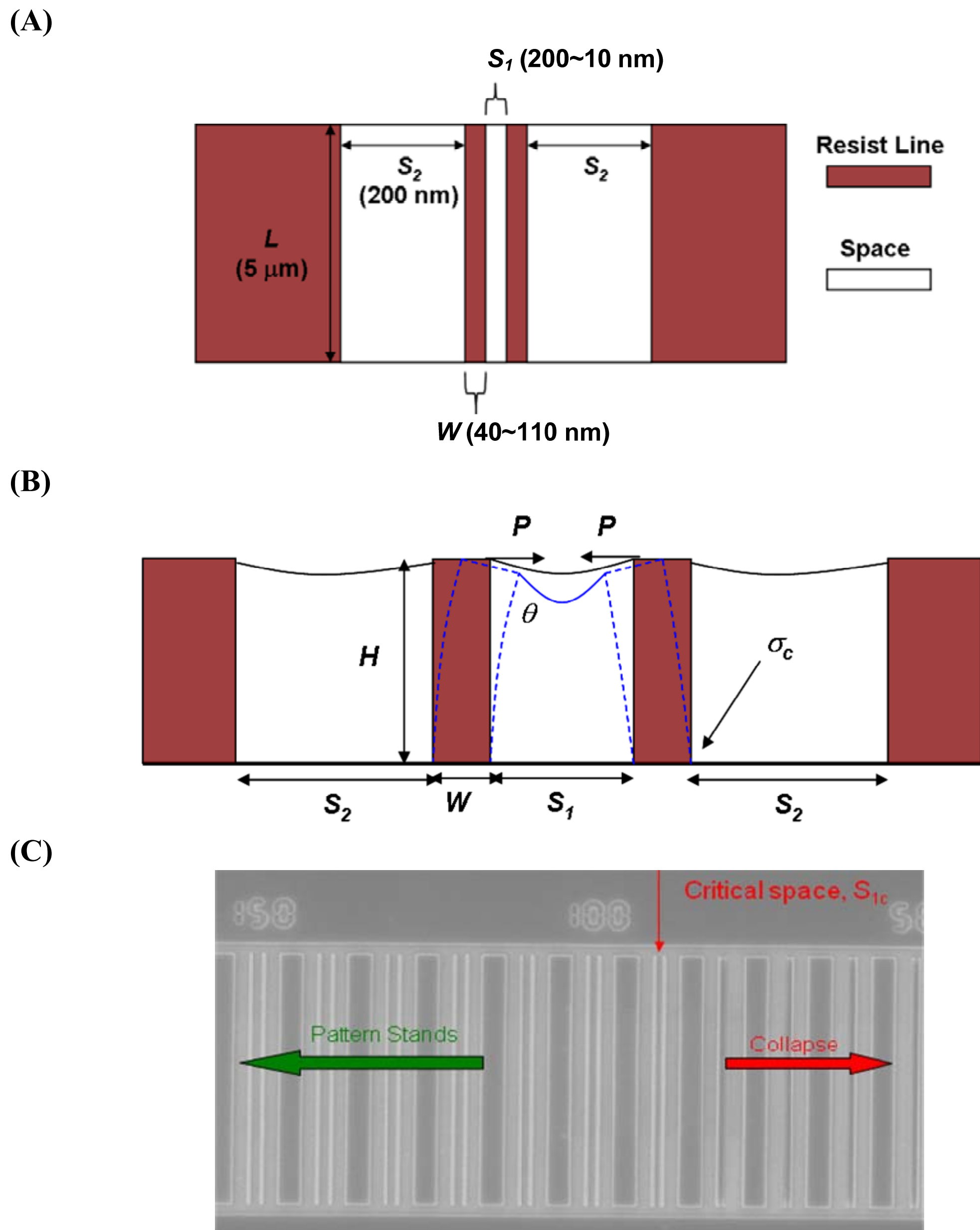

Figure 3.6 (A) Top view and (B) side view of pattern design used in this work for determining the critical stress at the point of pattern collapse; (C) An example for determining the critical position: SEM image of nominal 70 nm feature width line pair arrays used to identify the critical S_{1c} space.

(A)

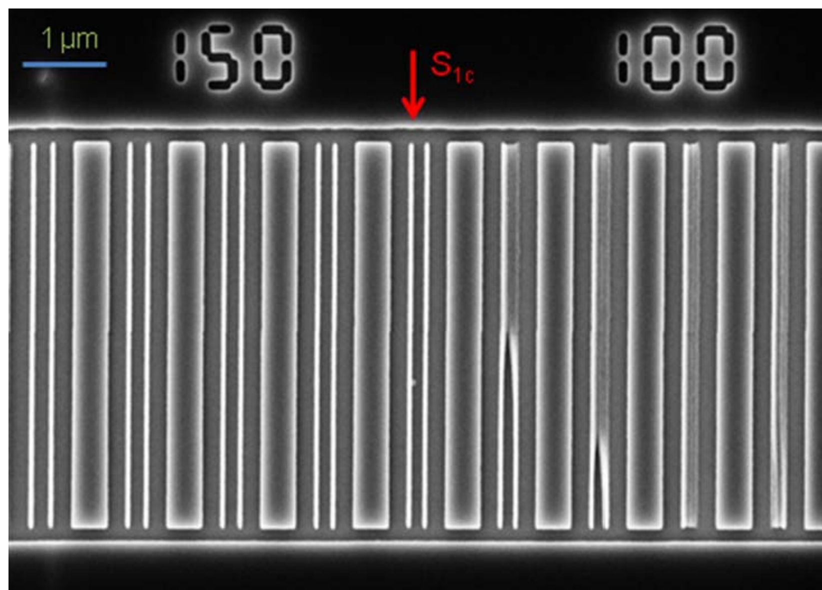

(B)

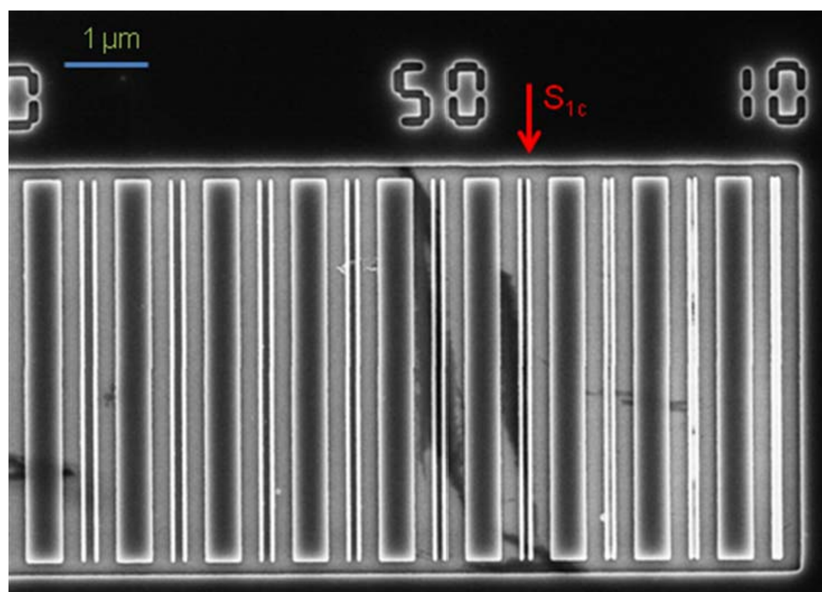

Figure 3.7 SEM images of nominal 70nm line widths on (A) the samples without reactive rinse, and (B) the samples with TMA reactive rinse. The numbers on the top of arrays represent the nominal S_1 space between two small lines. The arrows in the figure indicate the critical spaces (S_{1c}) which are the position in the pattern array with the smallest spacing between adjacent lines where resist lines can withstand the largest capillary stress before collapse.

Figure 3.8 shows the calculated critical stresses for the samples reactively rinsed with different acid crosslinkers. The critical stress (σ_c) is defined as the maximum stress that can be applied to the photoresist lines prior to pattern collapse and occurs in critical space, the smallest space position before the pair of resist lines collapse on the pattern structure we designed. The equation used to calculate the critical stress is expressed in equation (3.1), where γ is surface tension of rinse liquid (i.e. deionized water with γ=0.073 N/m), θ is the contact angle of the rinse liquid on the photoresist (i.e. deionized water with $\theta=77^{o}$ in ESCAP-1 case), height H is the thickness of the photoresist film, S_2 are the respective outside space widths between the lines of the pattern we designed, and S_{1c} is the critical pattern center space width where collapse is first indicated[5]. Line and space widths of the patterns were measured from SEM images using custom MATLAB software.

$$\sigma_c = 6\gamma \cos\theta \left(\frac{H}{W}\right)^2 \left(\frac{1}{S_{1c}} - \frac{1}{S_2}\right) \tag{3.1}$$

Critical stress is calculated at the final stress point before the resist lines collapses. It allows direct comparisons that are independent of pattern size and film thickness. The higher critical stress represents that resist lines have stronger resistance to the capillary stress. For the control samples which only underwent the process of AZ300MIF developer and DI water rinses (squares in Fig. 3.8), pattern lines displayed the lowest critical stress. For samples which received additional reactive rinses after development, their critical stresses are much higher than the control samples especially in the smaller feature width region. These results also confirm that the bifunctional and muti-functional acid units of the reactive rinse are able to form covalent crosslinks with phenolic groups of photoresists and increase the pattern resistance to the capillary stress. After PMA reactive rinse (blank stars), the pattern can withstand the highest capillary stress among these reactive rinse solutions. The contribution of TCA reactive rinse is about equivalent

to the AA rinse. The TMA and the BTCA rinses show similar values of critical stress. It may be because PMA with four carboxylic groups provides more active groups for EDC/NHS to form the ester intermediate to react with hydroxyl groups on ESCAP-1 resist. Therefore, the pattern treated with PMA reactive rinse solution shows the highest critical stress among these crosslinkers. However, the BTCA also has four carboxyl groups but the critical stress of the pattern treated with BTCA does not show better performance than crosslinkers with three functional groups such as TMA and TCA, even worse than TCA. It may be due to the intramolecular interaction and the molecular structure. For the crosslinkers with benzene core, adding more carboxylic functionality seems to help but hurt the ones for the alkyl chain. It may be because the alkyl chain is flexible and there may be some types of intramolecular hydrogen bonding which can occur and interfere with the crosslinking reaction. On the other hand, because the crosslinkers with benzene core are more rigid than alkyl chains, the intramolecular hydrogen bonding affects the crosslink reaction less. The critical stresses of patterns treated with BTCA and the TMA exhibit similar performance. It may be a trade off effect on the functionality and the core structure of crosslinkers. The TMA has fewer acid groups but a rigid core, and the BTCA has more acids but is flexible, which might actually be a bad combination. Furthermore, two important features of the critical stress data are the presentations of a plateau at larger feature width and transition in the critical stress occurring for feature width less than ~70 nm, with decreasing (control sample) or increasing modulus (samples with reactive rinses) at thinner feature widths. Previous literature on ultra-thin polymer films has suggested that the modulus of such films can be divided into a surface modulus, which has smaller modulus and is responsible for many of the abnormal interfacial/confinement trends observed with thin films, and a bulk modulus[10,18]. In the control case (solid square), without any reactive rinse treatment, for the larger feature width, the surface layer is only a small part of whole film. Therefore, the effect of soft surface layer on modulus is negligible and the effective modulus of the

pattern is independent of the film thickness and reaches a plateau. For the smaller feature width however, the ratio of the soft surface layer becomes comparable to the bulk layer, and strongly affects the overall properties of the film. The reduction of mechanical properties due to interfacial/confinement effect also impairs collapse resistance and results in the decrease of critical stress. In the reactive rinse cases, the critical stress increases with the decrease of feature width at the region of smaller feature width, showing the opposite trend to the control patterns. This increase of critical stress with decrease of feature width indicated that the reactive rinse treatment has a dramatic effect on the mechanical properties of pattern and increases the resistant to capillary stress because the crosslinked surface layer is a larger part of whole feature and dominates the mechanical properties of resist structures.

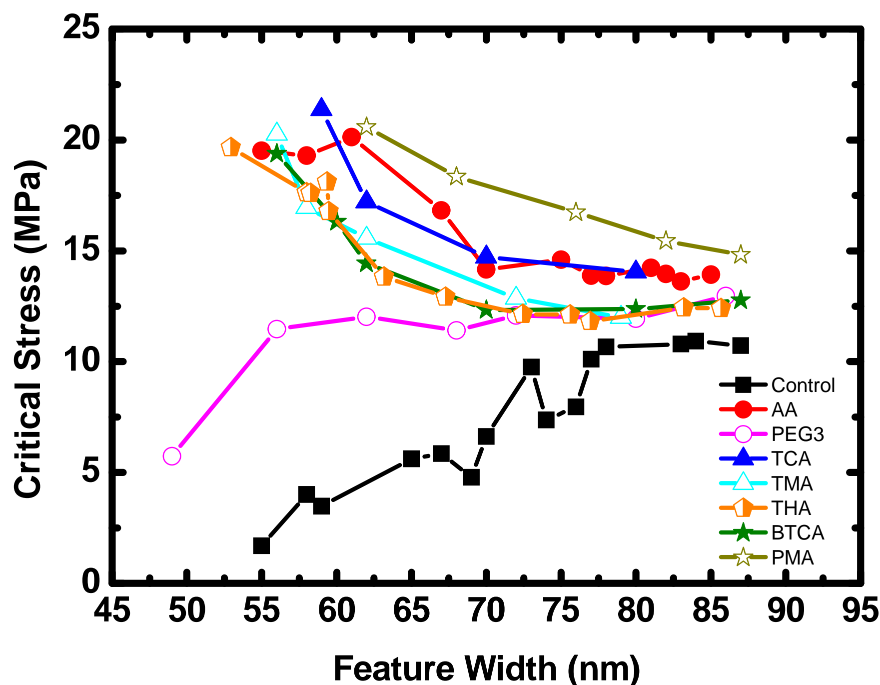

Figure 3.8 Critical stresses at the point of pattern collapse as a function of feature width in different rinse samples: ESCAP-1 control samples (solid squares); samples treated by AA reactive rinse (solid circles); samples treated by PEG3 reactive rinse (blank circles); samples treated by THA reactive rinse (half filled pentangles); samples treated by TCA reactive rinse (solid triangles); samples treated by TMA reactive rinse (blank triangles); samples treated by BTCA reactive rinse (solid stars); and samples treated by PMA reactive rinse (blank stars). All films are 252 nm thick.

The surface crosslink reaction may be not dependent on the functionality only but also on link length. Using the same procedure, rinse solutions with various chain lengths (listed in Fig. 3.2B) were applied in post-development step. The critical stresses of each pattern after reactive rinse were calculated and shown in Figure 3.9. PA reactive rinse samples showed the similar critical stress as the control sample which didn't apply reactive rinse and other acid linkers showed better critical stresses. These results also confirm the idea that the EDC/NHS reactive rinse forms a covalent crosslink with the phenolic groups on the surface of ESCAP-1 resist and improves pattern resistance to

capillary stress with enhancement of mechanical properties due to surface crosslink. Adipic acid samples (AA) and malonic acid (MA) samples showed the best performance, while sebacic acid (SeA) showed the worst. It indicated that the linker with longer chain length didn't provide significant benefit to the crssolink reaction because the linker with a longer chain may not match the distance between each -OH groups and provided less mechanical enhancement. AA and MA reactive rinse samples gave the higher critical stress. It may be because their linker lengths relatively match or close to the distance between each -OH groups on the surface and resulted in better mechanical benefit.

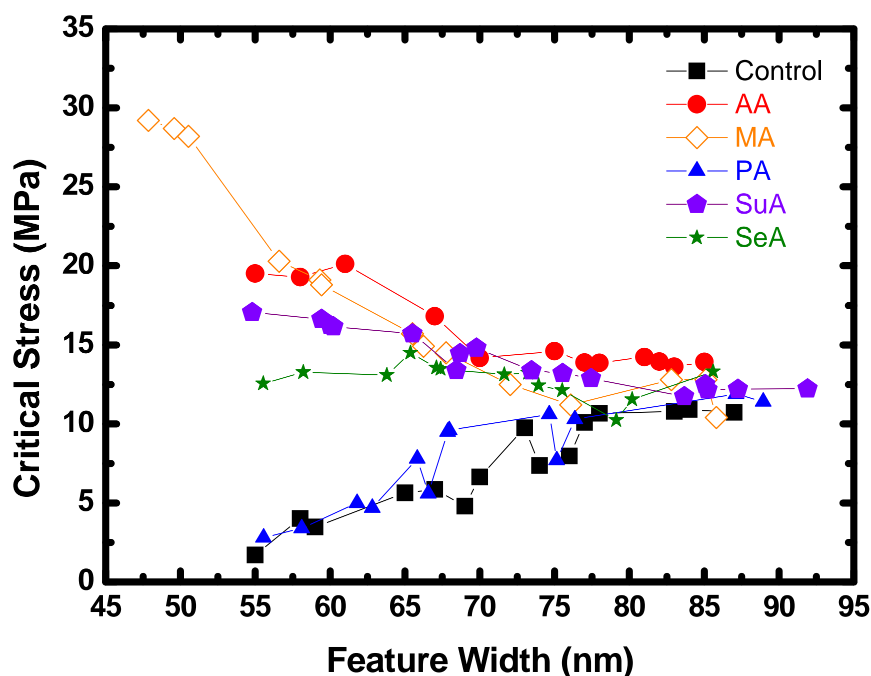

Figure 3.9 Critical stresses as a function of feature width in different samples: ESCAP-1 control samples (solid squares); samples treated by AA reactive rinse (solid circles); samples treated by MA reactive rinse (blank diamonds); samples treated by PA reactive rinse (solid triangles); samples treated by SuA reactive rinse (solid pentangles); and samples treated by SeA reactive rinse (blank stars). All films are 252 nm thick.

3.4 Conclusions

Pattern collapse occurs while the liquid is being dried off in the development process. To improve pattern collapse, we have developed a novel crosslinking strategy that is designed to covalently network the surface of phenolic-containing resins in the post-development step. Application of the reactive rinse showed an overall improvement in printing capabilities relative to samples where the rinse was not applied. Treatment with the rinse provided photoresist lines which could withstand higher stresses (which corresponds to lower S_1 space widths) when compared to their non-treated counterparts. The influence of crosslinkers with various functionalities and the crosslinker structures

on the observed critical stress was also discussed. It was shown that the patterns treated with multifunctional crosslinker with rigid core resulted in higher critical stress. The linker length is also another important factor on pattern performance. However increasing the linker chain didn't provide significant benefit to pattern performance. The linker length may have to match the distance between each functional groups of the resist surface to achieve the better surface crosslink reaction and mitigate the pattern collapse issue.

3.5 References

1. Huang, V.; Chiu, C. C.; Lin, C. A.; Chang, C. Y.; Gau, T. S.; Lin, B. J., Effect of novel rinsing material and surfactant treatment on the resist pattern performance. *Proc. SPIE* **2007,** *6519*, 65193C-9.

2. Drechsler, A.; Petong, N.; Bellmann, C.; Synytska, A.; Busch, P.; Stamm, M.; Grundke, K.; Wunnicke, O., Adsorption of cationic surfactants onto photoresist surfaces - A way to reduce pattern collapse in high aspect ratio patterning. *Can J Chem Eng* **2006,** *84* (1), 3-9.

3. Zhang, P.; Rao, M. B.; Jaramillo, J. M.; Horvath, B. t.; Ross, B.; Paxton, T.; Davis, T.; Cook, P. t.; Witko, D., Pattern collapse and line width roughness reduction by surface conditioner solutions for 248-nm lithography. *Proc. SPIE* **2005,** *5753*, 252-260.

4. Chai, J. J.; Zhang, X. G.; Huang, J.; Tan, X.; Dai, G. L., Microscopic model of nano-scale particles removal in high pressure CO(2)-based solvents. *J Supercrit Fluid* **2009,** *49* (2), 182-188.

5. Yeh, W. M.; Noga, D. E.; Lawson, R. A.; Tolbert, L. M.; Henderson, C. L., Comparison of positive tone versus negative tone resist pattern collapse bahavior. *J Vac Sci Technol B* **2010,** *28* (6), C6s6-C6s11.

6. Lee, C.-T.; Wang, M.; Jarnagin, N. D.; Gonsalves, K. E.; Roberts, J. M.; Yueh, W.; Henderson, C. L., Photosensitivity and line-edge roughness of novel polymer-bound PAG photoresists. *Proc. SPIE* **2007,** *6519*, 65191E-9.

7. Powell, H. M.; Boyce, S. T., EDC cross-linking improves skin substitute strength and stability. *Biomaterials* **2006,** *27* (34), 5821-5827.

8. Updegrove, T. B.; Correia, J. J.; Chen, Y. F.; Terry, C.; Wartell, R. M., The stoichiometry of the Escherichia coli Hfq protein bound to RNA. *Rna* **2011,** *17* (3), 489-500.

9. Everaerts, F.; Torrianni, M.; Hendriks, M.; Feijen, J., Biomechanical properties of carbodiimide crosslinked collagen: Influence of the formation of ester crosslinks. *J Biomed Mater Res A* **2008,** *85A* (2), 547-555.

10. Naue, N.; Fedorov, R.; Pich, A.; Manstein, D. J.; Curth, U., Site-directed mutagenesis of the chi subunit of DNA polymerase III and single-stranded DNA-binding protein of E-coli reveals key residues for their interaction. *Nucleic Acids Res* **2011,** *39* (4), 1398-1407.

11. Zhou, J.; Ma, Y. H.; Zhang, J.; Tong, J., Influence of Surface Photocrosslinking on Properties of Thermoplastic Starch Sheets. *Journal of Applied Polymer Science* **2009,** *112* (1), 99-106.

12. Marques, P. T.; Lima, A. M. F.; Blanco, G.; Laurindo, J. B.; Borsali, R.; Le Meins, J. F.; Soldi, V., Thermal properties and stability of cassava starch films cross-linked with tetraethylene glycol diacrylate. *Polymer Degradation and Stability* **2006,** *91* (4), 726-732.

13. VanLandingham, M. R.; Villarrubia, J. S.; Guthrie, W. F.; Meyers, G. F., Nanoindentation of polymers: An overview. *Macromol Symp* **2001,** *167*, 15-43.

14. Moy, C. K. S.; Bocciarelli, M.; Ringer, S. P.; Ranzi, G., Identification of the material properties of Al 2024 alloy by means of inverse analysis and indentation tests. *Mat Sci Eng a-Struct* **2011,** *529*, 119-130.

15. Zhao, J. H.; Kiene, M.; Hu, C.; Ho, P. S., Thermal stress and glass transition of ultrathin polystyrene films. *Appl Phys Lett* **2000,** *77* (18), 2843-2845.

16. Every, A. G., Measurement of the near-surface elastic properties of solids and thin supported films. *Meas Sci Technol* **2002,** *13* (5), R21-R39.

17. Yeh, W.-M.; Noga, D. E.; Lawson, R. A.; Tolbert, L. M.; Henderson, C. L., Thin film buckling as a method to explore the effect of reactive rinse treatments on the mechanical properties of resist thin films. *Proc. SPIE* **2010,** *7639*, 76391I-6.

18. Chung, J. Y.; Nolte, A. J.; Stafford, C. M., Surface Wrinkling: A Versatile Platform for Measuring Thin-Film Properties. *Adv Mater* **2011,** *23* (3), 349-368.

CHAPTER 4

DEVELOPMENT OF REACTIVE RINSES FOR CARBOXYLIC ACID FUNCTIONALIZED RESIST POLYMERS BASED ON POLYAMINE CROSSLINKERS AND EDC-NHS COUPLING

Pattern collapse is one of the important problems in the semiconductor industry. One of the primary modes of pattern collapse at small feature sizes is pattern bending or deforming due to weak mechanical restoring force of the resist features. The main forces which govern such pattern deformation are related to mechanical properties of the resist. Instead of synthesizing and changing the chemical formula of the resist, the quick way for achieving the mechanical enhancement is to crosslink the resist surface using surface reactive rinse via carbodiimide chemistry. Amine reactive rinse solution was applied on resist patterns to crosslink carboxylic acid groups on resist surface in post-development process. Pattern collapse test structures were fabricated and analyzed to quantify the impact of the use of amine reactive rinse treatment. XPS spectra, SEM images, and critical stress analysis of the resulting patterns confirmed that the use of reactive rinse can significantly enhance the mechanical properties of the resist and dramatically mitigate pattern collapse.

4.1 Introduction

As the semiconductor industry continues to push to smaller critical dimensions, pattern collapse caused by unbalanced capillary forces during the final rinse and drying process has become an important problem that can practically limit the resolution of a resist material long before its intrinsic resolution limit is reached. Typically the mode of

pattern deformation is categorized into two major failures: adhesion failure at the resist-substrate interface[1] and mechanical elastoplastic deformation[2]. Much of the previous work on the adhesion strength at the resist and substrate interface has involved the use of an underlayer[3,4] or a bottom anti-reflective coating (BARC)[5,6] which often have the added benefit of increasing the resist adhesion in addition to their primary benefits such as reflectivity control[6]. The common method for improving resist adhesion in industry is to apply hexamethyldisilazane (HMDS)[7] on the substrate to match the interfacial surface energy. In addition, the use of silane adhesion promoter has also reported to improve the interaction of resist and substrate using strong covalent bonding between photoresist and silicon substrate instead of matching the surface energies[8].

Most research groups focused on increasing the adhesion strength to improve pattern collapse issue but pay less attention on another mode of pattern collapse, elastoplastic deformation caused by the weak mechanical strength of the resist which couldn't support the increasing capillary stress. One approach to mitigating this type of collapse problem is to design a new resist composition by introducing benzyl or alicyclic groups that are robust enough to support capillary stress. However, such modification of resist physical properties for pattern collapse purposes is complicated and difficult to achieve through modified formula of the resist itself due to the complex set of requirements that a resist must satisfy and the complex set of physical and chemical phenomena that underlie the imaging processing itself. As a simple solution to this requirement, we have developed an alternative strategy of improving the resist mechanical properties after features are developed in the film but before they are dried and are subjected to significant capillary forces. In this chapter, the use of diamine to efficiently crosslink the surface of resist containing carboxylic acid groups through the formation of amide bonds using carbodiimide chemistry[9,10] has been explored. One advantage of this approach is that it is an aqueous process that is easily compatible with high volume, track-based lithographic processes. The total rinse process can complete in

2 minutes and is well-suited in the continuous lithography process. X-ray photoelectron spectroscopy (XPS) was used to characterize the surface crosslinking reaction after surface rinse treatment. Application of such amine reactive rinses was found to clearly result in an improvement in the resistance of the resists to pattern collapse as observed by SEM. A comparison of the critical stress at the point of pattern collapse as a function of resist feature size also clearly shows a significant improvement in mechanical resilience of resist samples processed with the reactive rinse treatment.

4.2 Experimental

Materials The model photoresist resin (DUP-A02, see Figure 4.1) used in this work was supplied by Intel. A model chemically amplified photoresist was formulated by combining the DUP-A02 resin, triphenylsulfonium nonaflate (TPS-Nf) photoacid generator (PAG), and a trioctylamine (TOA) base quencher, in cyclohexanone at loadings of 8 wt% total solids in cyclohexanone with 5 wt% TPS-Nf relative to A02 and 10 mol% of TOA relative to the TPS-Nf PAG. The developer, AZ300MIF, was supplied by AZ Electronic Materials Company. All other reagents used in this study were purchased from Sigma-Aldrich, VWR, Advanced ChemTech, or Alfa-Aesar.

Substrate Preparation Silicon nitride windowed (Si_xN_y) substrates were used as substrates for high-resolution electron beam imaging of resist materials. The preparation of Si_xN_y substrates have been described in our previous work[11]. The Si_xN_y windowed substrates is designed to eliminate electron backscattering from the substrate and thus produce extremely sharp aerial images and essentially vertical sidewalls in the final resist patterns. Si_xN_y substrates were primed with 1,1,3,3,3-hexamethyl-disilazane (HMDS) vapor at 70 torr and 110°C to enhance the adhesion strength of resist patterns before the resist was coated.

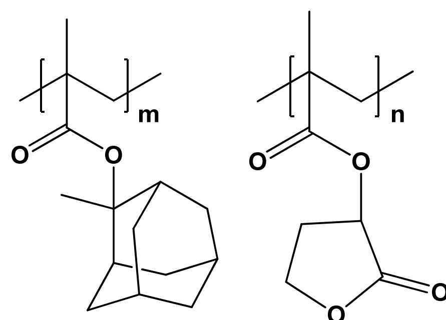

DUP-A02 (m:58, n:42)

Figure 4.1 Chemical structure of DUP-A02 photoresist we used in this work.

Amino Reactive Rinse Process *N*-Ethyl-*N′*-(3-dimethylaminopropyl) carbodiimide hydrochloride (EDC) and N-hydroxysuccinimide (NHS) was prepared for 0.1 M in deionized water (EDC/NHS). The resist processing consisted of spin coating the resist films at various spin speeds for 60 seconds to obtain films of varying thickness. The control films were then soft-baked (110 °C, 2 min), exposed and patterned via e-beam, post-exposure baked (110 °C, 1 min), developed (AZ300MIF, 30 sec), rinse by deionized water for 30 sec and finally dried with nitrogen stream. E-beam lithography was carried out using a JEOL JBX-9300FS e-beam lithography system with an accelerating voltage of 100 kV, a beam diameter of 8 nm, a 2 nA current, and a 10 nm shot pitch. The samples which underwent the reactive rinse were taken through the same procedure up through the development step. After the development step, the samples were placed in a 0.1 M solution of EDC/NHS solution for 1 minute, and then in 0.1 M 1,6-Hexanediamine (HA) aqueous solution for 1 minute. After two step rinses, the samples were then rinsed with deionized water for 30 seconds and dried with a stream of nitrogen in a manner identical to the control samples. Thermo K-Alpha X-ray Photoelectron Spectroscopy (XPS) with the source of Al Kα micro-focused monochromator at the pressure of 10^{-9} mbar was used

to characterize the reactive surface reaction. A value of 285 eV for the binding energy of the C_{1s} component was used to correct for charging under irradiation.

Pattern Performance Analysis An e-beam lithography pattern with a series of varying line and space widths was specifically designed in order to quantitatively study pattern collapse[12] as shown in Fig. 4.2. With our particular pattern design, as the S_1 spacewidth decreased from left to right starting from 200 nm down to 10 nm in the images shown for a set of lines with a constant line width W, pattern collapse would occur when a sufficiently small S_1 value was reached such that the stress applied to the resist exceeded the critical stress required for pattern bending and deformation as shown in Figure 4.2C. The critical space in the test patterns, S_{1c} is determined by identifying the point in each test structure array where the smallest S_1 is observed between a pair of adjacent lines in the test structure that exhibited no sign of collapse or deformation. Critical space (S_{1c}) and line widths (W) were measured precisely from high resolution SEM images using custom written MATLAB software designed for high resolution SEM feature analysis. Smaller critical S_1 space represents higher capillary stress and better pattern performance in our test arrays. The patterns we designed allowed us to qualitatively and quantitatively study pattern collapse and obtain consistent, reproducible results.

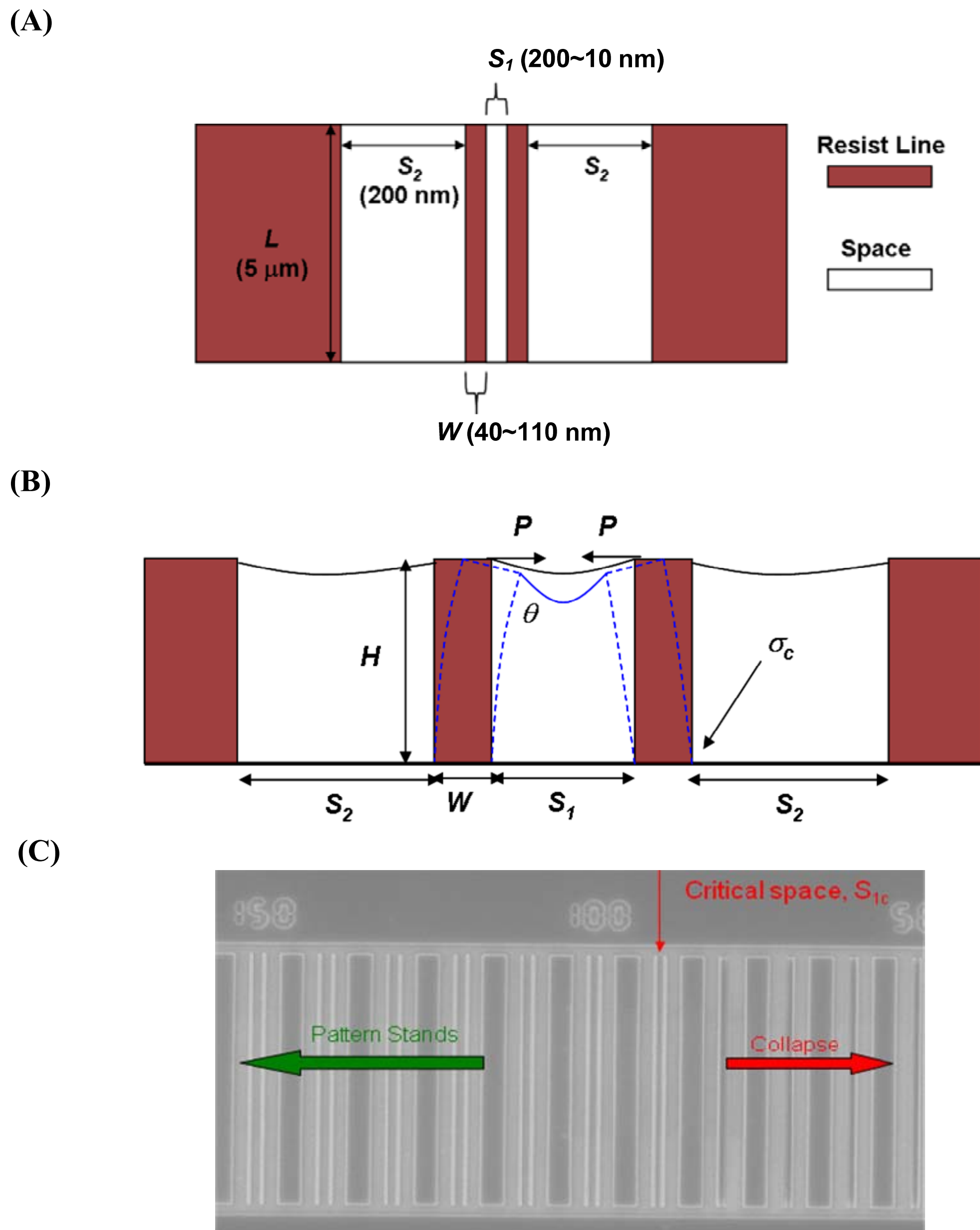

Figure 4.2 (A) Top view and (B) side view of pattern design used in this work for determining the critical stress at the point of pattern collapse; (C) An example for determining the position of critical stress: SEM image of nominal 70 nm feature width line pair arrays used to identify the critical S_{1c} space. The number on the top of array represents the space between two small lines (S_1).

4.3 Results and Discussion

A surface that mimics the condition of resist wall after development was made to study the amino reactive rinse process. Figure 4.3 shows the process for making the surface which mimics the condition of resist wall. Unformulated DUP-A02 resist in cyclohexanone solution was spin-coated on the silicon substrate and baked at 110 °C for 1 min. 3wt% TPS-Nf in isopropyl alcohol (IPA) solution was directly casted on the unformulated DUP-A02 resist film and exposed by DUV at 10 mJ/cm^2. After AZ 300MIF development, resist film was deprotected and formed the carboxylic groups on the top of unformulated A02 resist.

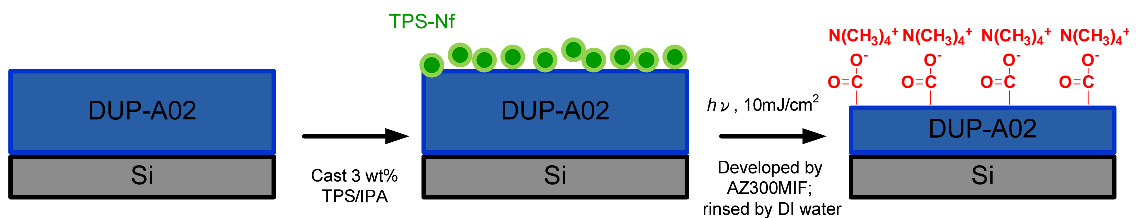

Figure 4.3 Schematic illustration of the process for making pedant COOR groups on the resist surface.

After this simple-cast method process, the resist films were characterized by the ellipsometer and water contact angle, and atomic force microscope (AFM), shown in Fig. 4.4. The plots in Fig. 4.4 show the normalized thickness and water contact angle as a function of DUV exposure doses. After the simple-cast process, the film thickness of DUP-A02 resist decreased and water contact angle of resist surface also dropped significantly. The decrease of film thickness and the formation of hydrophilic surface suggested that the top of DUP-A02 resist surface was partially developed and hydrophilic carboxylic surface was formed using our simple-cast method. Figure 4.4(B) and (C) are the 5μm by 5μm AFM images for DUP-A02 resist surfaces before simple-cast process

and for the DUP-A02 surface after 10 min DUV exposure and development, respectively. The root-mean-square (RMS) roughness of untreated DUP-A02 resist is 0.36 nm. After 10min exposure and AZ300 development, surface RMS increased by a factor of four in comparison to non-treated resist surface. RMS values also confirmed that the pedant COOR surface (referred to here as A02-COOR, R is $-N(CH_3)_4^+$ after AZ300MIF developer) was created using the simple-cast method. This mimic A02-COOR surface could be used for the study the impact of amine reactive rinse on the resist surface.

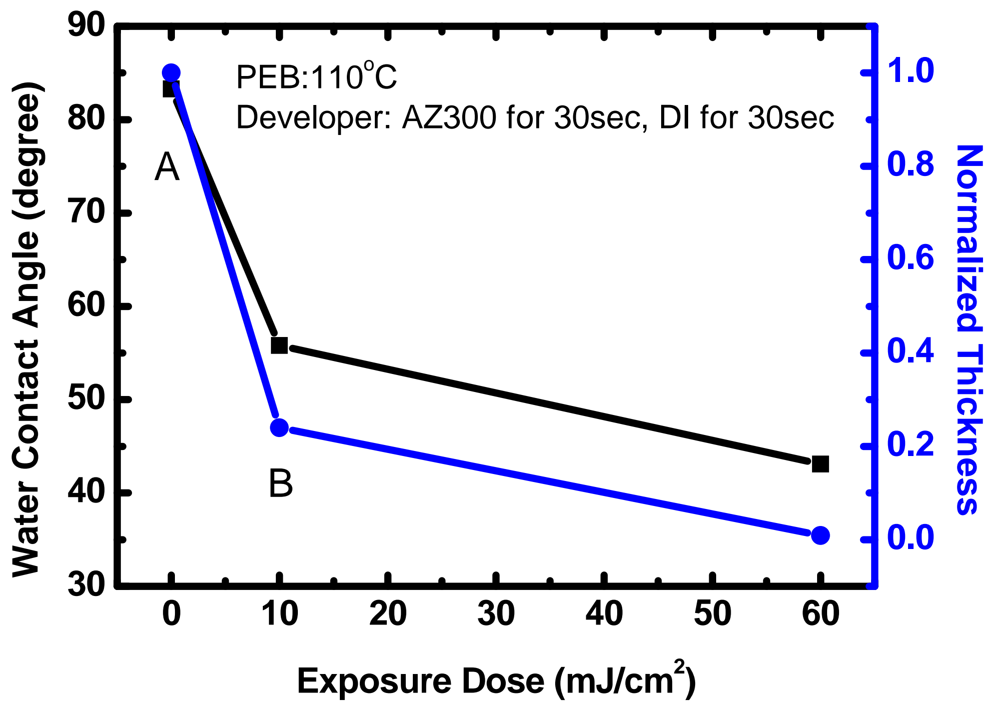

(A) (B)

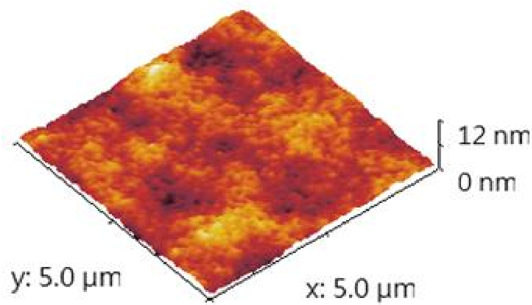

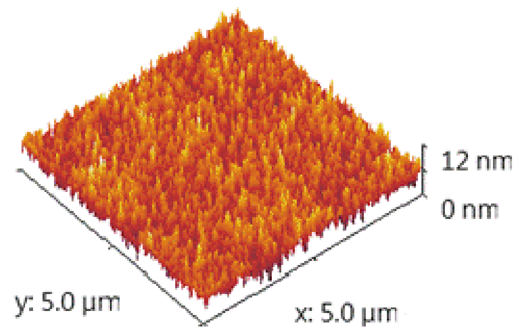

Figure 4.4 Resist surface conditions as a function of exposure dose. All samples were developed by AZ300MIF and rinsed by DI water. Solid squares on the top plot represent the water contact angle. Circles on the top plot represent the normalized thickness. (A) AFM image of unformulated DUP-A02 resist surface before exposure; (B) AFM image of resist surface exposed by 10 mJ/cm^2.

During deprotection reaction, adamantly groups in DUP-A02 photoresist were cleaved with photochemically-generated acid to form the carboxylic groups after development. Such carboxylic groups on the resist surface are capable of being used as reactive groups in conjunction with rinse additives to cross-link the surface of the patterns and films with functional amines. The schematic process of amino reactive rinse is shown in Fig. 4.5. After development process, carboxylic groups were generated on the resist wall. Carboxylic groups on the resist wall were then activated with EDC in the presence of *N*-Hydroxysuccinimide (NHS) and formed NHS esters. The NHS esters then easily reacted with nucleophiles, such as primary amine groups to form stable amide bonds. After the surface was activated by EDC/NHS, 1,6-hexanediamine (HA) with two reactive functional amine groups was applied as a crosslinker to covalently bind the carboxylic groups on the resist surface and enhance the resist mechanical properties.

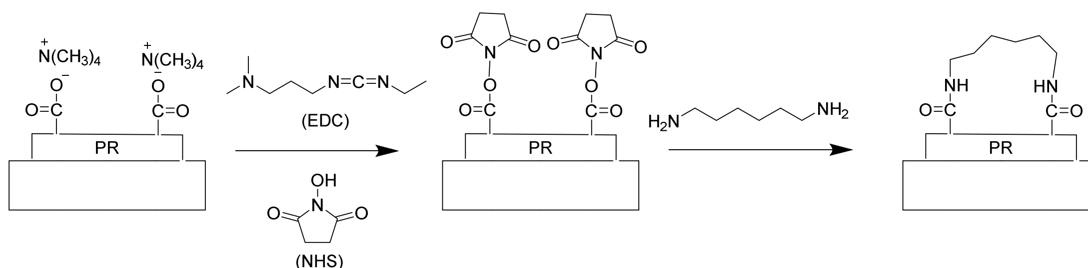

Figure 4.5 Schematic illustration of amine reactive rinse process.

Since DUP-A02 resist doesn't contain nitrogen elements, XPS tool can be used to detect the amine reactive rinse reaction based on the present nitrogen signal. Figure 4.6 shows the XPS survey spectra for A02-COOR resist surface made by simple-cast method and A02-COOR surface treated by amine reactive rinse. No nitrogen could be detected in the A02-COOR resist surface before amine reactive rinse. After 1,6-hexanediamine reactive rinse treatment, nitrogen peak could be found at 400 eV, shown in the top

spectrum in Figure 4.6. This indicated that di-amine is able to react with carboxylic groups on A02-COOR resist surface using carbodiimide chemistry.

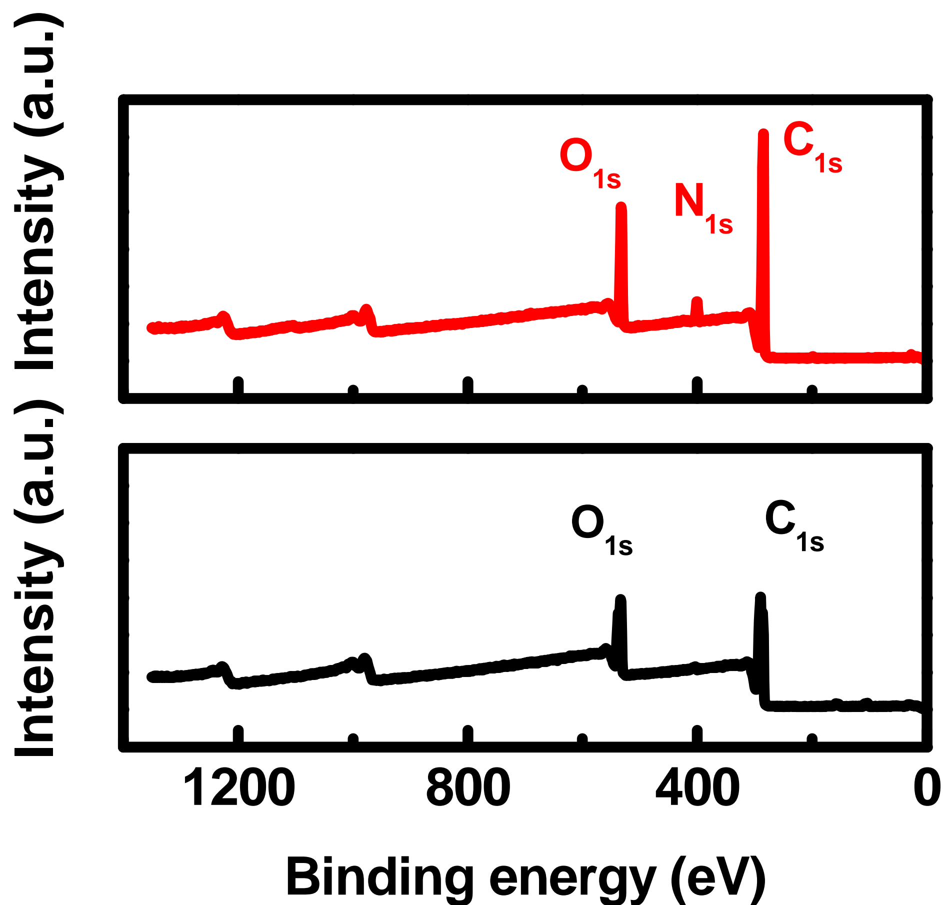

Figure 4.6 XPS survey spectra of the A02-COOR film (bottom) and A02-COOR film treated by amine reactive rinse (top).

An e-beam lithography pattern with a series of varying line and space widths was specifically designed in order to quantitatively study pattern collapse[12]. The pattern structure used in this work was designed so that the spacing (S) between two small parallel lines decreased from left to right starting from 200 nm down to 10 nm for a

constant line width (W). This pattern generates increasing stress in the pairs of resist lines as one moves across the pattern array and eventually a sufficiently small space value (critical space, S_{1c}) was reached in each array such that the stress applied to the resist exceeded the critical stress (σ_c) required for pattern bending and subsequently feature deformation and collapse occurred. Smaller spacing results in higher capillary stress on the pair of resist lines.

Figure 4.7 shows SEM images of resist samples which did not recieve amine reactive rinse and the samples treated by additional amine reactive rinse. The numbers on the top of the array structure represent the spaces between two small lines. The numbers on the left of array structure depict the width of small lines. The arrows in the figure indicate the critical spaces (S_{1c}) which are the position in the pattern array with the smallest spacing between small lines where resist lines can withstand the largest capillary stress before collapse. SEM images of such which did not receive amine reactive rinse (see Fig. 4.7A) showed that all patterns collapsed from 200 nm space S_1 to 10 nm space S_1 in the nominal 70 nm and 80 nm line widths. SEM images of samples where the amine reactive rinse was applied showed patterned line pairs collapsed at nominal 120 nm space S_1 (S_{1c}) in the nominal 70 nm line width and collapsed at 110 nm space S_1 (S_{1c}) in the 80 nm line width (see Fig. 4.7B). Smaller critical spaces represent the cases where the resist lines could endure higher capillary force without collapsing. SEM images showed that the use of the amine reactive rinse results in smaller critical space and enhanced pattern resistance to the capillary force compared to the samples without reactive rinse treatment.

(A)

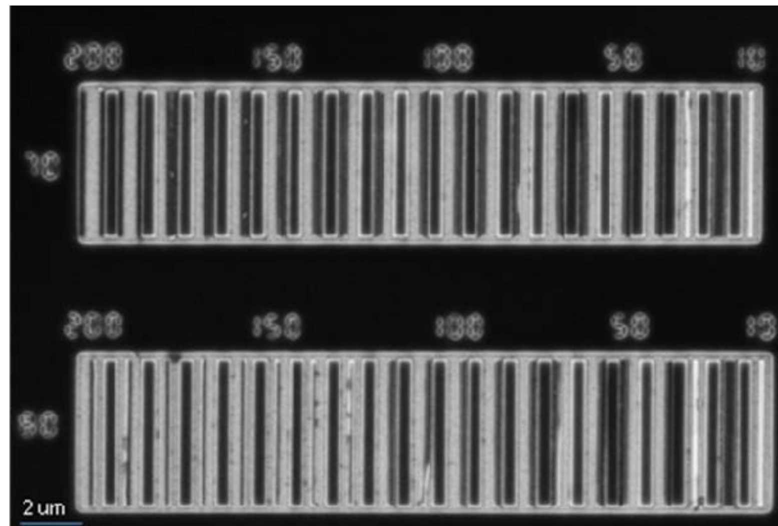

(B)

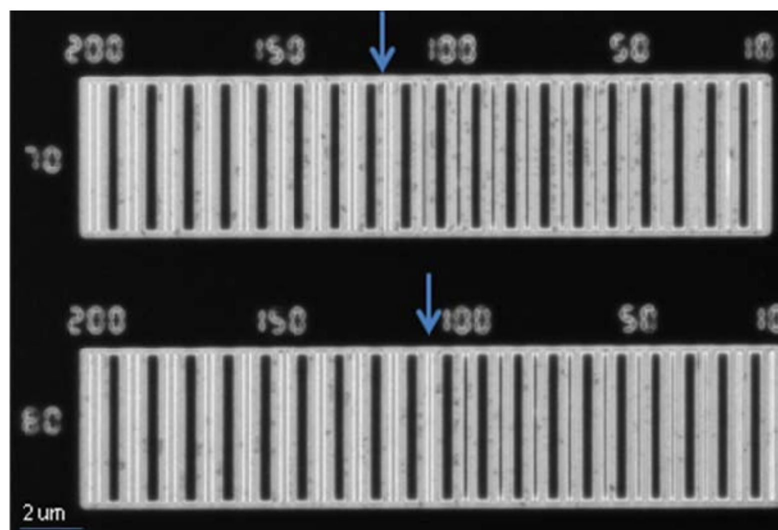

Figure 4.7 SEM images of nominal 70 nm and 80 nm line widths on (A) pattern sample which did not receive amine reactive rinse, and (B) pattern sample treated by amine reactive rinse. The numbers on the left of arrays represent the nominal widths of all small parallel lines. The numbers on the top of the arrays represent the nominal S_1 space widths between two small lines. The arrows in the figure indicate the critical spaces (S_{1c}) which are the position in the pattern array with the smallest spacing between two small lines where resist lines can withstand the largest capillary stress before collapse.

The critical stress (σ_c) is defined as the maximum stress that can be applied to the photoresist lines prior to pattern collapse and occurs in critical space, the last space before the pair of resist lines collapse on the pattern structure we designed. The equation used to calculate the critical stress is expressed in equation (4.1), where γ is surface tension of rinse liquid (i.e. deionized water with γ =0.073 N/m), θ is the contact angle of the rinse liquid on the photoresist (i.e. deionized water with θ=83° in DUP-A02 case), height H is the thickness of the photoresist film, S_2 are the respective outside space widths between the lines of the pattern we designed shown in Fig. 4.2, and S_{1c} is the critical pattern center space width where collapse is first indicated[12]. Critical stress analysis is allowed us to quantify the pattern performance and provide a reliable method to study the pattern collapse.

$$\sigma_C = 6\gamma\cos\theta\left(\frac{H}{W}\right)^2\left(\frac{1}{S_{1c}}-\frac{1}{S_2}\right) \tag{4.1}$$

Critical stresses were calculated in Fig. 4.8A and their chemical structures were also shown in Fig. 4.8B. The effects of the functionality and different type crosslinkers on the pattern performance were also discussed. 1,6-hexanediol and T-403 triamine were also applied on the test array we designed to discuss the impact of different type crosslinkers. The higher critical stress represents that resist lines have stronger resistance to the capillary stress and exhibit better performance. Resist samples which did not receive reactive rinse (squares in Fig. 4.8) have pattern lines with lowest critical stress. 1,6-hexanediol (circles in Fig. 4.8) and 1,6-hexanediamine (triangles in Fig. 4.8) treated samples showed similar critical stress values, but the 1,6-hexanediamine sample has slightly higher critical stress because the amine has stronger affinity to such carbodiimide reaction than alcohol. It is also seen that T-403 samples with three amine active groups showed highest critical stress among these crosslinkers. This result may be because three active groups provide more chance to react with surface carboxylic groups and result in

better mechanical improvement on the resist features than two functional crosslinkers, diol and diamine. These results also confirmed the idea of carboiimide reactive rinse that di-amine, diol, and tri-amine type crosslinkers are presumed to form covalent crosslink with the carboxylic groups on the surface of DUP-A02 resist after development, and improve the pattern resistance to capillary stress with the enhancement of mechanical properties due to surface crosslink.

Two prominent features were also observed in Fig. 4.8A. The first prominent feature is that transition in critical stress occurs for feature widths less than ~90 nm with decreasing (control DUP-A02 samples) or increasing (reactive rinse samples) for small feature width region. The second prominent feature of these data is the presence of a plateau in the critical stress of 1.5 MPa at ~90 nm feature width. Critical stress behavior is highly correlated to the mechanical properties of resist structures and several previous literatures on ultra-thin polymer films have suggested that the effective modulus of such films can be divided into two modulus combinations: robust bulk layer modulus, and surface layer modulus which has smaller modulus, and is responsible for many of the abnormal interfacial/confinement trends observed with thin films, and a bulk modulus[13,14]. The effective mechanical properties of the polymer film are the combination of soft surface layer and robust bulk layer. For the larger feature widths, the soft surface layer only plays a small part of whole film so the effect of soft surface layer on modulus is negligible. Because robust bulk layer is dominated the resist properties, the impact of surface crosslink doesn't provide significant improvement on the effective modulus and results in the similar critical stress at the region of larger feature width. For the smaller feature width region, the ratio of the soft surface layer becomes comparable to the bulk layer, and strongly affects the overall properties of the film[14]. Therefore, in the smaller feature width region, the effective modulus is dependent on the resist feature width and decreases with the decrease of the feature width, which was observed in the control DUP-A02 resist sample (squares in Fig. 4.8A). The reactive rinse was applied to crosslink the

pattern surface and also enhanced the mechanical properties of the surface layer, resulting in significant improvement on critical stress on the small feature region. This result also suggests that the effective modulus is very sensitive to the dimension of feature size, and reactive rinse treatment is suitable for improving the mechanical properties for the smaller features.

(A)

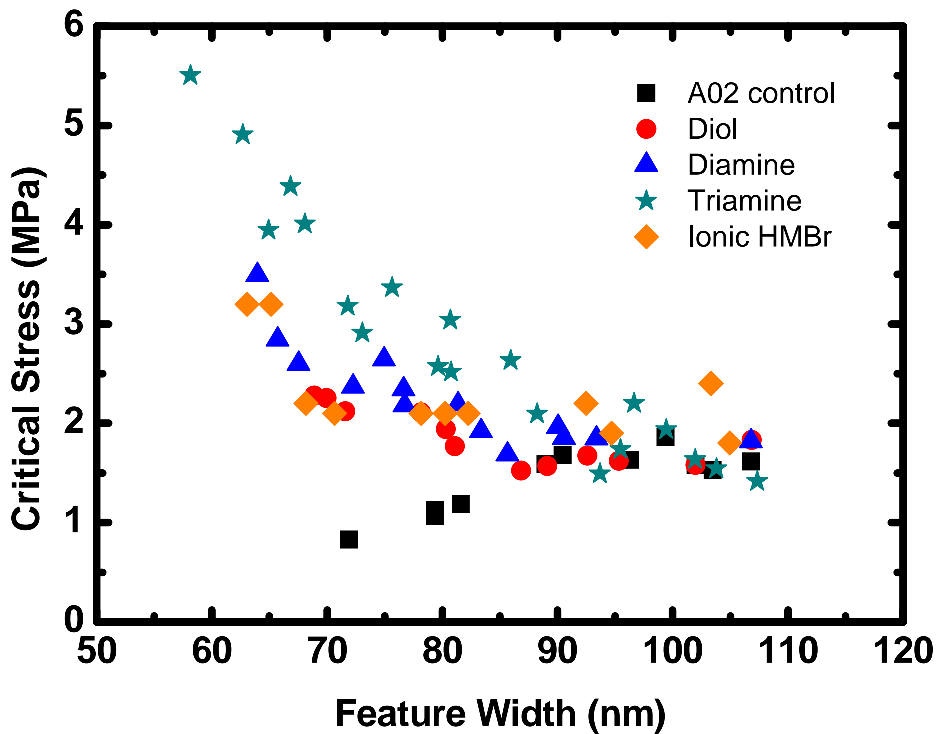

(B)

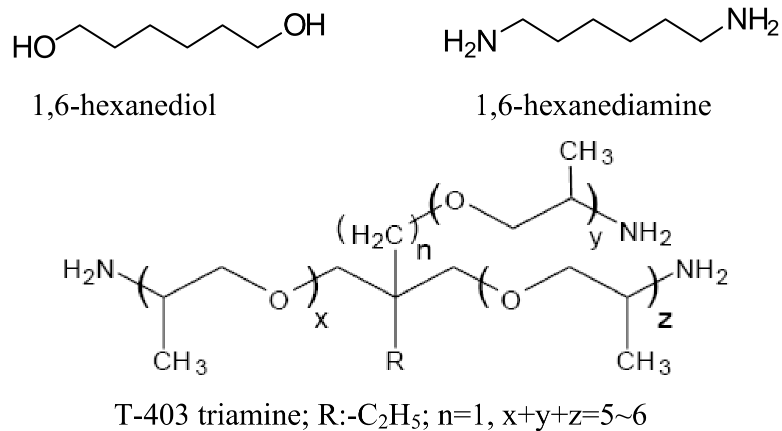

T-403 triamine; R:-C_2H_5; n=1, x+y+z=5~6

Figure 4.8 Critical stresses at the point of pattern collapse as a function of feature width in different rinse samples: DUP-A02 control samples (solid squares); samples treated by1,6-hexanediol reactive rinse (solid circles); samples treated by 1,6-hexanediamine reactive rinse (solid triangles); samples treated by T-403 triamine reactive rinse (solid stars). Film thicknesses are 252 nm.

4.4 Conclusions

Resist surface crosslinking using amino reactive rinse treatment to mitigate pattern collapse issue is presented in this chapter. Because the surface reaction is very fast and total process of reactive rinse only consist of two steps for two minutes total, the reactive rinse method is very well suited for the mitigation of pattern collapse issue in thin film lithography process. The surface which mimics the surface condition after development was created by simple-cast method and confirmed by the surface contact angle, thickness change results and AFM images. XPS spectra and pattern performance from SEM images also indicated that amine-based and alcohol-based crosslinkers were able to covalently crosslink the carboxylic groups and formed esters on DUP-A02 resist surface, and improved the pattern collapse issue. The critical stress results showed that multi-functionality crosslinker may be one of the important factors that can enhance the surface crosslink reaction.

4.5 References

1. Tanaka, T.; Morigami, M.; Atoda, N., Mechanism of Resist Pattern Collapse during Development Process. *Jpn J Appl Phys 1* **1993,** *32* (12B), 6059-6064.

2. Yoshimoto, K.; Stoykovich, M. P.; Cao, H. B.; de Pablo, J. J.; Nealey, P. F.; Drugan, W. J., A two-dimensional model of the deformation of photoresist structures using elastoplastic polymer properties. *J Appl Phys* **2004,** *96* (4), 1857-1865.

3. Guerrero, D. J.; Xu, H.; Mercado, R.; Blackwell, J., Underlayer Designs to Enhance EUV Resist Performance. *J Photopolym Sci Tec* **2009,** *22* (1), 117-122.

4. Takei, S.; Ogawa, T.; Willson, C. G., Study of fluorinated silicon-based resist material and photoreactive underlayer for defect reduction in step and repeat ultraviolet nanoimprint lithography. *Micro Nano Lett* **2011,** *6* (6), 422-424.

5. Kuroda, S.; Goto, T.; Tamada, O.; Sanada, M.; Kawai, A., Analysis of interface condition between BARC and resist film by FT-IR/ATR. *J Photopolym Sci Tec* **2007,** *20* (6), 807-808.

6. Guerrero, D. J.; Sullivan, D. M.; Mercado, R.-M. L., Resist double patterning on BARCs and spin-on multilayer materials. *Proc. SPIE* **2009**, 75200M-75200M.

7. Helbert, J. N.; Saha, N., Application of Silanes for Promoting Resist Patterning Layer Adhesion in Semiconductor Manufacturing. *J Adhes Sci Technol* **1991,** *5* (10), 905-925.

8. Yeh, W.-M.; Lawson, R. A.; Tolbert, L. M.; Henderson, C. L., A study of reactive adhesion promoters and their ability to mitigate pattern collapse in thin film lithography. *Proc. SPIE* **2011**, 79721W-79721W.

9. Powell, H. M.; Boyce, S. T., EDC cross-linking improves skin substitute strength and stability. *Biomaterials* **2006,** *27* (34), 5821-5827.

10. Damink, L. H. H. O.; Dijkstra, P. J.; vanLuyn, M. J. A.; vanWachem, P. B.; Nieuwenhuis, P.; Feijen, J., Cross-linking of dermal sheep collagen using a water-soluble carbodiimide. *Biomaterials* **1996,** *17* (8), 765-773.

11. Lee, C.-T.; Wang, M.; Jarnagin, N. D.; Gonsalves, K. E.; Roberts, J. M.; Yueh, W.; Henderson, C. L., Photosensitivity and line-edge roughness of novel polymer-bound PAG photoresists. *Proc. SPIE* **2007,** *6519*, 65191E-9.

12. Yeh, W. M.; Noga, D. E.; Lawson, R. A.; Tolbert, L. M.; Henderson, C. L., Comparison of positive tone versus negative tone resist pattern collapse bahavior. *J Vac Sci Technol B* **2010,** *28* (6), C6s6-C6s11.

13. Stafford, C. M.; Harrison, C.; Beers, K. L.; Karim, A.; Amis, E. J.; Vanlandingham, M. R.; Kim, H. C.; Volksen, W.; Miller, R. D.; Simonyi, E. E., A buckling-based metrology for measuring the elastic moduli of polymeric thin films. *Nat Mater* **2004,** *3* (8), 545-550.

14. Singh, L.; Ludovice, P. J.; Henderson, C. L., Influence of molecular weight and film thickness on the glass transition temperature and coefficient of thermal expansion of supported ultrathin polymer films. *Thin Solid Films* **2004,** *449* (1-2), 231-241.

CHAPTER 5

DEVELOPMENT OF A GENERAL REACTIVE RINSE PROCESS FOR RESIST PATTERN COLLAPSE MITIGATION BASED ON ION EXCHANGE OF POLYIONIC CROSSLINKERS TO THE DEVELOPED RESIST FEATURE SURFACE

Pattern collapse is one of important problems in the lithographic process during development process. One failure mode of pattern collapses is due to weak mechanical restoring force of resist features that can't handle the increasing capillary stress and results in resist feature bending or deforming. Instead of designing new robust resist materials, the quick and simple way for achieving the mechanical enhancement and preventing the resist structures from weak restoring force failure is to modify the resist surface. In this chapter, hexamethonium bromide reactive rinse was applied on resist patterns to ionically bond with carboxylate anions groups on the resist surface in post-development process in order to increase the mechanical properties of resist features. Pattern collapse test structures were fabricated and analyzed to quantify the impact of the use of hexamethonium bromide reactive rinse treatment. The resist moduli were measured using a homemade buckling stage, which revealed that the use of hexamethonium bromide rinse can significantly enhance the mechanical properties of the resist. XPS spectra, SEM images, and critical stress analysis of the resulting patterns also confirmed that the use of hexamethonium bromide rinse increased the pattern collapse resistance to capillary forces and improved the collapse issue.

5.1 Introduction

Pattern collapse caused by unbalanced capillary forces acting on the pattern walls during the final rinse and drying process in photolithography becomes an important issue for future nanodevice fabrications. Typically the mode of pattern deformation is categorized into two major types of failure: adhesion loss at the resist-substrate interface[1] and resist bending or breakage due to weak mechanical restoring force[2]. The most common method for improving resist adhesion in the industry is to apply hexamethyldisilazane (HMDS)[3] on the substrate, which is designed to match the interface surface energy to increase the interfacial adhesion strength. Several authors have investigated other approaches for adhesion improvement such as, the use of an underlayer[4,5] or a bottom anti-reflective coating (BARC)[6,7] which often have the added benefit of increasing the resist adhesion in addition to their primary benefits of reflectivity control[7]. Functional silane adhesion promoters have also been reported to form covalent bonding between the resist and silicon substrates to strengthen the interfacial interaction [8,9].

Most research groups have focused on increasing the adhesion strength to improve the former mode of pattern collapse but pay less attention to another mode of pattern collapse, mechanical deformation, caused by the weak mechanical strength of the resist which can't support the increasing capillary stress. One approach to mitigate this type of resist failure is to design new resist materials by introducing the bulky and robust groups (i.e. benzyl or alicylic groups) on the resist chemical structures in order to increase the mechanical restoring forces of resist features. However, design and synthesis of new resist materials that satisfy the imaging process in lithography requirement are very difficult. In order to implement effective solutions to improve pattern behavior, we have investigated the methods that are quick and compatible with lithographic process that can mitigate such pattern collapse in high resolution structures. We observed that negative tone photoresists which operate by crosslinking result in a covalently bonded

network and often exhibit superior patterning capabilities which can be attributed to the fact that the resist has adopted a networked macromolecular structure after exposure and most likely inherited superior mechanical properties relative to the unexposed polymeric structure. In our previous works[10,11], we have developed a surface rinse that used a diamine or aziridine solution to crosslink the functional groups on the surface of a photoresist through the formation of amide covalent bonds on the time scale of few minutes. It has been shown that such rinse methods are capable of increasing the mechanical properties of resist structures, confirmed by the increase of effective modulus after the rinse treatment. In addition to covalent crosslink approach, the carboxylate anions generated after base development are potentially linked with two functional ammonium salts. Also, quaternary ammonium cations are permanently charged and independent of the pH value of solution, which is a suitable candidate for an ionic bond rinse and also can be used to electrostatic interact with carboxylate anions formed on the resist wall surface after development process. In this chapter, ionic bonding on the resist surface using two functional quaternary ammoniums has been studied. X-ray photoelectron spectroscopy (XPS) was used to characterize and monitor the surface modification. The effective film modulus of the samples treated by ionic rinse was shown to increase using the e-beam resist, PMMA-co-PMAA and thin film buckling metrology. The use of such ionic reactive rinses was found to clearly result in an improvement in the resistance of the resists to pattern collapse as observed by SEM. A comparison of the critical stress at the point of pattern collapse as a function of resist feature size also clearly shows the significant improvement in mechanical resilience of resist samples processed with the rinse treatment.

5.2 Experimental

Materials The resist (DUP-A02, see Figure 5.1) used in this work was supplied by Intel. A model chemically amplified photoresist was formulated by combining the DUP-A02 resin, triphenylsulfonium nonaflate (TPS-Nf) photoacid generator (PAG), and a trioctylamine (TOA) base quencher, in cyclohexanone at loadings of 8 wt% total solids in cyclohexanone with 5 wt% TPS-Nf relative to A02 and 10 mol% of TOA relative to the TPS-Nf PAG. AZ300MIF (Tetramethylammonium hydroxide, TMAH) developer was supplied by AZ Electronic Materials Company. TOA was purchased from Alfa-Aesar. All other reagents used in this study were purchased from Sigma-Aldrich.

Substrate Preparation Silicon nitride windowed (Si_xN_y) substrates were used as substrates for high-resolution electron beam imaging of resist materials. The preparation of Si_xN_y substrates have been described in our previous work[12]. The Si_xN_y windowed substrates are designed to eliminate electron backscattering from the substrate and thus produce extremely sharp aerial images and essentially vertical sidewalls in the final resist patterns. Before the resist was coated, Si_xN_y substrates were primed with 1,1,3,3,3-hexamethyl-disilazane (HMDS) vapor at 70 torr and 110°C in vacuum oven for 10 minutes to enhance the adhesion strength of resist patterns and prevent the resist patterns collapsed due to adhesion failure.

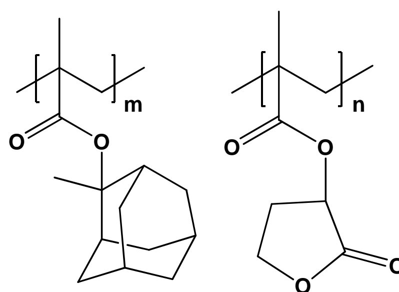

DUP-A02 (m:58, n:42)

Figure 5.1 Chemical structure of the DUP-A02 photoresist we used in this work.

Sample Preparation Hexamethonium bromide (HMBr) rinse solution was prepared for 0.1 M solution in deionized water. Resist films were made by spin-coating at various spin speeds for 60 seconds to obtain films of varying thickness. The control resist films were then soft-baked at 110 °C for 2 min, exposed and patterned via e-beam, post-exposure baked at 110 °C for 1 min, developed with AZ300MIF for 30 sec, rinsed with deionized water for 30 sec and finally dried with nitrogen stream. E-beam lithography was carried out using a JEOL JBX-9300FS e-beam lithography system with an accelerating voltage of 100 kV, a beam diameter of 8 nm, a 2 nA current, and a 10 nm shot pitch. The samples which underwent the HMBr ionic reactive rinse were taken through the same procedure up through the development step. After the development step, the samples were placed in a 0.1 M HMBr aqueous solution for 2 min, then rinsed with deionized water for 30 seconds and dried with nitrogen stream in a manner identical to the control samples. Thermo K-Alpha X-ray Photoelectron Spectroscopy (XPS) with the source of Al Kα micro-focused monochromator at the pressure of 10^{-9} mbar was used to characterize the surface modification. A value of 285 eV for the binding energy of the C_{1s} component was used to correct for charging under irradiation. Atomic force microscope (Agilent 5500, picoplus system) and water contact angle measurement were used to monitor the surface condition of the resist. The thickness of the resist films was measured by an M-2000 Variable Angle Spectroscopic Ellipsometer (VASE, J.A. Woollam).

Pattern Performance Analysis The pattern used to study the collapse of the formulated resist has been described previously[13]. An e-beam lithography pattern with a series of varying line and space widths was specifically designed in order to simulate the increasing capillary stress and quantitatively to study pattern collapse (Fig. 5.2). With our particular pattern design, as the spacewidth (S_1) between two small parallel lines decreased from left to right starting from 200 nm down to 10 nm in the images shown for a set of lines with a constant line width W, the capillary stress increased from left to right. Pattern collapse would occur when a sufficiently small S_1 value was reached such that the

stress applied to the resist exceeded the critical stress required for pattern bending and deformation as shown in Figure 5.2C. The critical space in the test patterns, S_{1c} is determined by identifying the position in each test structure array where two adjacent small lines in the test structure exhibit no sign of collapse or deformation (indicated by a red arrow on the top of SEM image). Critical space (S_{1c}), outside pool space (S_2) and line widths (W) were measured precisely from high resolution SEM images using custom written MALAB software designed for high resolution SEM feature analysis.

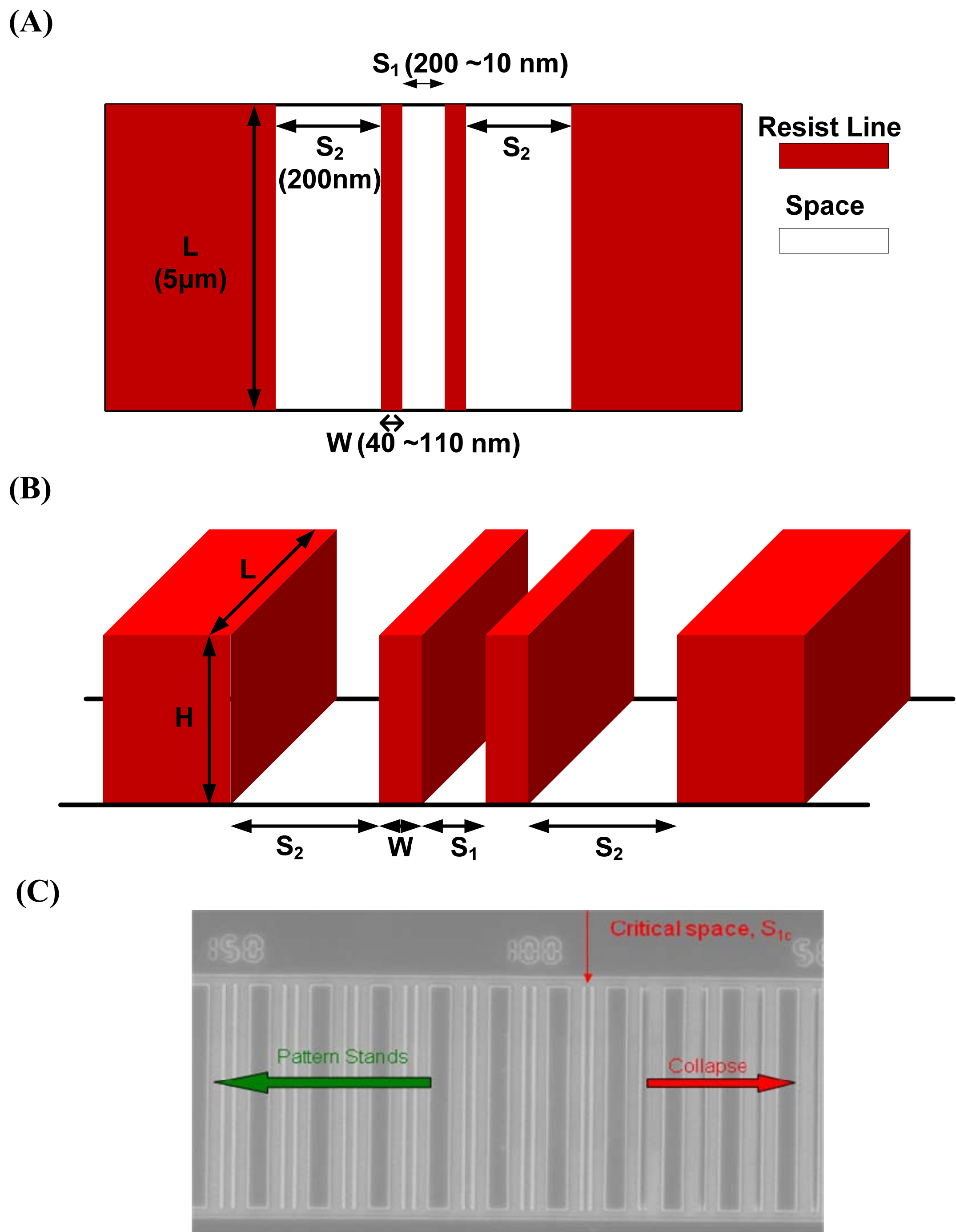

Figure 5.2 (A) Top view and (B) side view of pattern design used in this work for determining the critical stress at the point of pattern collapse; (C) An example for determining the position of critical stress: SEM image of nominal 70 nm feature width line pair arrays used to identify the critical S_{1c} space. The number on the top of array represents the space width (W) between two small lines (S_1).

5.3 Results and Discussion

To study the efficiency of ionic reactive rinse, the surface that mimics the condition of resist wall after development was created by the partial development on the resist film using the simple-cast process we designed in Figure 5.3. Unformulated DUP-A02 resist in cyclohexanone solution was spin-coated at 3000 rpm on the HMDS primed silicon substrate and baked at 110 °C for 1 min to obtain 220 nm thick resist film. 3wt% TPS-Nf in isopropyl alcohol (IPA) solution was directly casted on the unformulated DUP-A02 resist film and followed by DUV exposure of 10 mJ/cm^2. After AZ 300MIF rinse, resist film was partial developed and formed the carboxylate groups on the top of unformulated A02 resist film. After this simple-cast method process, the thickness of resist film decreased from 220nm to 64nm, measured by the ellipsometer and the static water contact angle on the resist surface also dropped from 83 to 54 degree. The decreases of film thickness and surface contact angle suggested that the top of DUP-A02 resist surface was partially developed and hydrophilic carboxylic surface that mimics the surface condition of resist side wall after development was successfully made. This mimic DUP-A02-COOR surface could be used for the study of the impact of ionic reactive rinse on the pattern collapse mitigation.

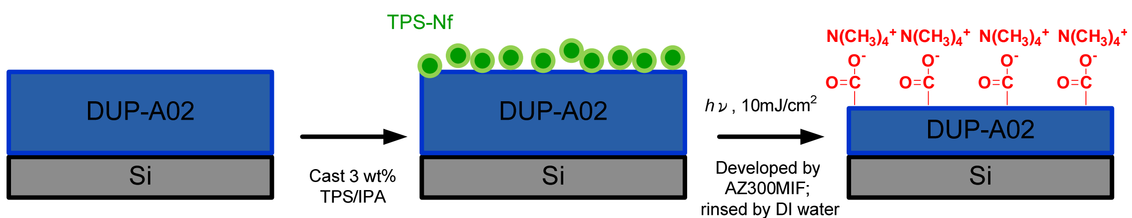

Figure 5.3 Schematic illustration of the process for making the resist surface that mimics the surface condition after development.

DUP-A02 photoresist surface is deprotected with photochemically-generated acid to form the carboxylate groups after development process. Such carboxylate groups on the resist surface is capable of being used as reactive groups in conjunction with rinse additives to bind the surface of the patterns and films with a functional cationic linker. In previous work, carboxylate groups on the resist wall were then activated with EDC in the presence of *N*-Hydroxysuccinimide (NHS) and formed NHS esters. The NHS esters then easily reacted with nucleophiles, such as primary amine groups to form stable amide bonds[10]. The functional diamine or diol can be used as a reactive crosslinker to covalently bond the carboxylate groups to the resist wall and enhance the resist mechanical properties. This covalently reactive rinse process contains two steps to crosslink the functional groups on the resist surface.

We observed the carboxylate anions on the resist surface generated after development. The developed resist surface can potentially be linked by one step ionic rinse using a cationic linker instead of covalent binding; however, the primary amine groups are very sensitive to the pH value of solution, so the use of di-amines or multi-amines to electrostatically react with carboxylate anions may be needed to carefully control the pH value of reaction solution. The quaternary ammonium cations are permanently charged and independent of the pH value of solution. Quaternary ammonium salts may be good candidates for new ionic interaction rinse to bond with carboxylate groups on the resist surface. The schematic process of HMBr ionic reactive rinse is illustrated in Fig. 5.4. Carboxylate anions groups were generated on the resist wall after the simple-cast process and development. Hexamethonium bromide (HMBr) salt with two quaternary ammonium cations was applied as a reactive linker for ionically bonding with the caroxylate anions on the resist surface and presumed to enhance the resist mechanical properties.

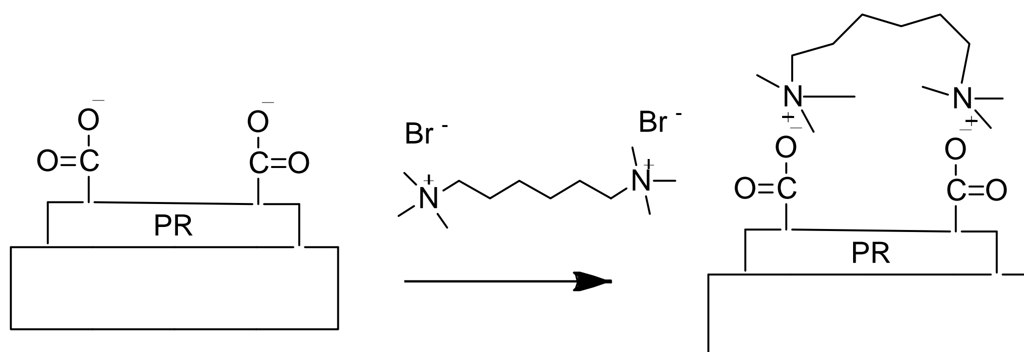

Figure 5.4 Schematic illustration of HMBr ionic rinse process.

XPS can be used to characterize the ionic interaction on the resist surface based on the present of nitrogen signal. Figure 5.5 shows the XPS results for various ionic rinse time. After AZ300MIF (contains 2.38wt tetra-methyl ammonium hydroxide, TMAH) development, the ionic complex of $COO^-NH_4^+$ was formed on the resist surface. The ammonium cations were replaced with H^+ by using a 10 min hydrogen chloride rinse to remove the nitrogen signal for XPS measurement (A02-COOR control sample in Fig 5.5A). The spectra of N_{1s} high resolution for various ionic rinse time are shown in Fig. 5.5A. A small amount of nitrogen (N_{1s}) was observed at ~400eV on A02-COOR control sample made by simple-cast method due to few ammonium salts remaining on the surface after hydrogen chloride ionic replacement. After HMBr rinse, an increase in the nitrogen peak could be found at 400 eV, indicating that HMBr is ionically bonded to carboxylate anions on the surface. The total amount of nitrogen reacted on the resist surface for each rinse time is characterized with the area ratio of nitrogen (N_{1s}) to silicon (Si_{2p}) on XPS spectra and shown in the Fig.5.5B. The area ratio of nitrogen to silicon increased as the rinse time increased and reached a plateau around 2 minutes, suggesting the 2 minute HMBr rinse reached the saturation point for the ionic interaction on the surface.

(A)

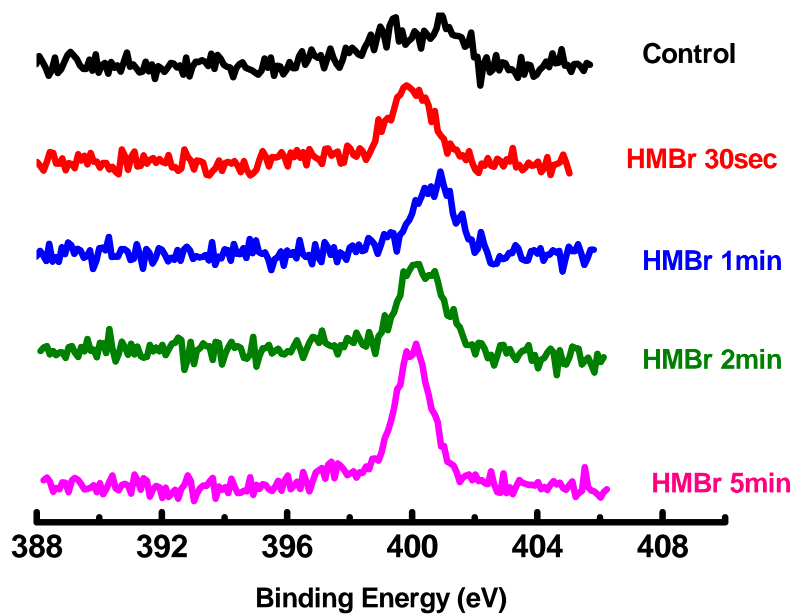

(B)

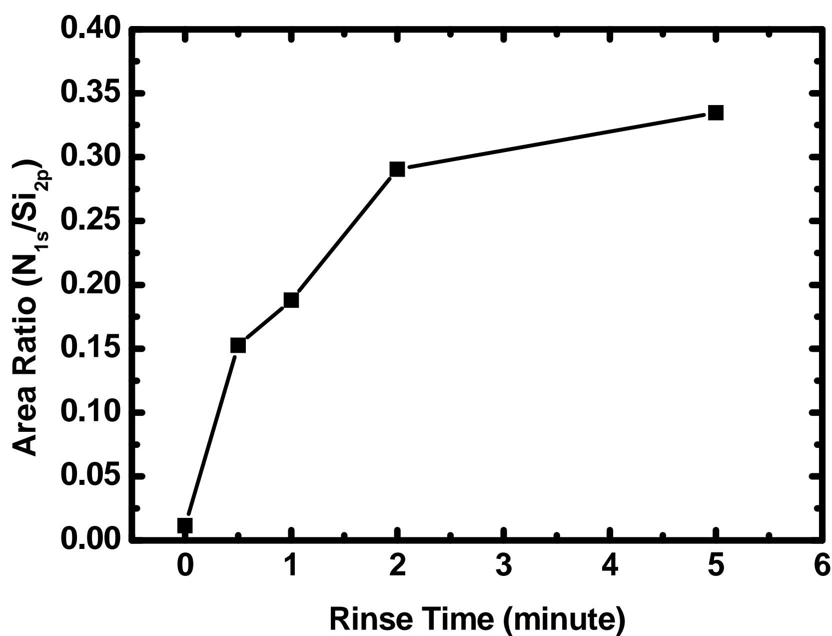

Figure 5.5 (A) High resolution N_{1s} spectra of the A02-COOR control film and films rinsed by HMBr for 30sec, 1min, 2min, and 5min. (B) The area ratio of N_{1s} and Si_{2p} as a function of HMBr rinse time.

The film modulus was measured to that an ionic rinse can link the carboxylate anions with HMBr and provides a mechanical property enhancement. The process of buckling method for film modulus measurement was described in our previous work[14]. A compressive stress was applied to the examined resist film using our homemade strain stage. The examined film surface underwent periodic buckling at a wavelength that correlated with the effective film modulus. Due to the adhesion issues on the transferring DUP-A02 resist films onto the homemade strain stage, the model PMMA-co-PMAA e-beam resist was used to test the impact of an ionic rinse on resist modulus. Figure 5.6 shows the effective film moduli for the 26 nm thick PMMA/PMAA and polystyrene (PS) films after 2-min HMBr rinse. The effective moduli of PMMA/PMAA films rinsed by HMBr ionic rinse increased significantly compared to the control film which did not receive HMBr rinse. Polystyrene with no carboxylate groups was used as a control sample. It can be seen that there is no significant modulus enhancement on polystyrene film after HMBr rinse. It indicated that the HMBr ionic reactive rinse could be used to link the surface carboxylate anions and improve the mechanical properties of nanoscale resist structures.

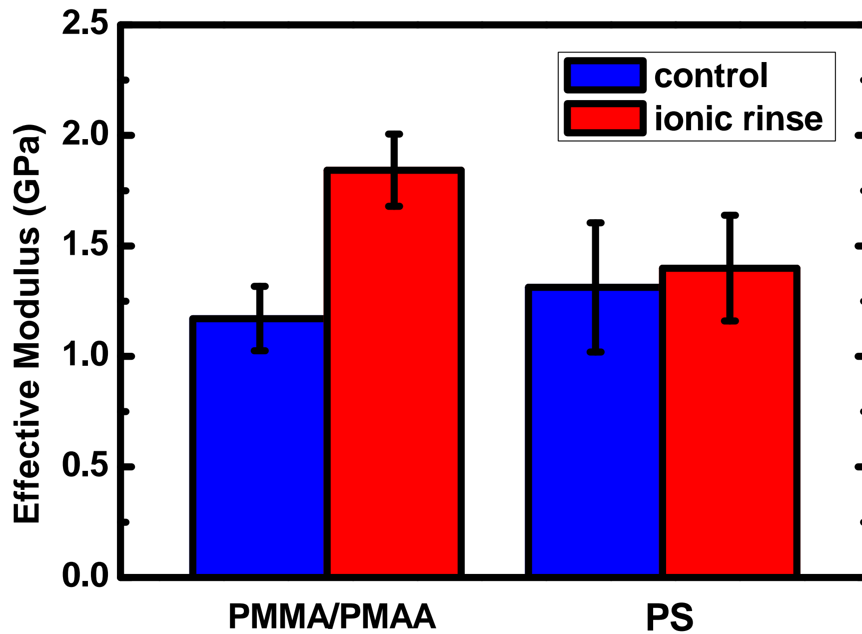

Figure 5.6 Effective moduli of PMMA/PMAA and PS film after HMBr reactive rinse.

The pattern structure used in this work was designed so that the spacing (S_I) between two small parallel lines decreased from left to right starting from 200 nm down to 10 nm for a constant line width (W) to simulate the increasing capillary stress. Eventually resist lines collapse at a sufficiently small space value which correspons to the critical stress required for pattern bending and subsequent feature deformation. Smaller spacing results in higher capillary stress on the pair of resist lines. A pair of resist lines that have not collapsed with a smaller critical S_I space represents higher capillary stress resistance and better pattern performance in our test arrays.

SEM images of a resist sample that did not receive on ionic reactive rinse and a sample treated by additional ionic reactive rinse after development are shown in Figure 5.7. The numbers on the top of array structures denote the spaces (S_I) between two small resist lines. The numbers on the left of array structure represent the width of each line

(W). The red arrows in the figures indicate the critical space (S_{1c}) which is the position in the pattern array with the smallest spacing between small lines where resist lines can withstand the largest capillary stress before collapse. SEM images of control sample which did not rinse with HMBr solution (see Fig. 5.7A) showed that all patterns collapsed from 200 nm space S_1 to 10 nm space S_1 in the nominal 70 nm and 80 nm line widths. For the sample where the HMBr ionic rinse was applied, it showed patterned line pairs collapsed at nominal 170 nm space S_1 (S_{1c}) in the nominal 70 nm line width and collapsed at 100 nm space S_1 (S_{1c}) in the 80 nm line width (see Fig. 5.7B). Smaller critical spaces represent the cases where the resist lines could endure higher capillary stress without collapse. SEM images showed that the use of the HMBr ionic rinse resulted in a smaller critical space and enhanced pattern collapse resistance to the capillary stress compared to the sample which didn't rinse with HMBr solution. Buckling results and SEM images both suggest that the HMBr rinse is capable of ionically bonding with carboxylate anions on the resist surface and enhancing the mechanical properties of resist features.

(A)

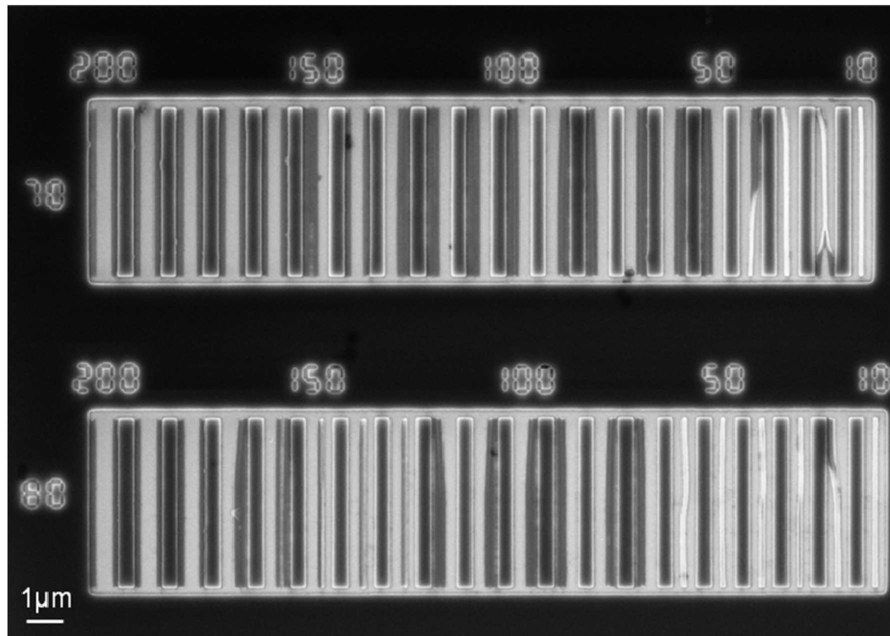

(B)

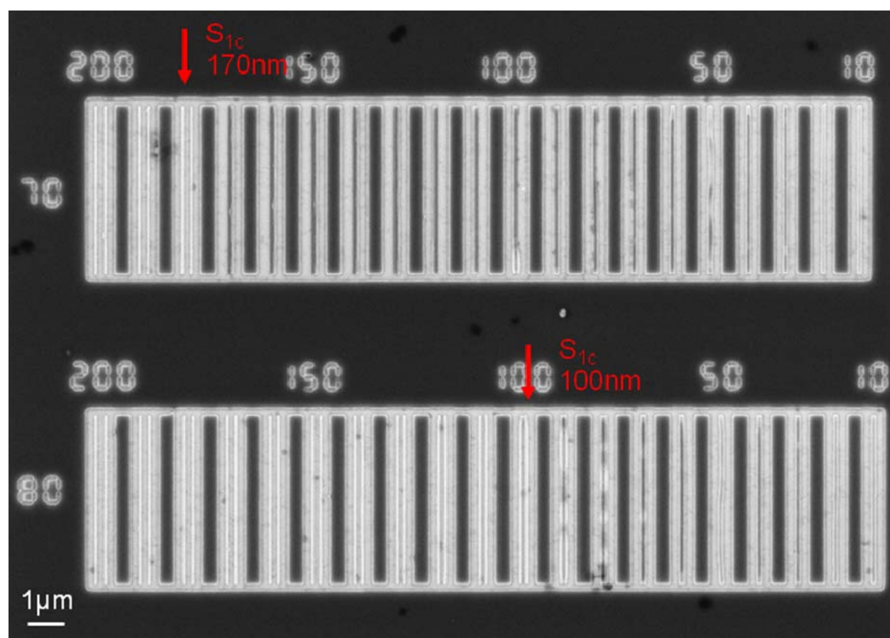

Figure 5.7 SEM images of nominal 70 nm and 80 nm line widths on (A) pattern samples which did not receive HMBr rinse, and (B) pattern samples treated by HMBr rinse. The numbers on the left of arrays represent the nominal widths of all small parallel lines. The numbers on the top of arrays represent the nominal S_1 space widths between two small lines. The arrows in the figure indicate the critical spaces (S_{1c}) which are the position in the pattern array with the smallest spacing between two small lines where resist lines can withstand the largest capillary stress before collapse.

The critical stress (σ_c) is defined as the maximum stress that can be applied to the photoresist lines prior to pattern collapse and occurs at critical spacing, the last space/position before the pair of resist lines collapses on the pattern structure we designed. It can be used to characterize and quantify the pattern behavior. The equation used to calculate the critical stress is expressed in equation (5.1), where γ is surface tension of rinse liquid (i.e. deionized water with γ=0.073 N/m), θ is the contact angle of the rinse liquid on the photoresist (i.e. deionized water with θ=83° in DUP-A02 case), height H is the thickness of the photoresist film, S_2 is the respective outside space width between the lines of the pattern we designed shown in Fig. 5.2, and S_{1c} is the critical pattern center space width where collapse is first indicated[13]. Critical space (S_{1c}), outside pool space (S_2) and line widths (W) were measured precisely from high resolution SEM images using custom written MALAB software designed for high resolution SEM feature analysis.

$$\sigma_C = 6\gamma \cos\theta \left(\frac{H}{W}\right)^2 \left(\frac{1}{S_{1c}} - \frac{1}{S_2}\right) \quad (5.1)$$

For the further comparison on different approaches of reactive rinse, covalently reactive rinses were also used to crosslink the carboxylate groups on the resist surface. Two other functionality crosslinkers, 1,6-hexanediamine and 1,6-hexanediol were also applied on the test array we designed. Figure 5.8 shows the chemical structures and calculated critical stresses of surface linkers we used in this study. The higher critical stress indicates that resist features exhibit better collapse resistance to the capillary stress. Resist samples that did not reactive rinse or ionic rinse (squares in Fig. 5.8), pattern lines show lowest critical stress and a plateau in the larger feature region. Samples rinsed by 1,6-hexanediol (circles in Fig. 5.8), 1,6-hexanediamine (triangles in Fig. 5.8), or hexamethonium bromide salt (diamonds in Fig. 8) showed almost the similar critical stress values and have higher critical stress compared to unrinsed samples (squares). These results confirmed the ideas of ioinically reactive rinse that ammonium salts are

able to form ionic links with the carboxylate groups on the surface of DUP-A02 resist and improve the pattern resistance to capillary stress with the enhancement of mechanical properties. The presence of a plateau in the critical stress of 1.5MPa at feature width of ~90 nm was observed on each sample. Several groups have reported confinement behavior on ultra-thin polymer films where polymer properties are not constant and depend on polymer film thickness. For instance, the glass transition temperature (Tg) of polymer film was found to decrease with decreasing film thickness below a critical film thickness of approximately 10 times the polymer radius of gyration[15]. The effective modulus of polymer films decreased as the film thickness decreased below 40 nm[16]. Many studies have suggested the presence of a mobile, rubberlike surface on polymer films[17] which is responsible for this such confinement effect. The effective mechanical properties of total polymer film are due to both the soft surface layer and the robust bulk layer. For the case of thicker films or larger feature widths, the soft surface layer only plays a small part of whole film so the effect of soft surface layer on film modulus is negligible. In this case, all resist properties are dominated by robust bulk layer and polymer properties are almost independent of film thickness and features size, revealing a plateau at larger feature width region. As the film thickness or feature width shrinks, the ratio of soft surface layer becomes comparable to bulk layer and contributes strong effects to the overall properties of the polymer film. Therefore, in the smaller feature width region, the effective modulus is dependent on the resist feature width and decreases with the decrease of the film thickness or feature width, which observed in the control DUP-A02 resist sample because the critical stress is highly related to mechanical properties of resist structures (squares in Fig. 5.8A). For the samples risned by diol, diamine, or HMBr reactive solutions, mechanical properties of the surface layer were improved through surface modifications due to diol, diamine, or HMBr crosslinked or ionically bonded the carboxylate groups on the resist surface. The mechanical improvement due to surface modification becomes significant at small feature region due

to the increasing ratio of surface layer, resulting in the trend that critical stress of resist lines increased as the resist feature size shrank. This result also suggests that diol, diamine, or HMBr reactive rinse provided significant mechanical improvement.

(A)

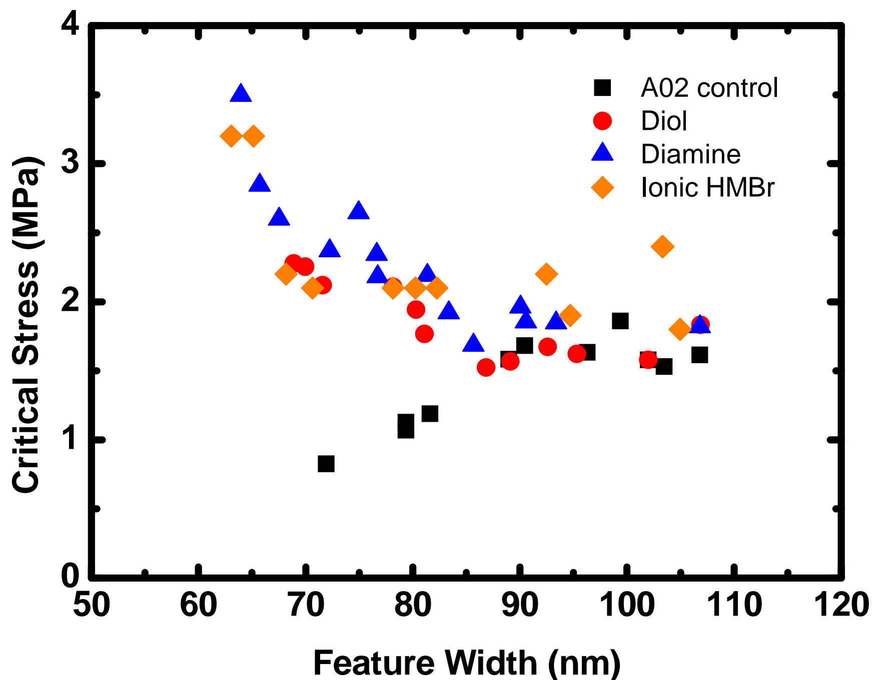

(B)

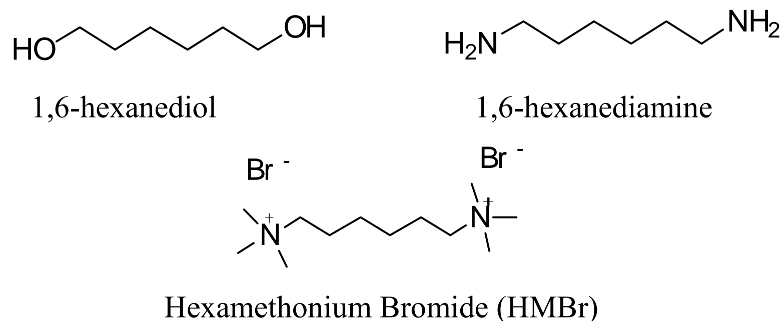

Figure 5.8 (A) Critical stresses at the point of pattern collapse as a function of feature width in different rinse samples: DUP-A02 control samples (squares), samples treated with diol reactive rinse (circles), samples treated with diamine reactive rinse (triangles), and samples treated with HMBr rinse (diamonds). All samples thicknesses are 252 nm. (B) Chemical structures of the linkers in this work.

5.4 Conclusions

The application of ionic rinse in the post-development to mitigate pattern collapse issue is presented. A test pattern array was designed to simulate the capillary stress for resist collapse quantification. Hexamethonium bromide with two quaternary ammoniums on both ends was applied to ionically bond with carboxylate anions on the resist surface. The effective modulus of resist film was found to improve significantly after hexamethonium bromide ionic rinse treatment, confirmed by our homemade strain stage. The mechanical property data were also consistent with the critical stress results that surface rinse can enhance the resist collapse resistance to capillary stress. The critical stress results also showed that the HMBr ionic rinse and covalent reactive rinses provide similar resistance to resist collapse. This approach is an aqueous process and compatible with high volume, track-based lithographic processes. Total rinse process consists of only one step rinse and completes in 2 minutes. This ionic rinse approach is well-suited in the continuous lithography processes.

5.5 References

1. Tanaka, T.; Morigami, M.; Atoda, N., Mechanism of Resist Pattern Collapse during Development Process. *Jpn J Appl Phys 1* **1993,** *32* (12B), 6059-6064.

2. Yoshimoto, K.; Stoykovich, M. P.; Cao, H. B.; de Pablo, J. J.; Nealey, P. F.; Drugan, W. J., A two-dimensional model of the deformation of photoresist structures using elastoplastic polymer properties. *J Appl Phys* **2004,** *96* (4), 1857-1865.

3. Helbert, J. N.; Saha, N., Application of Silanes for Promoting Resist Patterning Layer Adhesion in Semiconductor Manufacturing. *J Adhes Sci Technol* **1991,** *5* (10), 905-925.

4. Guerrero, D. J.; Xu, H.; Mercado, R.; Blackwell, J., Underlayer Designs to Enhance EUV Resist Performance. *J Photopolym Sci Tec* **2009,** *22* (1), 117-122.

5. Takei, S.; Ogawa, T.; Willson, C. G., Study of fluorinated silicon-based resist material and photoreactive underlayer for defect reduction in step and repeat ultraviolet nanoimprint lithography. *Micro Nano Lett* **2011,** *6* (6), 422-424.

6. Kuroda, S.; Goto, T.; Tamada, O.; Sanada, M.; Kawai, A., Analysis of interface condition between BARC and resist film by FT-IR/ATR. *J Photopolym Sci Tec* **2007,** *20* (6), 807-808.

7. Guerrero, D. J.; Sullivan, D. M.; Mercado, R.-M. L., Resist double patterning on BARCs and spin-on multilayer materials. *Proc. SPIE* **2009**, 75200M-75200M.

8. Yeh, W.-M.; Lawson, R. A.; Tolbert, L. M.; Henderson, C. L., A study of reactive adhesion promoters and their ability to mitigate pattern collapse in thin film lithography. *Proc. SPIE* **2011**, 79721W-79721W.

9. Prucker, O.; Naumann, C. A.; Ruhe, J.; Knoll, W.; Frank, C. W., Photochemical attachment of polymer films to solid surfaces via monolayers of benzophenone derivatives. *J Am Chem Soc* **1999,** *121* (38), 8766-8770.

10. Yeh, W.-M.; Lawson, R. A.; Tolbert, L. M.; Henderson, C. L., Resist surface crosslinking using amine-based reactive rinses to mitagate pattern collapse in thin film lithography. *Proc. SPIE* **2012**, 83251X-83251X.

11. Yeh, W.-M.; Lawson, R. A.; Tolbert, L. M.; Henderson, C. L., Application of aziridine reactive rinses in a post-development process to reduce photoresist pattern collapse. *Proc. SPIE* **2012**, 83251Y-83251Y.

12. Lee, C.-T.; Wang, M.; Jarnagin, N. D.; Gonsalves, K. E.; Roberts, J. M.; Yueh, W.; Henderson, C. L., Photosensitivity and line-edge roughness of novel polymer-bound PAG photoresists. *Proc. SPIE* **2007,** *6519*, 65191E-9.

13. Yeh, W. M.; Noga, D. E.; Lawson, R. A.; Tolbert, L. M.; Henderson, C. L., Comparison of positive tone versus negative tone resist pattern collapse bahavior. *J Vac Sci Technol B* **2010,** *28* (6), C6s6-C6s11.

14. Yeh, W.-M.; Noga, D. E.; Lawson, R. A.; Tolbert, L. M.; Henderson, C. L., Thin film buckling as a method to explore the effect of reactive rinse treatments on the mechanical properties of resist thin films. *Proc. SPIE* **2010,** *7639*, 76391I-6.

15. Singh, L.; Ludovice, P. J.; Henderson, C. L., Influence of molecular weight and film thickness on the glass transition temperature and coefficient of thermal expansion of supported ultrathin polymer films. *Thin Solid Films* **2004,** *449* (1-2), 231-241.

16. Stafford, C. M.; Vogt, B. D.; Harrison, C.; Julthongpiput, D.; Huang, R., Elastic moduli of ultrathin amorphous polymer films. *Macromolecules* **2006,** *39* (15), 5095-5099.

17. Fischer, H., Thermal probe surface treatment of a bulk polymer: Does a surface layer with a lower glass transition than the bulk exist? *Macromolecules* **2002,** *35* (9), 3592-3595.

CHAPTER 6

THE USE OF REACTIVE ADHESION PROMOTERS TO MITIGATE PATTERN COLLAPSE IN THIN-FILM LITHOGRAPHY

Pattern collapse has become an issue of increasing importance in semiconductor lithography as the size of critical features continues to shrink. One of the primary modes of pattern collapse at small feature sizes is adhesion failure caused by loss of adhesion of the resist to the substrate during the drying process. The main forces which govern pattern collapse by adhesion failure are related to substrate/resist interactions. In this chapter, a reactive adhesion promoter capable of covalently attaching to hydroxystyrene-based positive tone resist copolymers has been developed and demonstrated. A vinyl-ether-modified silane was prepared and effectively applied using a solution silanization reaction. A model hydroxystyrene-based positive tone resist was applied and subjected to post apply bake to cause reaction of the surface modifier with the photoresist to occur prior to patterning using e-beam lithography. Pattern collapse test structures were fabricated and analyzed after development and drying on the different substrates to quantify the impact of the use of the covalent surface linker and compare it to more standard adhesion promoter processes such as those utilizing hexamethyldilazane (HMDS). Ultimately, the results of critical stress analysis and SEM studies of the resulting patterns confirmed that use of surface priming agents that covalently attach the resist to the substrate can significantly enhance resist-substrate adhesion and dramatically reduce pattern collapse.

6.1 Introduction

As integrated circuit fabrication continues to advance towards the 22 nm node and below, it has become clear that although line edge roughness and resolution are important, other issues such as pattern collapse must be addressed in order for technology to continue to progress. Pattern collapse is caused by unbalanced capillary forces present during the final drying step of the standard lithographic process. One of primary modes of pattern collapse is adhesion failure at the resist-substrate interface[1]. Most research groups have studied the use of alternative rinses and drying processes to mitigate the capillary force, such as the use of surfactants in final rinse liquids[2,3], the use of supercritical fluid in drying process[4,5], and the combination of surfactant and supercritical fluid[6]. However, swelling and additional shrinkage issues have been found in the case that the surfactants are applied in rinse liquids[3,7]. Also the equipment of supercritical fluid may be not well-compatible in the present lithographic process. Therefore, the alternative method to mitigate the adhesion failure is to enhance the interaction strength between the resist and the substrate using surface adhesion promoters.

Much of the previous work on the adhesion strength at the resist and substrate interface has involved the use of an underlayer[8] or a bottom anti-reflective coating (BARC) which often has the added benefit of increasing the resist adhesion in addition to their primary benefits such as reflectivity control[9,10,11]. The industry standard method for improving resist adhesion is to make a surface more organophillic by treatment with hexamethyldisilazane (HMDS)[12]. However, HMDS treatments only modify adhesion by manipulating Van der Waals forces and interaction energies between resist molecules and functional groups on the surface, and such interactions are relatively weak compared to covalent bond energies. One potential approach towards addressing adhesion related defects and the resulting failure which occurs is to design a surface modifier that can covalently attach to both the substrate and the resist (Figure 6.1).

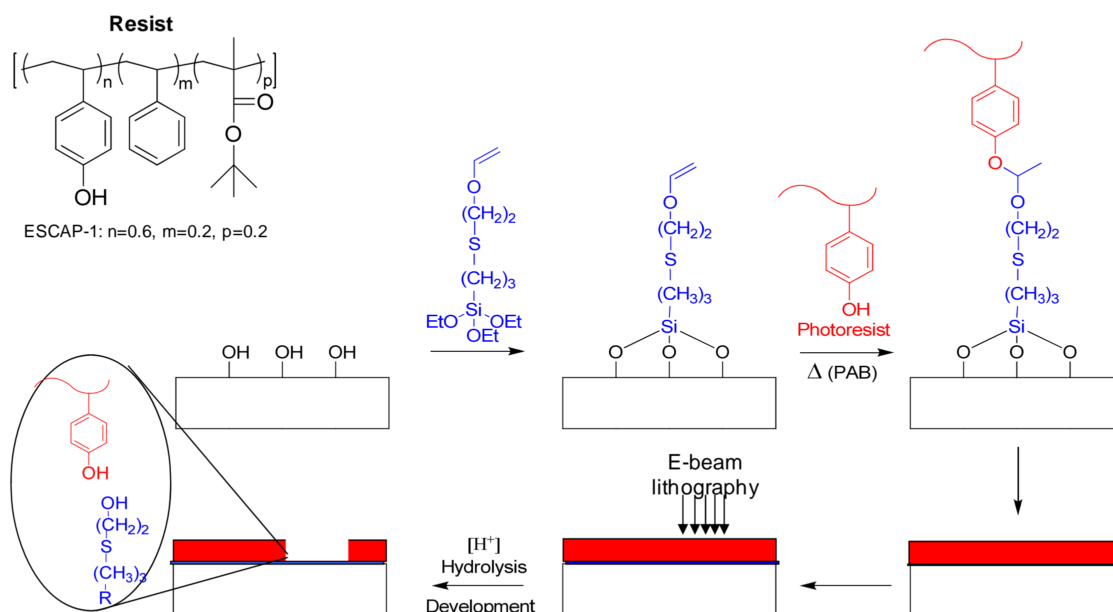

Figure 6.1 (top left) Structure of the model resist used in this work, referred to here as ESCAP-1, which is a copolymer of hydroxystyrene, styrene, and t-butyl acrylate. (bottom) Schematic of the surface modification technique investigated in this work to enhance photoresist adhesion using a reactive vinyl ether silane.

The use of various silanes to modify hydroxyl-containing surfaces has been well established in the literature[13,14]. In this work, a triethoxysilane compound was synthesized and used to modify the Si_xN_y surface of substrates used for high resolution patterning tests of a model resist system. The primary innovation tested in this work is the inclusion of a reactive moiety in the surface modifier that can form a covalent bond with the resist film coated on top of it. In the case presented here, a reactive vinyl ether functionality was selected to fulfill this function in order to take advantage of the reactivity of phenolic groups present in the particular model resist used here[15]. E-beam lithography was performed using a previously described pattern[16], and SEM analysis of the resulting features were compared to samples treated using HMDS and different baking conditions. The results of these tests clearly demonstrate the positive effect of the new adhesion

promoter over traditional methods like HMDS treatment. Our previous adhesion model also indicated that the use of vinyl ether silanes we synthesized showed significant improvement on the resist-substrate interaction.

6.2 Experimental

Materials and Equipments The model photoresist resin (ESCAP-1, see Figure 6.1) used in this work was supplied by JSR and Intel. The developer, AZ300MIF was supplied by AZ Electronic Materials Company. All other reagents used in this study were purchased from Sigma-Aldrich, VWR, or Alfa-Aesar. A model chemically amplified photoresist was formulated by combining the ESCAP-1 resin, triphenylsulfonium nonaflate (TPS-Nf) photoacid generator (PAG), and a trioctylamine (TOA) base quencher, in propylene glycol methyl ether acetate (PGMEA) at loadings of 3.6 wt% total solids in PGMEA with 5 wt% TPS-Nf relative to ESCAP-1 and 10 mol% of TOA relative to the TPS-Nf PAG. E-beam lithography was performed using a JEOL JBX-9300FS e-beam lithography system with an accelerating voltage of 100 kV, a beam diameter of 8 nm, a 2 nA current, and a 10 nm shot pitch. The Si_xN_y windowed substrates used in this study have been described elsewhere and were utilized to allow for extremely high resolution imaging of the chemically amplified resist (CAR)[17]. Electron beam exposures on such thin nitride windows eliminate electron backscatter from the substrate and thus produce extremely sharp aerial images and essentially vertical sidewalls in the final resist patterns. Such perfectly rectangular resist profiles make analysis of the resulting pattern collapse much simpler and more reliable than in the case of the rounded profiles that can be obtained from degraded aerial images produced using other exposure sources such as optical projection systems. This high resolution fidelity of the e-beam process also helped ensure that pattern failure was due to adhesion failure or other collapse modes and not due to errors or defects in the printing. SEM images were taken

using a Zeiss Ultra 60 scanning electron microscope. The original image was off-line processed with background intensity subtraction and adaptive Gaussian-noise filtering to determine feature width. High resolution X-ray photoelectron spectroscopy (XPS) measurements were performed using Thermo K-Alpha XPS with a source of Al Kα micro-focused monochromator at the pressure of 10^{-9} mbar to characterize the surface modification. A value of 285 eV for the binding energy of the C_{1s} component was used to correct for charging under irradiation.

Synthesis of Vinyl Ether Silane Vinyl ether silane **1** (VE) was prepared according to a standard procedure found in the literature[18] as shown in Figure 6.2. Briefly, 3-mercaptopropyl-1-triethoxysilane and excess 2-chloroethyl vinyl ether were added to a flask equipped with a condenser along with potassium carbonate, tetra-*n*-propylammonium bromide, potassium iodide, hydroquinone, and acetonitrile. The reaction mixture was heated to 80°C and stirred overnight. The solids were removed by filtration, and the reaction mixture was further purified by removing the volatiles using rotary evaporation. The resulting brown oil was dissolved in anhydrous dichloromethane and filtered through a HMDS-passivated silica plug, and the solvent was removed to give the vinyl ether silane **1** as yellow oil.

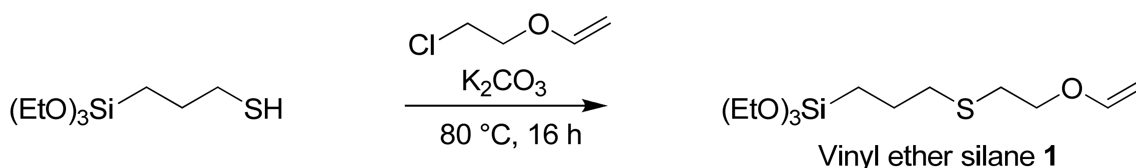

Figure 6.2 Synthetic procedure used to prepare of vinyl ether silane **1**.

Surface Modification Process Si_xN_y substrates were treated by oxygen plasma for 15 minutes to oxygenate the surface and generate surface hydroxyl groups as indicated by the low water contact angle measured immediately after plasma treatment

(~0°). The substrates were then modified with vinyl ether silane **1** by immersing the substrate in a 0.1% by volume silane solution in anhydrous dichloromethane (DCM) for different reaction time. Residual non-covalently attached silanes were removed by washing with fresh anhydrous DCM and absolute ethanol. HMDS vapor-primed Si_xN_y windowed substrates, which were used as a control substrate for adhesion testing, were prepared by vapor deposition in a vacuum oven heated to 150°C at 70 torr with a deposition time of 10 minutes.

Resist Processing The resist process consisted of spin coating of the resist films (2000 rpm, 60 sec; 97nm thick), softbaking the film at different baking conditions, e-beam exposure, post-exposure baking of the film (110°C, 1 min), development (AZ300MIF, 30 sec), rinsing of the structures in deionized water, and finally drying of the patterned film with nitrogen stream.

6.3 Results and Discussion

Vinyl ether functionalized triethoxy silane (VE) used in this work can potentially thermally crosslink to the phenolic groups in a resist, such as the ESCAP-1 resist used here, during the PAB as shown in Figure 6.1. To understand the VE process and its impact on adhesion, studies were conducted to identify conditions under which dense monolayers of VE could be deposited. 0.1% by volume VE silane solution in anhydrous dichloromethane (DCM) was used to treat a Si_xN_y window substrate used for high resolution e-beam patterning for periods of 30 minutes, 1 hour, 2 hours, and 3 hours. Residual non-covalently attached silane was removed by washing with fresh anhydrous DCM and absolute ethanol. The surface modifications were monitored by observing a change in the water contact angle of the surface. The water contact angle results for different VE reaction time are shown in the Figure 6.3A. The Si_xN_y substrate was also immersed in anhydrous DCM solution as a control test, denoted by blank triangles. The

water contact angle of the original nitride surface before oxygen plasma treatment is ~35°, star point in Fig. 6.3A. After oxygen plasma cleaning for 15 minutes, the substrate surface became highly hydrophilic due to the formation of pendant hydroxyl groups on the surface. It was also seen that the surface contact angles of DCM control increased slightly as the treatment time increases, most likely due to deposition of trace contaminants in the DCM onto the surface. With a long alkyl chain on VE structure, the VE modified surface resulted in a more hydrophobic surface condition compared to the bare silicon nitride surface itself. Surface contact angles of the VE treated surface increased with increasing VE solution reaction time and eventually reached a plateau (at less than one hour treatment) which also indicated the VE modification on the surface achieved a saturated condition fairly quickly. Since Si_xN_y thicknesses on different samples varied, separate blank silicon surface samples were used to estimate the layer thickness of vinyl ether silane formed on the surface as a function of reaction time via spectroscopic ellipsometry measurement of the film thickness. The thickness of the VE layer measured by ellipsometry on the silicon wafer for different modification times is shown in Figure 6.3B. The thicknesses of the VE layer on the silicon substrates measured by ellipsometry are also consistent with the estimated layer thickness of 11.5 Å for the VE compound as obtained from simple molecular models of the compound in an extended alkyl chain conformation. Since ESCAP-1 resist doesn't contain sulfur elements, XPS measurements can be used to detect the VE surface modification based on the presence of sulfur signal. Figure 6.4 shows the S_{2p} high resolution XPS spectra under different modification time. Although the sulfur composition is relatively slow compared to all resist composition, it still can be observed that S_{2p} signal at around 166 eV increased as the VE modification time increased. Ellipsometry data and XPS results both supported the idea that even the shortest treatment time used in this study reach dense surface coverage. To ensure dense VE coverage on the silicon nitride substrates, a two

hour modification was used to test the impact of VE in patterning performance and pattern collapse.

(A)

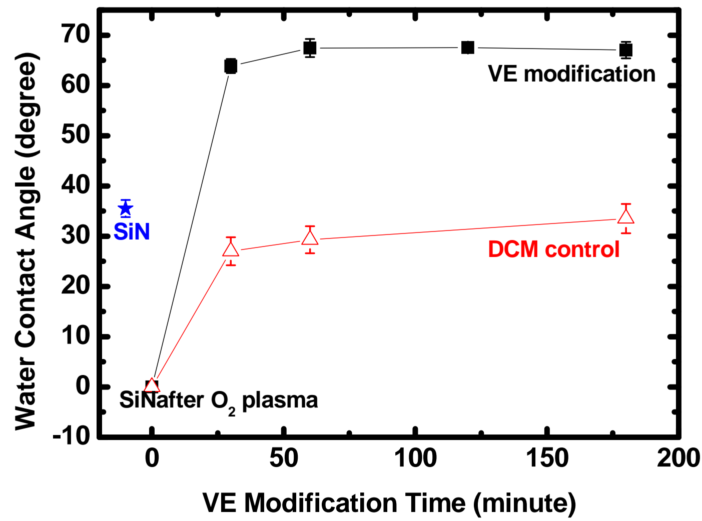

(B)

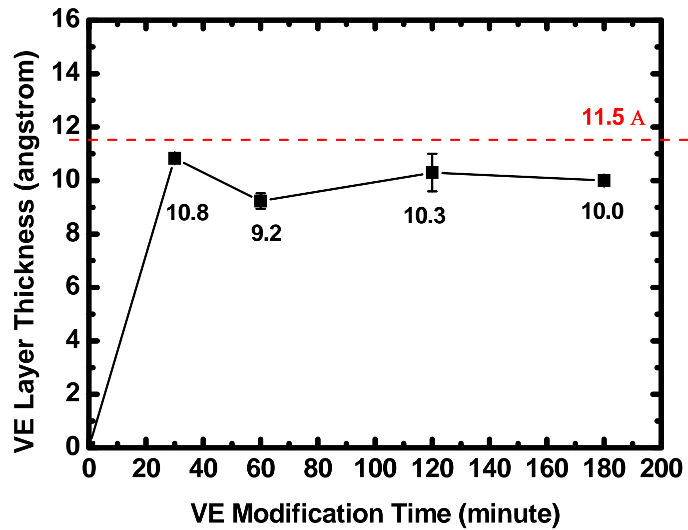

Figure 6.3 (A) Water contact angles, (B) thicknesses, and for different VE modification time. The dash line in (B) represents the thickness obtained from molecular modeling.

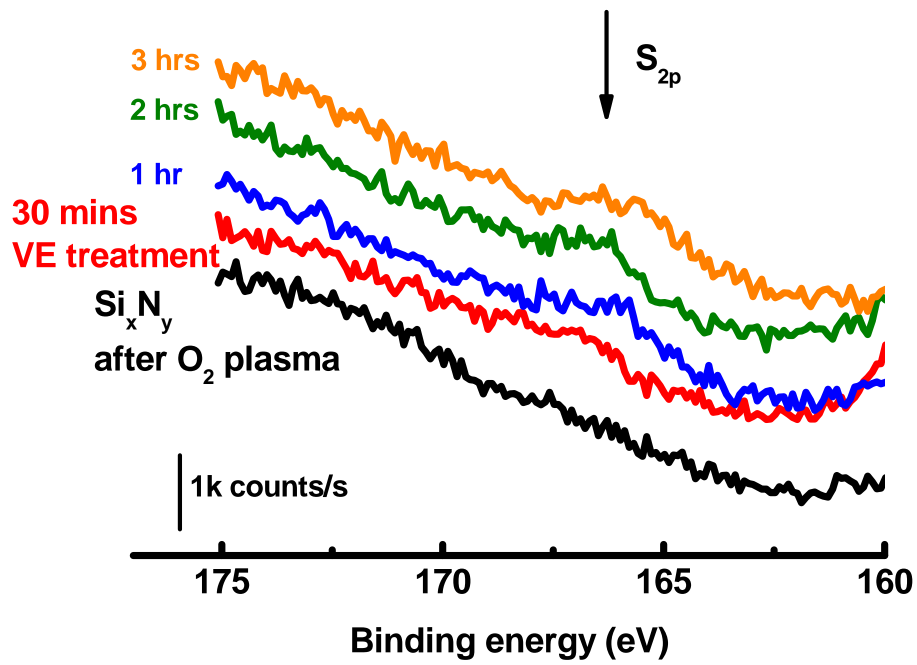

Figure 6.4 S_{2p} high resolution XPS spectra for different VE modification time.

An e-beam lithography pattern with a series of varying line and space widths was specifically designed in order to quantitatively study pattern collapse[16]. The pattern structure used in this work was designed so that the spacing (*S*) between two small parallel lines decreased from left to right varing from 200 nm down to 10 nm for a constant line width. This pattern generates increasing stress in the pairs of resist lines as one moves across the pattern array and eventually a sufficiently small space value (critical space, S_{1c}) was reached in each array such that the stress applied to the resist exceeded the critical stress (σ_c) required for pattern bending and subsequently feature deformation and collapse occurred. Smaller spacing results in higher capillary stress on the pair of resist lines. These patterns we designed allowed us to qualitatively and quantitatively study pattern collapse and obtain consistent, reproducible results.

Bare silicon nitride and HMDS vapor primed samples were also prepared for comparison, as HMDS is often used to modify the hydroxyl functional groups of surfaces, rendering them hydrophobic and more amenable towards photoresist film formation with suitable adhesive properties for lithographic purposes. Both bare silicon nitride and HMDS vapor primed samples underwent the same extended post-apply bake that was used on the vinyl ether modified samples (130 °C , 10 min) in order to eliminate any confounding effects, both positive or negative, that might be caused by the extended high temperature bake. To study the pattern failure due to the loss of adhesion and the impact of adhesion promoters, thin resist films were used which resulted in low aspect ratio beams that were spaced at large distances apart to ensure that the collapse mechanism being observed was indeed adhesion related defects and not pattern collapse by bending. The adhesion model[19] we developed suggests that pattern lines of 97 nm thick ESCAP-1 resist fail due to the loss of adhesion strength and that the collapse mechanism is dominated by adhesion strength as the line width is larger than 40 nm. Therefore, 97 nm thick ESCAP-1 resist films were used to discuss the adhesion failure. Resist films were spin-coated and baked at 130 °C for 10 min on bare silicon nitride, HMDS primed silicon

nitride, and VE modified silicon nitride substrates. E-beam lithography was used to pattern the ESCAP-1 films on the various substrates and then dried with nitrogen flow after development and rinse. The SEM images after imaging and development were shown in Figure 6.5. The arrows in the figure indicate the critical space (S_{1c}) which is the position in the pattern array with the smallest spacing between adjacent lines where resist lines can withstand the largest capillary stress before collapse. Smaller critical spaces represent cases where the resist lines could endure higher capillary force without collapse. In Figure 6.5, the first column shows the images of nominal 50 nm line width for bare silicon nitride, HMDS primed, and VE modified samples. The images of nominal 60nm line width are shown in the second column. The bare silicon substrate without any surface treatment displayed very serious adhesion failure in Figure 6.5A and D. No lines remain on the test structure. For the HMDS vapor primed sample (Figure 6.5B and E), the adhesion failure was improved and pattern lines can stand at smaller critical space. It was also seen that the use of the VE silane as an adhesion promoter (Figure 6.5C and F) resulted in smallest critical space and enhanced adhesion relative to bare silicon nitride samples and simple HMDS vapor primed samples.

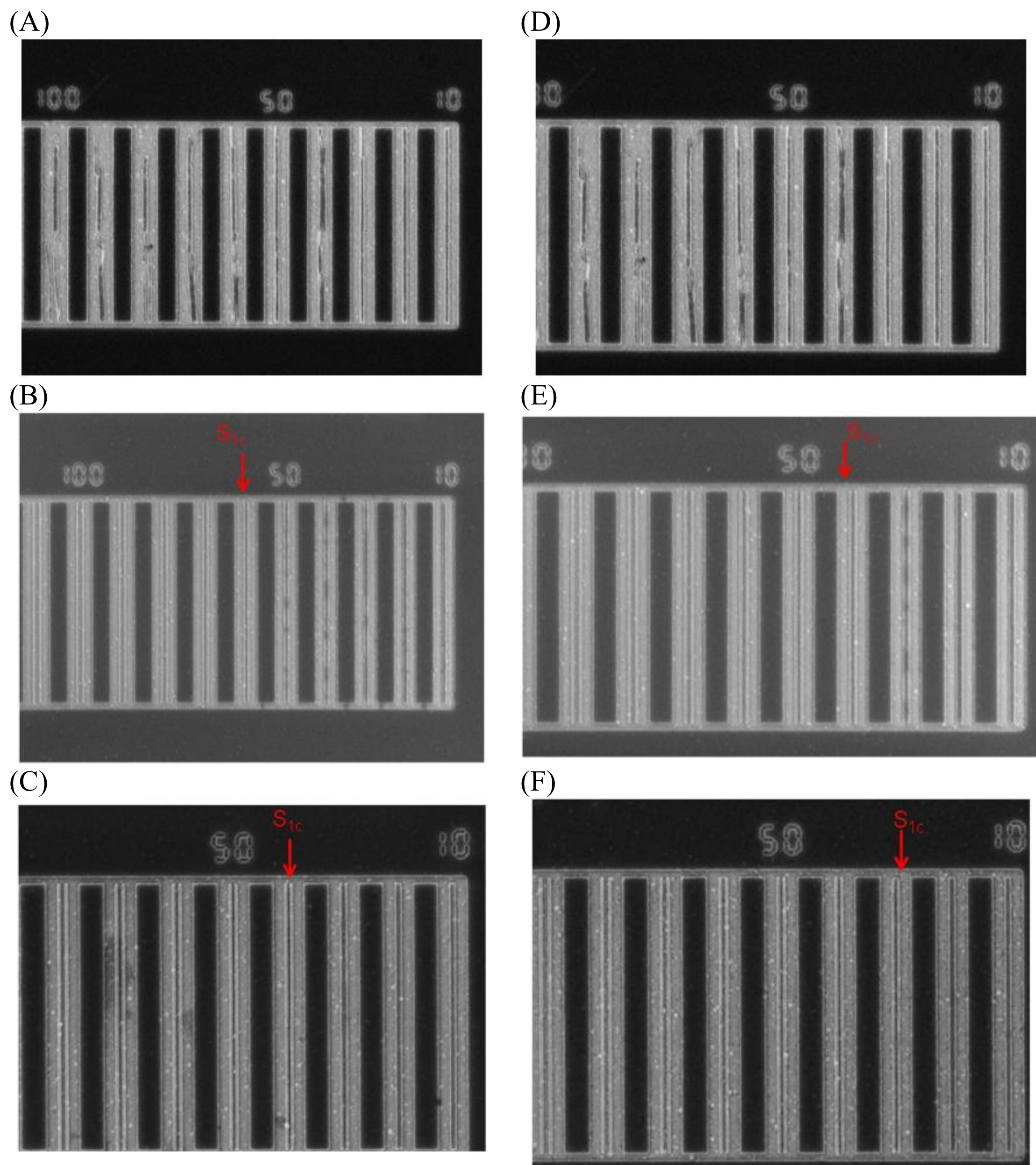

Figure 6.5 SEM images for different substrate treatments. Images of nominal 50 nm line width: (A) Bare Si_xN_y, (B) HMDS primed Si_xN_y, and (C) VE modified Si_xN_y; Images of nominal 60 nm line width: (D) Bare Si_xN_y, (E) HMDS primed Si_xN_y, and (F) VE modified Si_xN_y.

In this chapter, vinyl ether functionality was chosen due the fact that it has been well-established that such groups are capable of forming covalent bonds with phenolic hydroxyl moieties at elevated temperatures[14]. Therefore, the effect of soft-bake condition is very important for the reaction of covalently binding the ESCAP-1 with the VE modified substrate. SEM images of resist patterns of nominal 50 nm line widths formed on VE samples made using different soft baking conditions were taken and shown in Figure 6.6. Increasing the soft bake temperature to 140 ^{o}C for 20 minutes showed more serious adhesion failure. There is no complete line surviving on the sample made using the baking condition of 140 ^{o}C for 20 minutes as shown in Figure 6.6A. For the VE sample of 130 ^{o}C for 10 minutes (Figure 6.6B), the critical space is 60 nm resist and lines below critical space all collapsed. For the VE sample baked at 120 ^{o}C for 10 minutes, the critical space shifted from 60 nm to 30 nm. It is indicated that lower bake temperature resulted in better adhesion strength and better pattern behavior.

Figure 6.7 shows the critical stresses for different substrates and baking conditions. The critical stress (σ_c) is defined as the maximum stress that can be applied to the photoresist lines prior to pattern collapse and occurs in critical space, the last space before the pair of resist lines collapse on the pattern structure we designed. The equation used to calculate the critical stress is expressed in equation (6.1), where γ is surface tension of rinse liquid (i.e. deionized water with γ =0.073 N/m), θ is the contact angle of the rinse liquid on the photoresist (i.e. deionized water with θ=77° in ESCAP-1 case), height H is the thickness of the photoresist film, S_2 is the respective outside space width between the lines of the pattern we designed, and S_{1c} is the critical pattern center space width where collapse is first indicated. More detail about this critical stress analysis has been published in our previous work[16].

$$\sigma_C = 6\gamma \cos\theta \left(\frac{H}{W}\right)^2 \left(\frac{1}{S_{1c}} - \frac{1}{S_2}\right) \tag{6.1}$$

Critical stress is measured at the final stress point before the resist lines collapses. It allows direct comparisons that are independent of pattern size and film thickness. The higher critical stress represents that resist lines have stronger resistance to capillary stress. In figure 6.7, without any surface modification, bare silicon nitride samples displayed a lowest critical stress, and a worse general patterning performance. For the samples treated with HMDS priming, critical stress was better than for the bare silicon nitride substrates. For the samples treated with the VE (SiN/VE) reactive adhesion promoter, resist adhesion and resistance to pattern collapse was even better than in the case of HMDS substrates. While baking conditions had little effect on the HMDS primed samples in terms of resist adhesion and pattern collapse, the baking conditions used in the VE samples had a significant impact on such behavior. Of the three temperatures chosen for the post-apply bake (i.e. PAB or soft bake), the lowest temperature of 120 °C was found to give the best resistance to pattern collapse in comparison to 130 °C and 140 °C samples. For the VE sample soft baked at 120 °C for 10 min, resistance to pattern collapse was improved for small resist features, with the samples exhibiting a critical stress of ~4 MPa as compared to only a ~2.5 MPa critical stress for samples made with a 140 °C PAB. The higher temperature may enhance the reaction of covalently binding the ESCAP-1 with the VE modified substrates but may also have a negative impact on the Si-O bonding. The optimization of baking condition can potentially improve pattern adhesion even more.

(A)

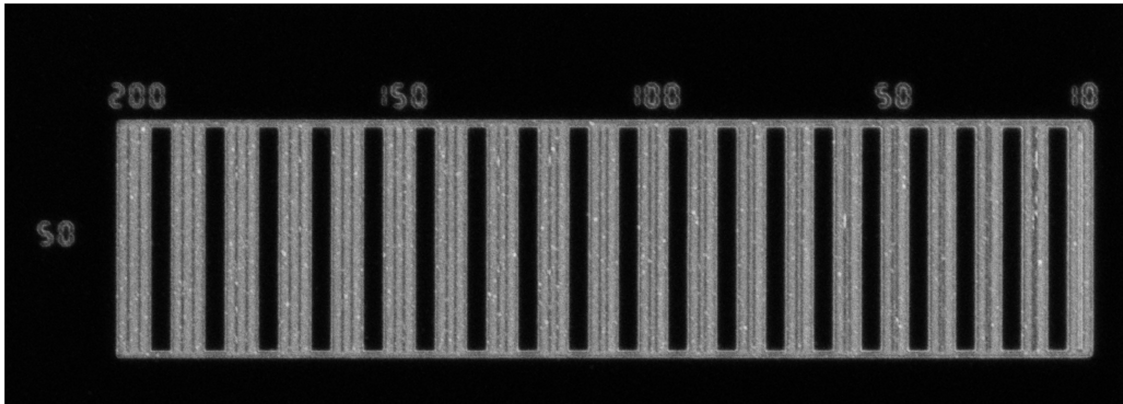

(B)

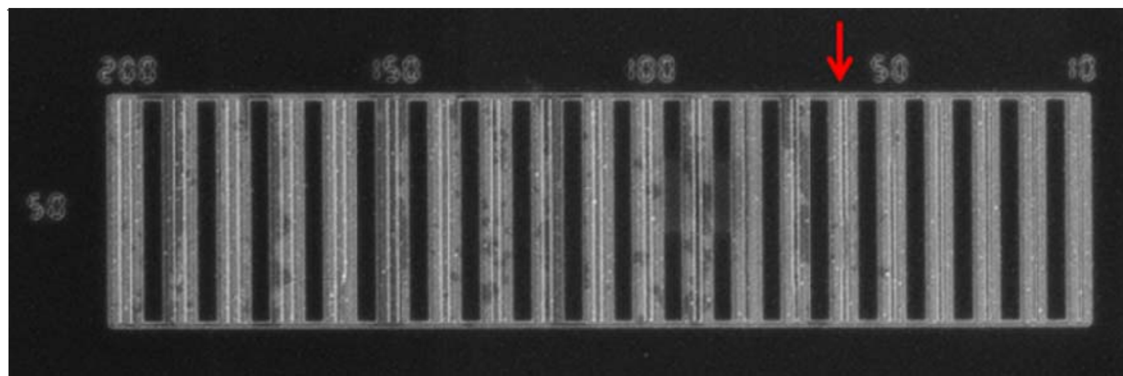

(C)

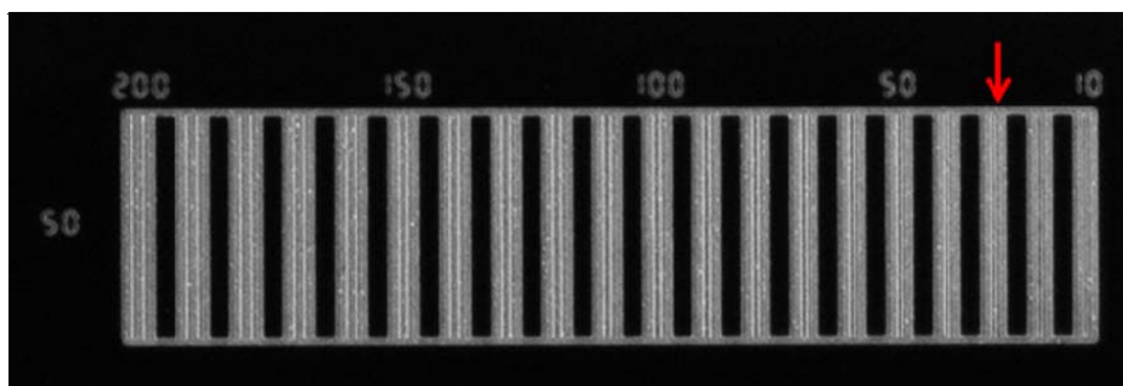

Figure 6.6 SEM images of nominal 50nm line widths on VE samples using different soft-bake conditions: (A) 140°C for 20 min, (B) 130°C for 10 min, and (C) 120°C for 10 min.

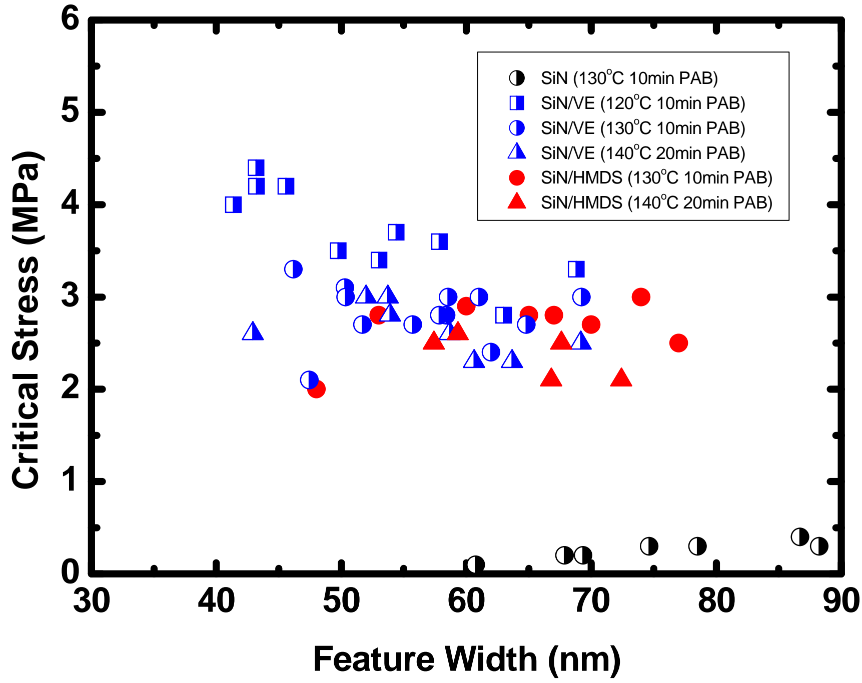

Figure 6.7 Critical stresses at the point of pattern collapse as a function of feature width in different substrates and baking conditions. All films are 97 nm thick.

In previous study[19], our adhesion model based on use of a Hamaker constant (A) description of the resist-surface interaction appears to describe collapse behavior well on HMDS surfaces at low aspect ratios. The adhesion model is described in equation (6.2).

$$S_{1c} = \frac{12\pi h_0^{\ 3} H\gamma \cos\theta \cdot S_2}{AWS_2 + 12\pi h_0^{\ 3} H\gamma \cos\theta} \tag{6.2}$$

Different resist-substrate conditions resulted in different values of Hamaker constant (i.e. effective Hamaker constant, A_{eff}). Therefore, the experimental data from VE treatment can be used to calculate the effective Hamaker constant using the parameter fitting in our adhesion model. Figure 6.8 shows the critical stress comparison for experimental data and the fitting results from our adhesion model. The Hamaker constant is defined as the body-body interaction. High effective Hamaker constant represents

stronger interaction force and better adhesion strength. Effective Hamaker constants for HMDS and VE substrates are 0.8 and 1.2×10^{-20} J respectively. VE treatment results in 50% improvement in effective Hamaker constant and better adhesion strength compared to HMDS vapor priming samples.

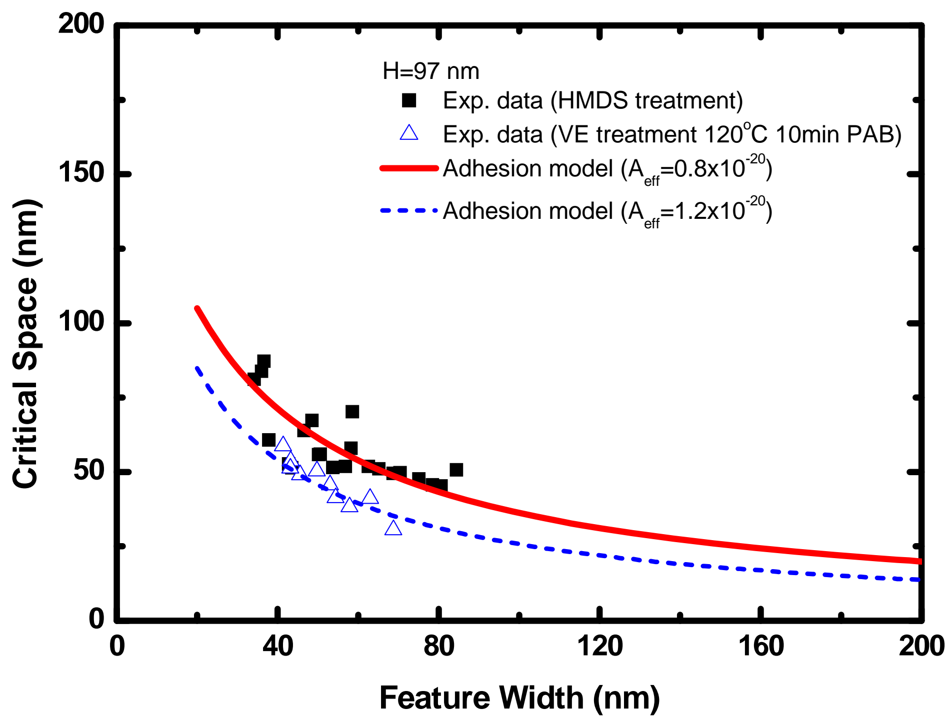

Figure 6.8 Critical spaces of experimental data and modeling results for HMDS and VE samples.

6.4 Conclusions

We have developed a reactive adhesion promoter composed of a vinyl ether functionalized silane (VE) capable of covalently attaching phenolic resists to the substrate surface during the post-apply bake process. Compared to traditional HMDS vapor primed substrates, the implementation of the VE adhesion promoter resulted in a significant improvement in the adhesion and resistance to adhesion based pattern collapse failure in small sub-60 nm resist features. Soft bake conditions have also been discussed. The lower baking temperature for vinyl ether modified samples can enhance the pattern adhesion and resist lines can stand in higher capillary stress. Effective Hamaker constants obtained from our adhesion model also confirmed that the VE modified sample showed significant improvement in pattern collapse based on adhesion failure and resulted in 50% improvement in resist-substrate interaction.

6.5 References

1. Tanaka, T.; Morigami, M.; Atoda, N., Mechanism of Resist Pattern Collapse during Development Process. *Jpn J Appl Phys 1* **1993,** *32* (12B), 6059-6064.

2. Alvine, K. J.; Ding, Y. F.; Douglas, J. F.; Ro, H. W.; Okerberg, B. C.; Karim, A.; Lavery, K. A.; Lin-Gibson, S.; Soles, C. L., Effect of Fluorosurfactant on Capillary Instabilities in Nanoimprinted Polymer Patterns. *J Polym Sci Pol Phys* **2009,** *47* (24), 2591-2600.

3. Huang, V.; Chiu, C. C.; Lin, C. A.; Chang, C. Y.; Gau, T. S.; Lin, B. J., Effect of novel rinsing material and surfactant treatment on the resist pattern performance. *Proc. SPIE* **2007,** *6519*, 65193C-9.

4. Zweber, A. E.; Wagner, M.; DeYoung, J.; Carbonell, R. G., Mechanism of Extreme Ultraviolet Photoresist Development with a Supercritical CO(2) Compatible Salt. *Langmuir* **2009,** *25* (11), 6176-6190.

5. Ouyang, C. Y.; Lee, J. K.; Ober, C. K., Studies of Environmentally Friendly Solvent-based Developers. *J Photopolym Sci Tec* **2011,** *24* (2), 239-240.

6. Lee, M. Y.; Do, K. M.; Ganapathy, H. S.; Lo, Y. S.; Kim, J. J.; Choi, S. J.; Lim, K. T., Surfactant-aided supercritical carbon dioxide drying for photoresists to prevent pattern collapse. *J Supercrit Fluid* **2007,** *42* (1), 150-156.

7. Drechsler, A.; Belmann, C.; Synytska, A.; Petong, N.; Grundke, K.; Stamm, M.; Reichelt, J.; Wunnicke, O., The adsorption of cationic surfactants on photoresist surfaces and its effect on the pattern collapse in high aspect ratio patterning. *Colloid Surface A* **2007,** *311* (1-3), 83-92.

8. Guerrero, D. J.; Xu, H.; Mercado, R.; Blackwell, J., Underlayer Designs to Enhance EUV Resist Performance. *J Photopolym Sci Tec* **2009,** *22* (1), 117-122.

9. Kawai, A.; Moriuchi, T.; Niiyama, T.; Kishioka, T.; Maruyama, D.; Sakaida, Y.; Matsumoto, T., Adhesion improvement of ArF resist pattern depending on BARC material. *Microelectron Eng* **2006,** *83* (4-9), 659-662.

10. Kurano, K.; Kishioka, T.; Hiroi, Y.; Ohashi, T.; Kawai, A., Peeling analysis of ArF resist pattern on BARC by using AFM. *J Photopolym Sci Tec* **2007,** *20* (6), 825-826.

11. Park, E. M.; Choi, J.; Kang, B. H.; Dong, K. Y.; Park, Y.; Song, I. S.; Ju, B. K., Investigation of the effects of bottom anti-reflective coating on nanoscale patterns by laser interference lithography. *Thin Solid Films* **2011,** *519* (13), 4220-4224.

12. Helbert, J. N.; Saha, N., Application of Silanes for Promoting Resist Patterning Layer Adhesion in Semiconductor Manufacturing. *J Adhes Sci Technol* **1991,** *5* (10), 905-925.

13. Cho, W. K.; Kong, B.; Park, H. J.; Kim, J.; Chegal, W.; Choi, J. S.; Choi, I. S., Long-term stability of cell micropatterns on poly((3-(methacryloylamino)propyl)-dimethyl(3-sulfopropyl)ammonium hydroxide)-patterned silicon oxide surfaces. *Biomaterials* **2010,** *31* (36), 9565-9574.

14. Song, J. H.; Sailor, M. J., Chemical modification of crystalline porous silicon surfaces. *Comment Inorg Chem* **1999,** *21* (1-3), 69-84.

15. Moon, S.; Kamenosono, K.; Kondo, S.; Umehara, A.; Yamaoka, T., 3-Component Photopolymers Based on Thermal Cross-Linking and Acidolytic De-Cross-Linking of Vinyl Ether Groups - Effects of Binder Polymers on Photopolymer Characteristics. *Chem Mater* **1994,** *6* (10), 1854-1860.

16. Yeh, W. M.; Noga, D. E.; Lawson, R. A.; Tolbert, L. M.; Henderson, C. L., Comparison of positive tone versus negative tone resist pattern collapse bahavior. *J Vac Sci Technol B* **2010,** *28* (6), C6s6-C6s11.

17. Lee, C.-T.; Wang, M.; Jarnagin, N. D.; Gonsalves, K. E.; Roberts, J. M.; Yueh, W.; Henderson, C. L., Photosensitivity and line-edge roughness of novel polymer-bound PAG photoresists. *Proc. SPIE* **2007,** *6519*, 65191E-9.

18. Youssef, B.; Lecamp, L.; Garin, S.; Bunel, C., New synthesis of photocurable silanes and polysiloxanes bearing heterocyclic or olefinic functions. *Nucl Instrum Meth B* **1999,** *151* (1-4), 313-317.

19. Yeh, W. M.; Lawson, R. A.; Henderson, C. L., A comprehensive model and method for model parameterization for predicting pattern collapse behavior in photoresist nanostructures. *Proc. SPIE* **2011,** *7972* (1), 79721X.

CHAPTER 7

EFFECT OF DRYING RATE ON PATTERN COLLAPSE BEHAVIOR IN THIN FILM LITHOGRAPHY

Pattern collapse during development and drying can have a substantial impact on process viability in nanolithography. Pattern collapse in, general, is caused by unbalanced capillary forces generated during final drying. Significant research has focused on developing methods to reduce such capillary forces and ameliorate pattern collapse. However, it appears that relatively little attention has been paid to other process-dependent factors which may also significantly impact such behavior. For example, another factor which may affect pattern collapse is drying time, during which the resist features are actually stressed. In this work, test structures were dried using a variety of drying conditions, and the impact of these different methods on pattern collapse was quantified. Drying rate had a dramatic impact on pattern collapse. In addition, spin drying also exhibited a significant pattern orientation dependence of pattern collapse at small scale.

7.1 Introduction

As the semiconductor industry continues to push the limits of the lithography processes used to fabricate integrated circuits, pattern collapse during development becomes a limiting factor. Pattern collapse is caused by capillary forces acting on the structures during drying. The main factors affecting pattern collapse can be classified into three groups[1,2]: (1) pattern geometry; (2) physical properties of the photoresist; (3) capillary forces induced by drying of the rinse liquid. In general, the first two factors are

determined by device design and by the physical properties required in the resist for acceptable imaging performance. These are not easily adjustable to compensate for pattern collapse problems. Therefore, significant research has focused on developing methods to reduce capillary forces and to improve the pattern collapse performance. Several groups have studied the use of alternative lithographic rinse and drying processes, including reducing capillary forces by use of surfactants in final rinse liquids. Drechsler and coworkers found that a rinse with cationic surfactants yields a reduction in observed pattern collapse for small photoresist test structures[3]. Other groups reported that the use of surfactant rinse in the development step provides significant improvement in photoresist patterning behavior, including reduced pattern collapse and reduced line width roughness[4,5]. Although appropriate surfactants in the development step can reduce the surface tension of rinse solvent and the contact angle of rinse liquid on the resist wall, patterns rinsed with surfactant appear to suffer shrinkage and deformation if the surfactant penetrates too deep into the resist[3,5]. Another approach for the reduction of surface tension is to apply a supercritical fluid. Supercritical carbon dioxide drying has also been demonstrated to eliminate the capillary forces naturally present during normal drying[6,7].

In contrast, relatively little attention has been paid to other process-dependent factors which may also significantly impact such collapse behavior. Our goal was to probe the extent to which the time during which a resist structure is subjected to capillary force-induced loads affects the pattern collapse behavior of such structures. This focus is on modulating drying rate of the final rinse liquid (water) and quantifying the observed changes in pattern collapse. The different methods used in this work are: (1) drying slowly by normal evaporation in stagnant room air, (2) drying in a vacuum oven, (3) drying in a flowing nitrogen stream, and (4) spin-drying. The effect of these different drying methods on the resulting pattern collapse behavior has been quantified by measuring the change in the critical stress at the point of pattern collapse using simple

parallel line resist test structures subjected to the different drying conditions. E-beam lithography was used as previously described to generate these pattern collapse test structures[8,9] and SEM analysis of the resulting features was used to compute the critical stress at the point of collapse for resist lines of varying widths under the different drying conditions. The effect of pattern orientation with respect to the wafer radius during spin drying was also analyzed.

7.2 Experimental

Materials and Equipments A model photoresist, consisting of a resin supplied by JSR and Intel (referred to here as ESCAP-1--a terpolymer of hydroxystyrene, styrene, and *t*-butyl methylmethacrylate consisting of monomer mole fractions of 0.6, 0.2, 0.2 respectively, see Figure 7.1), a triphenylsulfonium nonaflate (TPS-Nf) photoacid generator, and a trioctylamine (TOA) base quencher, was created by dissolving all the components in propylene glycol methyl ether acetate (PGMEA) at loadings of 7.4 wt% total solids in PGMEA with 5 wt% TPS-Nf relative to ESCAP-1 and 10 mol% TOA relative to the TPS-Nf PAG. All reagents, with the exception of the resin, were purchased from Sigma-Aldrich, VWR, or Alfa-Aesar. E-beam lithography was carried out using a JEOL JBX-9300FS e-beam lithography system with an accelerating voltage of 100 kV, a beam diameter of 8 nm, a 2 nA current, and a 10 nm shot pitch. Si_3N_4 windowed substrates, used in order to eliminate electron backscatter from the substrate and thus produce extremely sharp aerial images and essentially vertical sidewalls, have been described elsewhere[10]. Such perfectly rectangular resist profiles make analysis of the resulting pattern collapse much simpler and more reliable than in the case of the rounded profiles that can be obtained from degraded aerial images produced using other exposure tools such as optical projection lithography systems. SEM images of the resulting high

resolution resist test structures were collected using a Zeiss Ultra 60 scanning electron microscope.

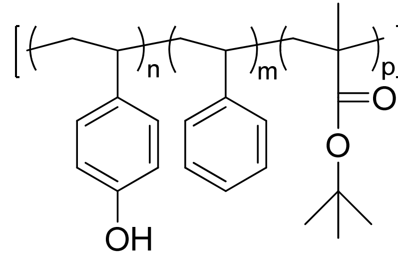

Figure 7.1 The model resist used in this work: ESCAP-1 (mole fractions n:m:p = 0.6:0.2:0.2).

Resist and Drying Processing Before coating of the photoresist, the Si_3N_4 substrates were modified by HMDS vapor priming to improve adhesion. The resist process consisted of spin coating of a 252nm resist film (3700 rpm, 60 sec), soft-baking (110°C, 2 min), exposing the pattern using a 50 μC/cm^2 dose, post-exposure baking (110°C, 1 min), development (AZ300MIF, 30 sec), rinsing in deionized water, and drying of the patterned film under different methods as described above.

Process Pattern Collapse Analysis An e-beam lithography pattern with a series of varying line and space widths was designed specifically to quantitatively study pattern collapse (see Figure 7.2). With our particular pattern design, as the S_1 spacewidth decreased from left to right in the images shown for a set of lines with a constant line width W, pattern collapse would occur when a sufficiently small S_1 value was reached such that the stress applied to the resist exceeded the critical stress required for pattern bending and deformation as shown in Figure 7.2. The initial pressure difference acting on the resist lines can be described using equation (7.1) where γ is the surface tension of the final rinse liquid (i.e. deionized water with γ=0.073 N/m in ESCAP-1 case), θ is the contact angle of the rinse liquid on the photoresist (i.e. deionized water with θ=~77° in

ESCAP-1 case), and S_1 and S_2 are the respective inside and outside space widths between the lines of the pattern. Features W and outside widths space S_2 of the patterns were measured from SEM images using custom MATLAB software.

$$\Delta P = 2\gamma \cos\theta \left(\frac{1}{S_1} - \frac{1}{S_2} \right) \tag{7.1}$$

$$\sigma_c = 6\gamma \cos\theta \left(\frac{H}{W} \right)^2 \left(\frac{1}{S_{1c}} - \frac{1}{S_2} \right) \tag{7.2}$$

The critical space width in the test patterns, S_{1c} was determined by identifying the point in each test structure array for which the smallest S_1 was observed between a pair of adjacent lines in the test structure that exhibited no collapse or deformation. In this way, using S_{1C} it is possible to estimate the maximum stress a photoresist line can withstand before pattern deformation and collapse occurs. The equation used to calculate this critical stress is shown in equation (7.2), where W is the width of the resist feature, height H is the thickness of the photoresist film, and S_{1C} is the critical pattern center space width for which smaller S_1 space widths clearly exhibited some formation or collapse. Additional details about this critical stress analysis have been previously published[8].

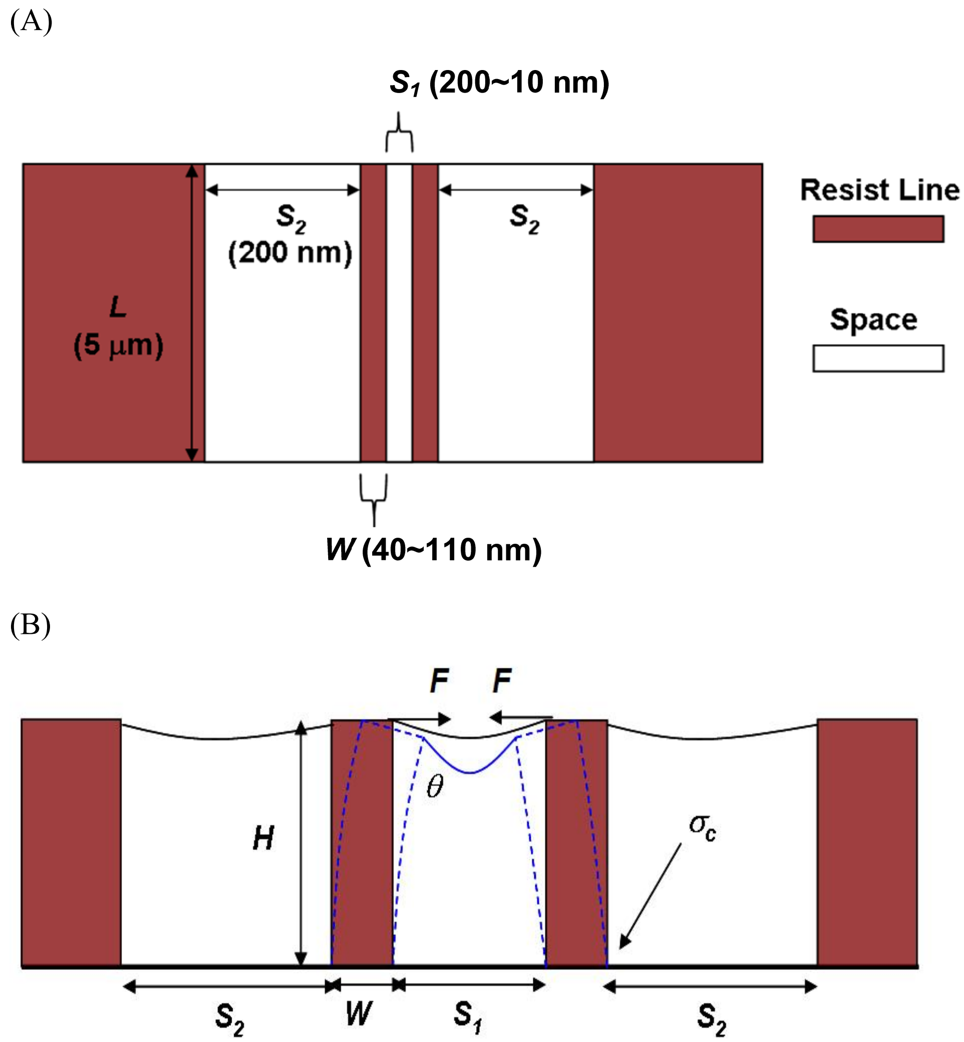

Figure 7.2 (A) Top view and (B) side view of one parallel line test pattern element in the large test pattern array design used for studying pattern collapse in this work.

7.3 Results and Discussion

The different drying methods used in this work are: (1) samples dried slowly by normal evaporation in stagnant room air, (2) samples dried in a vacuum oven, (3) samples dried by a flowing nitrogen stream, and (4) samples dried by the spin dryer at 4500rpm for 3mins. The experimental process is shown schematically in Figure 7.3. Different drying methods resulted in different lengths of time during which the resist features were actually stressed during drying. The sample dried in stagnant room air took the longest time, and samples dried by flowing nitrogen stream and dried by the spin dryer dried very quickly. Figure 7.4 shows SEM images of nominal 70nm wide line pattern pair arrays after drying via these different methods. Samples dried in the atmosphere and in the vacuum also showed somewhat unusual collapse behavior. In these cases, there was a relatively large range of S_I space widths over which only a portion of the resist line collapsed. These ranges of S_I space widths over which only a portion of the resist line collapsed are highlighted in the red boxes in Figure 7.4. What of course might be expected is that once the S_I space width decreased below a critical value (i.e. S_{IC}), that the stress exerted on the resist line would be sufficient to collapse the entire resist line over virtually its complete length. The number of different S_I widths over which this partial pattern collapse was observed to occur also appears to be correlated with the drying rate, with the slowest drying rate (i.e. in stagnant air) exhibiting the largest range of such behavior. The arrows in the SEM images shown in Figure 7.4 indicate the position of critical space S_{IC} selected from each test pattern array. Based on equation (2), smaller critical space (S_{IC}) values represent cases where the resist lines can withstand higher critical stress values and still not exhibit pattern collapse. Since one would expect that the S_{IC} value would be constant for a given resist material coated at a particular film thickness and imaged at a particular line size (i.e. that the critical stress is determined by either the adhesion energy of the resist on the surface (i.e. for adhesion based pattern failure) or the effective modulus and yield behavior of the polymer nanostructure (i.e. for

elastoplastic deformation) depending on the mode of pattern collapse observed), the results shown in Figure 7.4 suggest that the drying method has a significant effect on the critical stress that a resist nanostructure can withstand. The SEM images shown in Figures 7.4C and 7.4D reveal that patterns dried by spin drying and by flowing dry nitrogen gas exhibit superior resistance to pattern collapse.

Tilted SEM images of nominal 90nm line pattern pairs from these pattern collapse test arrays are shown in the Figure 7.5. The tilted images also reveal that samples dried by flowing nitrogen and by spin drying show superior resistance to pattern collapse.

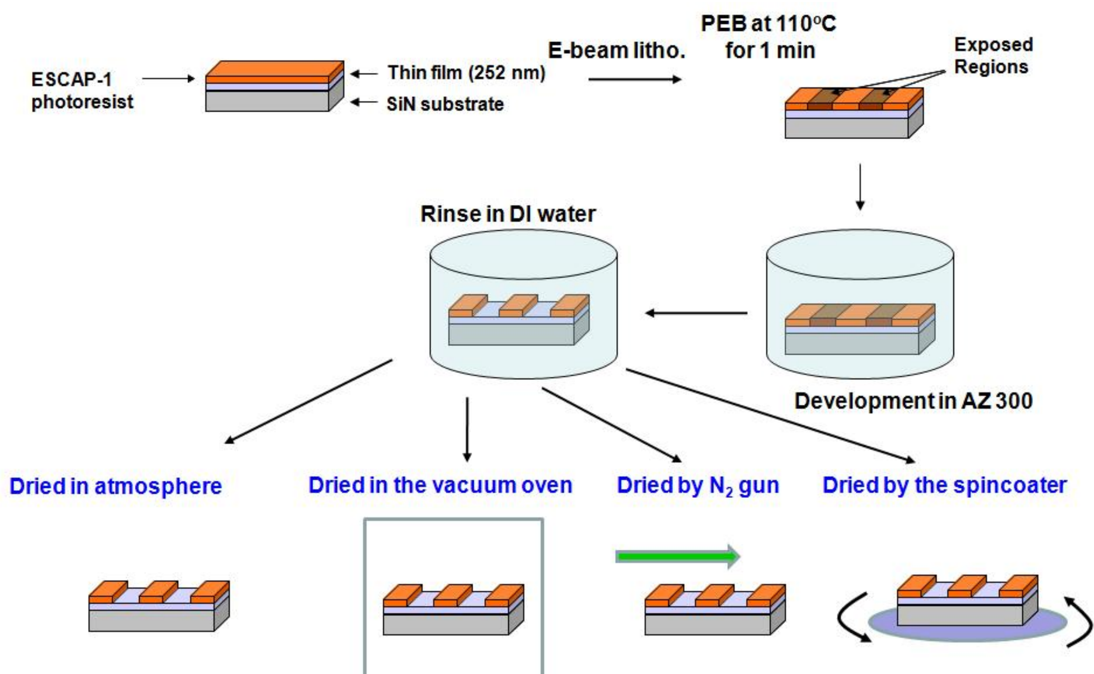

Figure 7.3 A flow chart of experimental process.

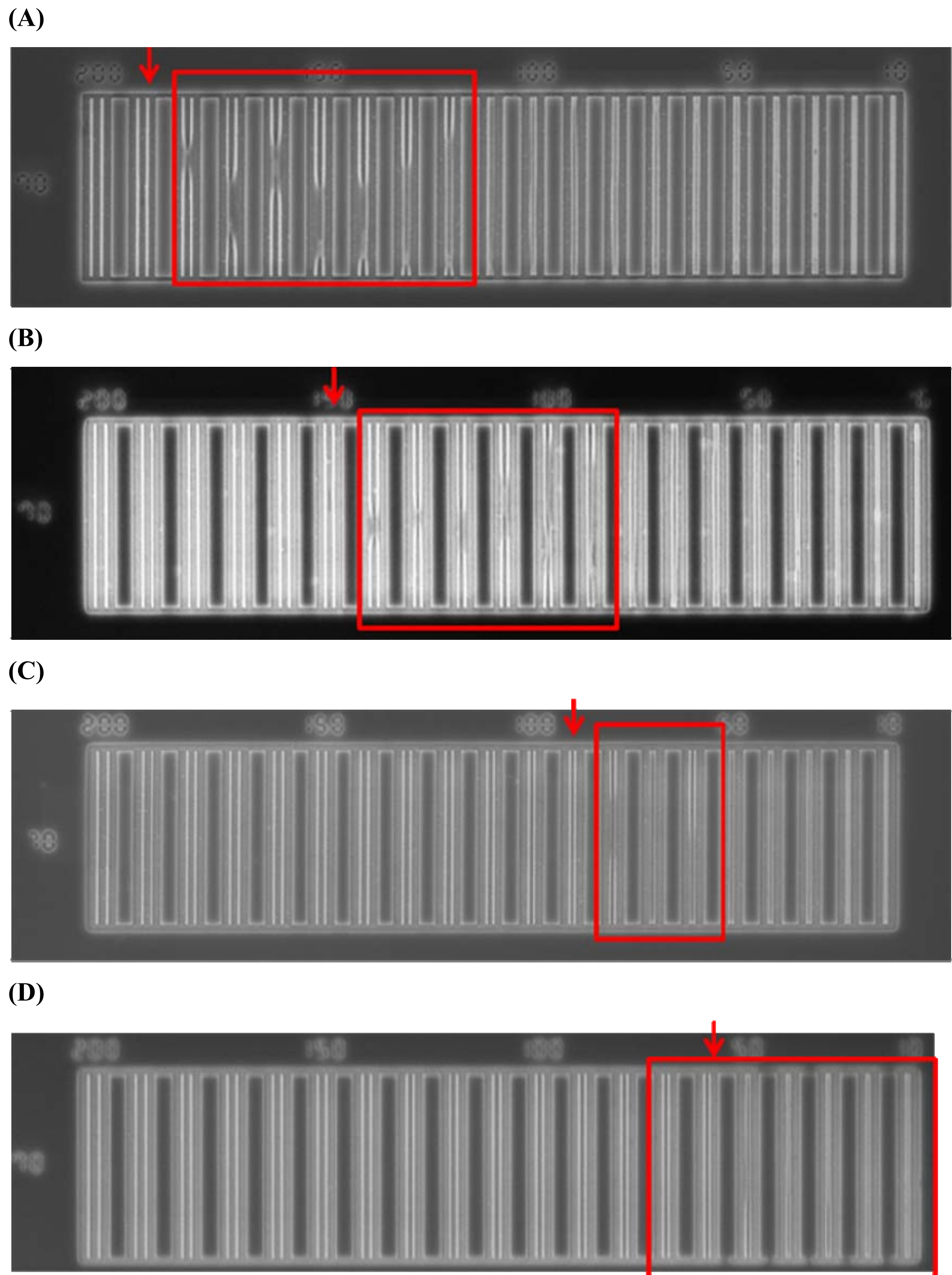

Figure 7.4 SEM images for different drying methods. Nominal 70 nm wide line pairs dried (A) in stagnant room air, (B) in a vacuum oven, (C) under flowing dry nitrogen gas, and (D) by spin drying at 4500rpm for 3mins.

(A)

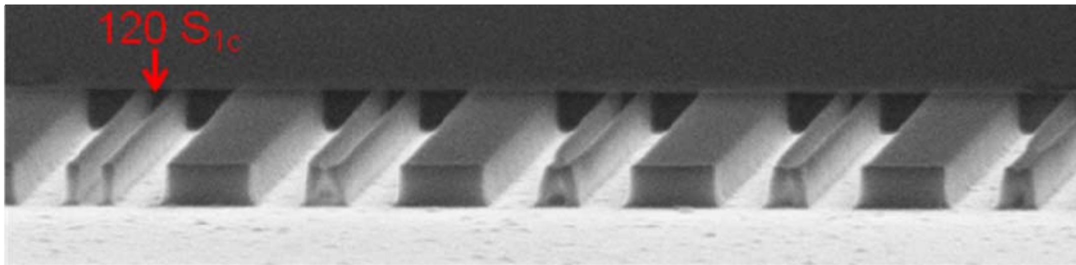

(B)

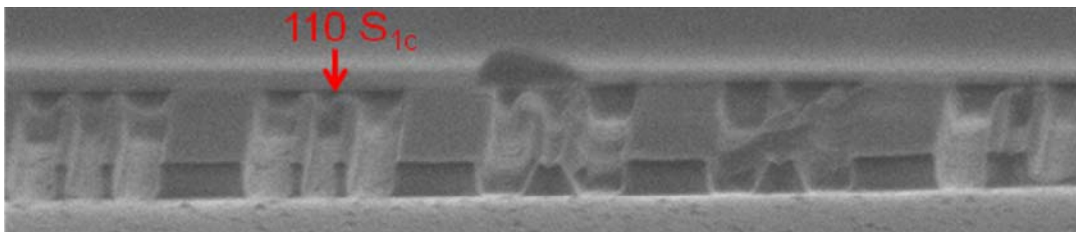

(C)

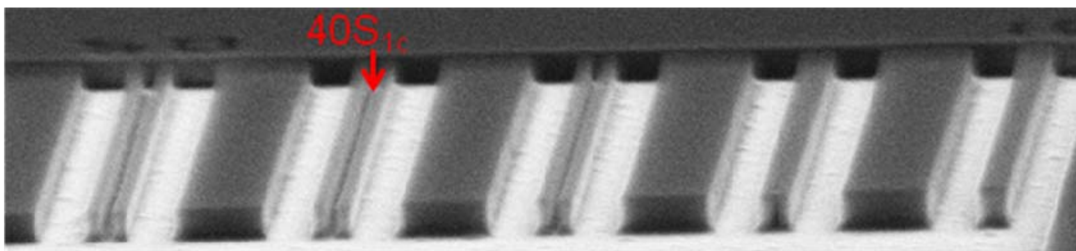

(D)

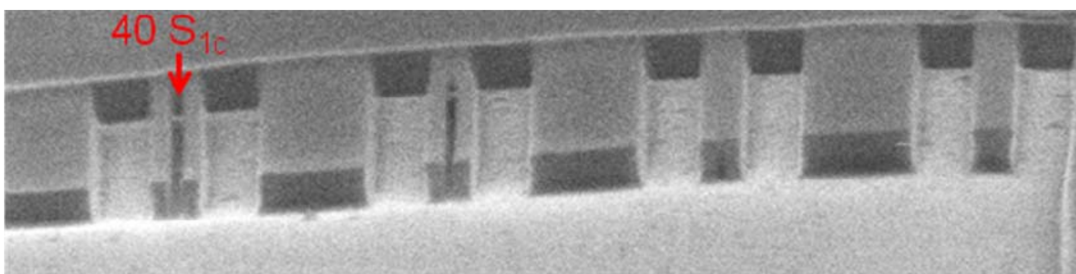

Figure 7.5 Tilted SEM images for different drying methods. Nominal 90 nm line width dried (A) in atmosphere, (B) in the vacuum oven, (C) by nitrogen blow, and (D) by the spinner with 4500rpm for 3mins.

Figure 7.6 shows the critical stress as a function of feature width calculated using the S_{IC} data collected from the pattern test arrays for the different drying methods used in this work. The critical stress (σ_c) can be defined as the maximum stress that can be applied to the photoresist lines prior to pattern collapse. This plot of critical stress versus feature width indicates that pattern collapse becomes worse (i.e. lower critical stress at the point of collapse) when slower drying rate drying processes are used. This data suggests that it is not simply a critical force or stress (e.g. a yield stress) which is exceeded to cause collapse, but rather that it is the combination of a force or stress exerted over a period of time. This suggests that it is possible that polymer creep phenomena may be involved in the collapse behavior of polymer resist nanostructures dried at slower drying rates.

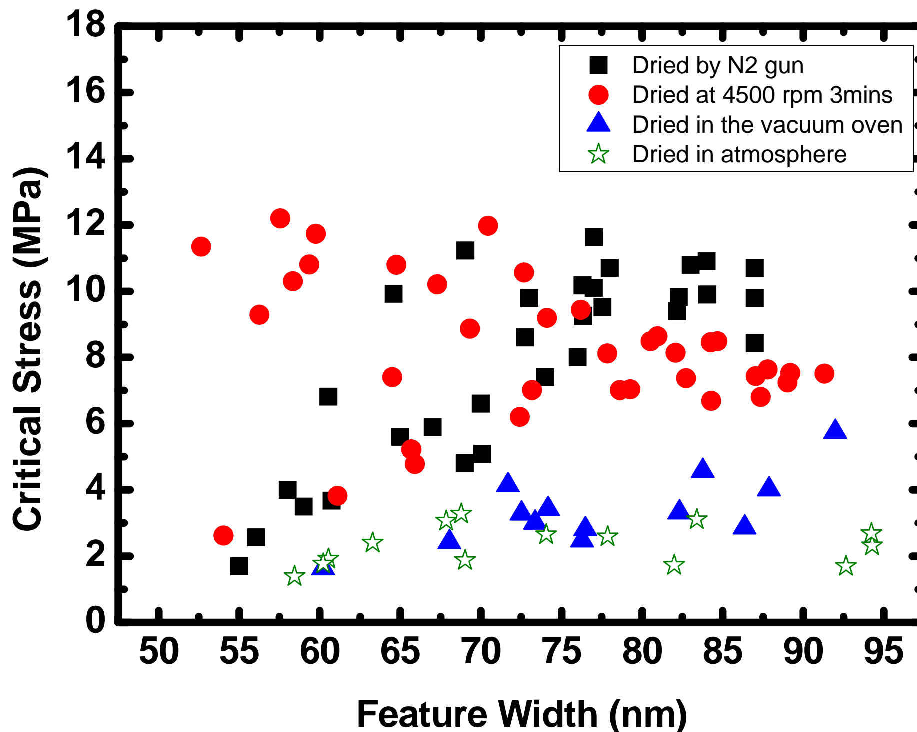

Figure 7.6 Critical stresses as a function of feature width for different drying methods.

Another remarkable discovery in Figure 7.6 is that seemingly different critical stress trends were observed within the overall data set collected for the samples dried by spin drying (red circles). This divergence of the critical stress data into two populations or trends for small line widths in the spin dried samples was not observed in other samples dried with other techniques. Therefore, we speculate that pattern orientation with respect to wafer radius may be a controlling factor in this behavior if fluid flow effects are involved in the forces responsible for collapse. A schematic of the array design on the substrate is shown in Figure 7.7A. Each test sample contains a 6 row by 7 column array of thin SiN membrane windows on top of which the high resolution pattern collapse test structures are patterned using e-beam lithography. The patterns in the upper 4 rows (i.e. green box in Figure 7.7A) of the array contain high resolution line pair pattern collapse test structure arrays (see Figure 7.2) where each array appears as shown schematically in Figure 7.7B. These test structures are the ones from which the critical stress data are collected. The bottom two rows of the array contain open ended line pair arrays (see Figure 7C for a schematic of the test structure design that appears in those windows of the array) that are used for tilted and cross-section imaging as shown in Figure 7.5. Since the test structures in each of the arrays shown in the green box in Figure 7.7A are nominally identical, it is possible to determine the effect of their orientation with respect to the sample center and radius from center on the observed critical stress and collapse behavior. The patterned line features in the upper 4 rows of the array are all oriented such that their lines and spaces run length-wise up and down as shown in the schematics in Figure 7.7A and 7.7B. Therefore, the fourth column of the array has features that are oriented with their lines running parallel to the wafer sample radius during spin drying (i.e. the column shown with the blue dashed line in Figure 7.7A). The sample is mounted such that the fourth row of the array has features that are oriented perpendicular to the wafer sample radius during spin drying (i.e. the row shown with the red dashed line in Figure 7.7A). The other windows in the array contain lines that have orientations that are

to varying degrees set at some angle diagonal to the wafer sample radius during spin drying. By looking at windows that are in a position where their row number and column number are equal, the effect of having the lines at an approximately 45 degree angle to the wafer sample radius can be determined. Such a grouping of the pattern orientations with respect to the sample radius during spin drying reveals what appears to be some effect of fluid flow/centrifugal forces on the observed pattern collapse as shown in Figure 7.8. While the current data set is limited, it appears that the critical stress of lines oriented perpendicular to the wafer radius during spin drying exhibit substantially smaller critical stress and worse collapse than lines oriented parallel or even diagonal to sample radius. It is, of course, not surprising that forces perpendicular to the resist lines should have the greatest effect. However, further experiments and data analysis are needed to confirm these results.

(A)

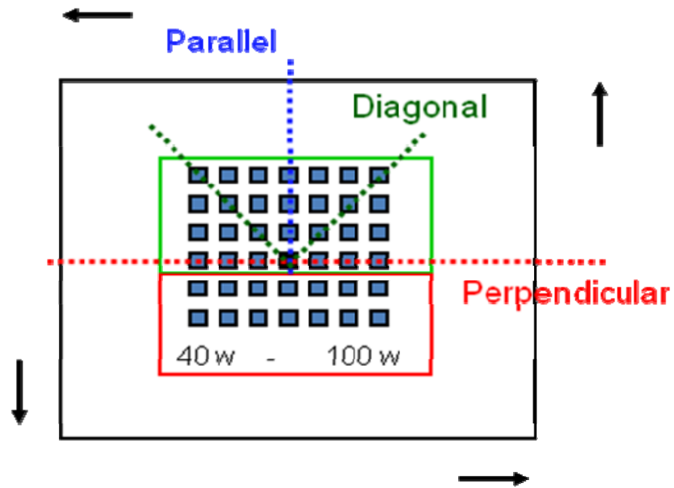

(B)

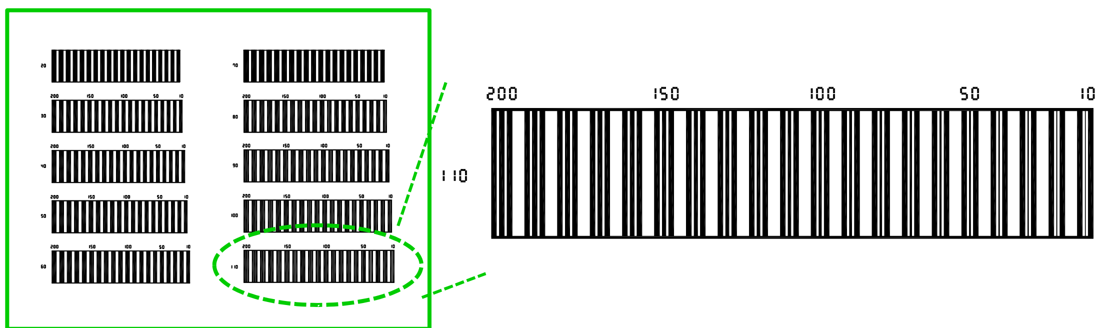

(C)

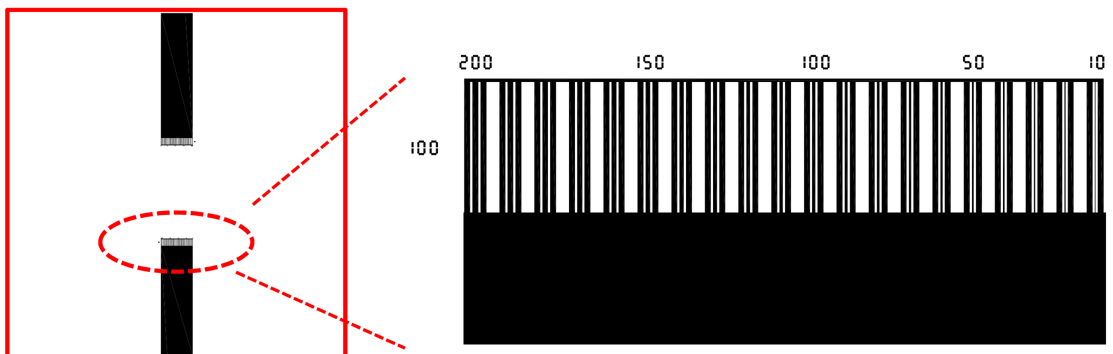

Figure 7.7 (A) Schematic of 6 x 7 SiN window array used for patterning of high resolution pattern collapse test structures with e-beam lithography in this work. Also shown are line orientations in those patterns with respect to the sample radius during spin drying. (B) Pattern design in the top-row windows used for calculating critical stress, (C) Pattern design in the bottom-row windows used for tilted images.

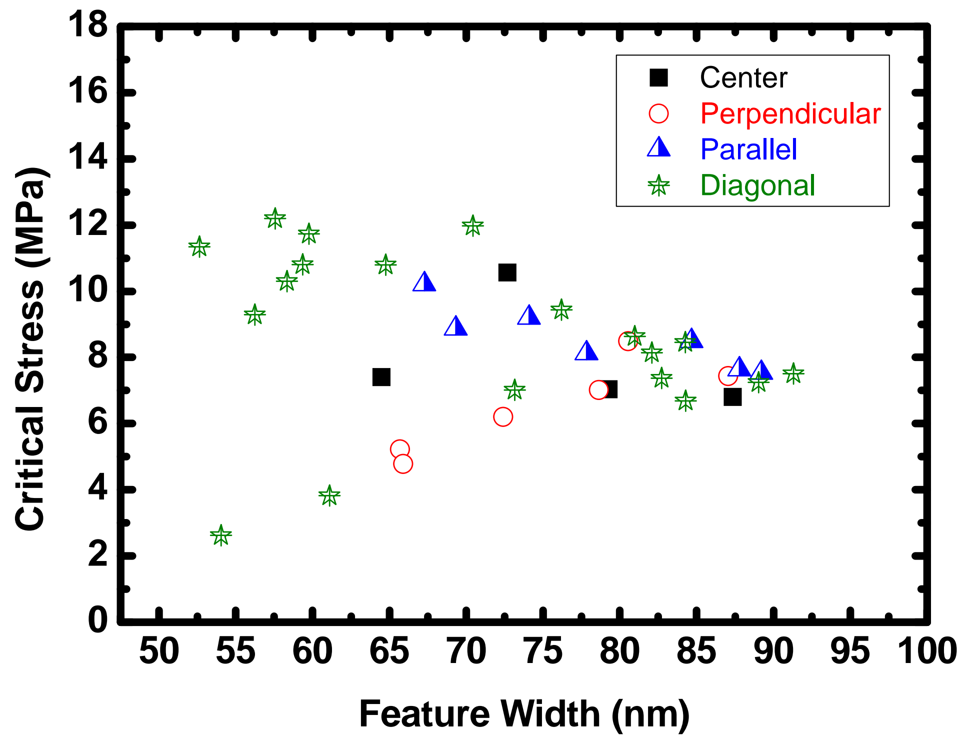

Figure 7.8 Critical stresses as a function of feature width under different pattern orientations.

7.4 Conclusions

We have investigated the effect of drying rate on pattern collapse using different drying methods. The SEM images and critical stress results show that the drying method has a significant impact on pattern collapse behavior. Comparing the different methods, slower drying rates in which pattern lines are stressed by capillary forces for longer times result in smaller critical stresses and unusual collapse behavior. Patterns dried by faster drying rates withstand higher critical stresses. Pattern orientation with respect to the wafer radius has an important effect on collapse behavior in spin drying. The pattern lines oriented perpendicular to the centrifugal force resulted in worse collapse behavior.

7.5 References

1. Tanaka, T.; Morigami, M.; Atoda, N., Mechanism of Resist Pattern Collapse during Development Process. *Jpn J Appl Phys 1* **1993,** *32* (12B), 6059-6064.

2. Chini, S. F.; Amirfazli, A., Understanding Pattern Collapse in Photolithography Process Due to Capillary Forces. *Langmuir* **2010,** *26* (16), 13707-13714.

3. Drechsler, A.; Belmann, C.; Synytska, A.; Petong, N.; Grundke, K.; Stamm, M.; Reichelt, J.; Wunnicke, O., The adsorption of cationic surfactants on photoresist surfaces and its effect on the pattern collapse in high aspect ratio patterning. *Colloid Surface A* **2007,** *311* (1-3), 83-92.

4. Zhang, P.; Rao, M. B.; Jaramillo, J. M.; Horvath, B. t.; Ross, B.; Paxton, T.; Davis, T.; Cook, P. t.; Witko, D., Pattern collapse and line width roughness reduction by surface conditioner solutions for 248-nm lithography. *Proc. SPIE* **2005,** *5753*, 252-260.

5. Huang, V.; Chiu, C. C.; Lin, C. A.; Chang, C. Y.; Gau, T. S.; Lin, B. J., Effect of novel rinsing material and surfactant treatment on the resist pattern performance. *Proc. SPIE* **2007,** *6519*, 65193C-9.

6. Goldfarb, D. L.; de Pablo, J. J.; Nealey, P. F.; Simons, J. P.; Moreau, W. M.; Angelopoulos, M., Aqueous-based photoresist drying using supercritical carbon dioxide to prevent pattern collapse (vol 18, pg 3313, 2000). *J Vac Sci Technol B* **2001,** *19* (2), 600-600.

7. Lee, M. Y.; Do, K. M.; Ganapathy, H. S.; Lo, Y. S.; Kim, J. J.; Choi, S. J.; Lim, K. T., Surfactant-aided supercritical carbon dioxide drying for photoresists to prevent pattern collapse. *The Journal of Supercritical Fluids* **2007,** *42* (1), 150-156.

8. Yeh, W. M.; Noga, D. E.; Lawson, R. A.; Tolbert, L. M.; Henderson, C. L., Comparison of positive tone versus negative tone resist pattern collapse bahavior. *J Vac Sci Technol B* **2010,** *28* (6), C6s6-C6s11.

9. Noga, D. E.; Yeh, W.-M.; Lawson, R. A.; Tolbert, L. M.; Henderson, C. L., Methods to explore and prevent pattern collapse in thin film lithography. *Proc. SPIE* **2010,** *7639*, 76392O-6.

10. Lee, C.-T.; Wang, M.; Jarnagin, N. D.; Gonsalves, K. E.; Roberts, J. M.; Yueh, W.; Henderson, C. L., Photosensitivity and line-edge roughness of novel polymer-bound PAG photoresists. *Proc. SPIE* **2007,** *6519*, 65191E-9.

CHAPTER 8

A COMPREHENSIVE MODEL AND METHOD FOR MODEL PARAMETERIZATION FOR PREDICTING PATTERN COLLAPSE BEHAVIOR IN PHOTORESIST NANOSTRUCTURES

Pattern collapse has become an issue of increasing importance in semiconductor lithography as the size of critical features continues to shrink down to sub-20 nm. Although models have been proposed to explain the observed pattern collapse behavior, the ability of such models to quantitatively predict the collapse behavior has been limited without significant model fitting to experimental pattern collapse behavior. Such a need to collect extensive collapse data before these models can provide any predictive capability limits their use and in general does not provide further insight into the underlying root causes of the observed behavior in many cases. This is particularly true at small feature sizes for resist lines smaller than approximately 70 nm in width. In this chapter, a comprehensive pattern collapse model that accounts for both adhesion based pattern failure and elastoplastic deformation-based failure was developed. Furthermore, the required model parameters were extracted from basic experiments on the resist materials and substrates themselves without the need for actual patterning experiments. For example, the resist mechanical modulus behavior was determined from simple thin film buckling experiments. The results of these simple tests were quantitatively predictive pattern collapse models for a particular resist-substrate combination that capture complex effects such as the dependence of the collapse behavior on resist film thickness and feature size due to feature size dependent polymer modulus behavior. Application of these models and methods to an experimental resist and comparisons of the model

predictions versus actual experimental pattern collapse data were shown and discussed to validate the methodology.

8.1 Introduction

As integrated circuit fabrication continues to advance towards the 22 nm node and below, it has become clear that although line edge roughness and resolution are important, other issues such as pattern collapse must be addressed in order for technology to continue to progress. Pattern collapse is caused by unbalanced capillary forces present during the final drying step of the standard lithographic process. Main factors affecting pattern collapse can be classified into three groups: (1) pattern geometry; (2) photoresist physical properties; (3) the capillary forces induced by drying of the final rinse liquid. The particular pattern geometry of interest can generally be characterized by a resist line height, resist line width and a space between the resist line and adjacent features, whereby all these properties are determined by a combination of the device layer design being patterned and the etch requirements for subsequent processing of the resist layer. Changing pattern geometry to mitigate the pattern collapse is not an option. Second, the physical properties of the photoresist material that are important in the context of such collapse behavior include Young's modulus, yield stress, and strength of interaction with the substrate. One approach to improve the collapse caused by mechanical failure (e.g. Young's modulus, yield stress etc.) is to design new resist materials by introducing the bulky and robust groups (i.e. benzyl or alicylic groups) on the resist structures in order to increase the mechanical restoring forces of resist features. For the strength of interaction with the substrate, the most common method for improving resist adhesion in the industry is to applied hexamethyldisilazane (HMDS)[1] or an functional underlay[2,3,4] on the substrate and designed to match the interface surface energy to increase the adhesion

strength. The rinse liquid and its capillary forces can be considered in the context of a Laplace pressure, ΔP, that is created during drying and which results in forces that are exerted on the resist structures during drying[5]. Several groups have studied the use of surfactant in the rinse to reduce the capillary stress and improve the pattern behavior[6,7].

A comprehensive pattern collapse model should consider each of the parameters in these three groups and be able to determine its affect on pattern collapse behavior. Many research groups have published different theoretical models to study the pattern collapse issue. Namatsu and coworkers utilized plastic beam bending equation to predict the smallest critical space that could be created between silicon nanolines before collapse would occur based on the structure's dimensions[8]. However, such a purely plastic deformation model only considers the plastic deformation therefore can not make any predictions about other possible collapse modes such as elastic deformation or adhesion failure. A purely elastic model has been developed by Tanaka and coworkers and considered the line structure patterns as a perfectly elastic cantilever without other types of deformations[9]. This simple elastic model again only considers elastic mechanical response and hence ignores the potential for yielding and plastic deformation observed by Namatsu. Therefore, Yoshimoto and coworkers noticed that an apparent plastic bending can occur near the substrate-resist interface and suggested that a photoresist pattern can undergo both elastic and plastic deformation[10]. As a result, they developed a combined model that includes both elastic and plastic deformation modes for polymer resist feature collapse, but there is not much experimental data to support their results. These earlier modeling efforts only included behavior based on the assumed bulk mechanical property behavior of resist polymers. However, it has been observed that many polymer film properties, including the glass transition temperature (Tg)[11] and effective polymer modulus, change as a function of film thickness [12,13]. Therefore, one of the goals of this work was to investigate the degree to which such polymer dimension-dependent

mechanical property behavior would affect resist pattern collapse. In another collapse mode, Jouve and coworkers were one of the first to develop a model for adhesion failure-based pattern collapse. However, the adhesion model they proposed only applied to low aspect ratio structure[14,15]. In this work, a comprehensive pattern collapse model that accounts for both adhesion based pattern failure and elastoplastic deformation-based failure has been developed and compared to experimental data. The required model parameters (i.e. film modulus) are extracted from basic experiments on the resist materials and substrates themselves without the need for actual patterning experiments. Patterning experiments on our designed structures are performed to validate the work.

8.2 Experimental

Materials and Equipments A model photoresist, (referred to here as ESCAP-1, a terpolymer of hydroxystyrene, styrene, and *t*-butyl methylmethacrylate consisting of monomer mole fractions of 0.6, 0.2, and 0.2 respectively) was supplied by JSR and Intel. A triphenylsulfonium nonaflate (TPS-Nf) photoacid generator (PAG), and a trioctylamine (TOA) base quencher, were made by dissolving all the components in propylene glycol methyl ether acetate (PGMEA) at loadings of 7.4 or 3.7 wt% total solids in PGMEA with 5 wt% TPS-Nf relative to ESCAP-1 and 10 mol% TOA relative to the TPS-Nf PAG. The developer, AZ300MIF was supplied by AZ Electronic Materials Company. All other reagents used in this study were purchased from Sigma-Aldrich, VWR, or Alfa-Aesar. E-beam lithography was carried out using a JEOL JBX-9300FS e-beam lithography system with an accelerating voltage of 100 keV, a beam diameter of 8 nm, a 2 nA current, and a 10 nm shot pitch. The Si_xN_y windowed substrates used in this study have been described elsewhere[8]. Electron beam exposures were performed on such thin nitride windows in order to eliminate electron backscatter from the substrate and thus produce extremely sharp aerial images and essentially vertical sidewalls in the final resist patterns. Such

perfectly rectangular resist profiles make analysis of the resulting pattern collapse much simpler and more reliable than in the case of the rounded profiles that can be obtained from degraded aerial images produced using other exposure tools such as optical projection lithography systems. SEM images of the resulting high resolution resist test structures were collected using a Zeiss Ultra 60 scanning electron microscope. Feature width and space widths of the patterns were measured from SEM images using custom MATLAB software. The thickness of the resist films was measured by an M-2000 Variable Angle Spectroscopic Ellipsometer (VASE, J.A. Woollam).

Pattern Geometry The particular pattern collapse test structure geometry used in this work is shown in Figure 8.1. Each individual pattern collapse test structure consists of two long photoresist lines of equal width (W) separated from each other by an inner space of controlled width (S_1) and separated from large outlying test pattern separation features by relatively large equal width spaces (S_2). This geometry effectively creates two free standing photoresist beams that are experienced the unbalance capillary stress produced from the rinse liquid in the inner (S_1) and outer spaces (S_2). Figure 8.1A depicts the three-dimensional pattern geometry in which the two different resist beams are surrounded by these two spaces (i.e. S_1 and S_2) and the larger block beams are used to separate each unit set. Figure 8.1B is the cross-section view of designed pattern structures. It is assumed that the final rinse liquid during drying is trapped in these spaces between the resist beams, thus creating large unbalanced forces acting on the resist lines due to differences in the curvature of the liquid interfaces created as a result of differences in the S_1 and S_2 space widths. This type of individual line pair test structure is repeated a large number of times in a large square array in which the resist line width W is varied systematically in different rows of the array and the inner space width S_1 is varied systematically in different columns of the array. In the particular pattern design used in this work, the S_1 space width decreases from left to right in the SEM images shown for a row of lines of constant line width W. Figure 8.1C is an example of 70 nm feature line

pair arrays. The numbers on the top represent the inner S_I spaces between two small lines. Numbers decrease from left to right, providing the increasing capillary stress from left to right. Pattern collapse is observed to occur in these arrays when a sufficiently small S_I value (called as critical S_I) is reached such that the stress applied to the resist exceeds a critical stress (σ_c) required for either: (1) pattern bending and deformation (blue dashed borders, as shown in Figure 8.1B) or (2) loss of adhesion of the resist feature from the substrate. The critical stress (σ_c) is defined as the maximum stress that can be applied to the photoresist lines prior to pattern collapse and occurs in critical space, the last space/position before the pair of resist lines collapse on the pattern structure we designed. It can also be used to characterize and quantify the pattern collapse behavior. The equation used to calculate the critical stress is expressed in equation (8.1), where γ is surface tension of rinse liquid (i.e. deionized water with γ =0.073 N/m), θ is the contact angle of the rinse liquid on the photoresist (i.e. deionized water with θ=75° in ESCAP-1 case), height H is the thickness of the photoresist film, S_2 is the respective outside space width between the lines of the pattern we designed shown in Fig. 8.1, and S_{Ic} is the critical pattern center space width where collapse is first indicated[16].

$$\sigma_C = 6\gamma \cos\theta \left(\frac{H}{W}\right)^2 \left(\frac{1}{S_{1c}} - \frac{1}{S_2}\right) \qquad (8.1)$$

(A)

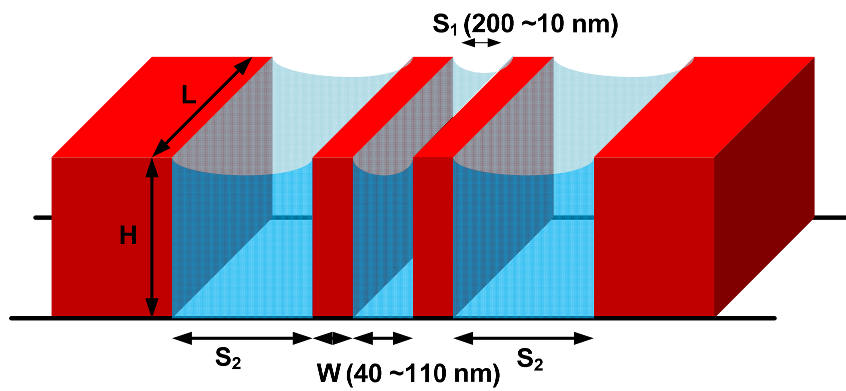

(B)

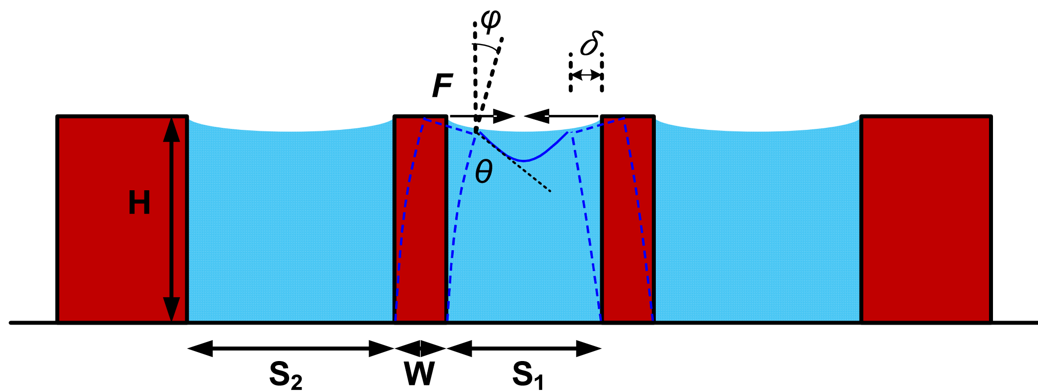

(C)

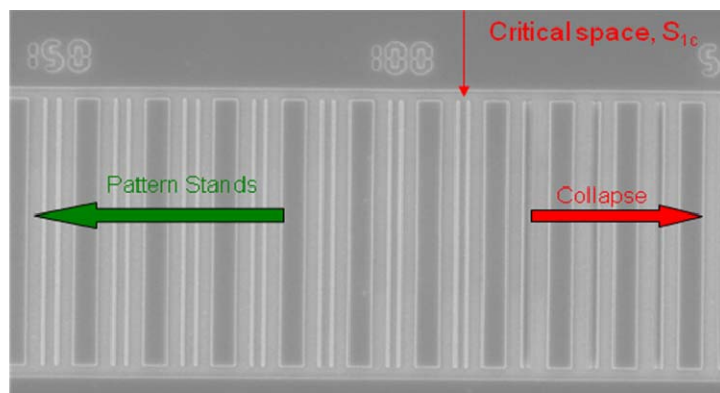

Figure 8.1 (A) Top view and (B) side view of pattern design used in this work for determining the critical stress at the point of pattern collapse; (C) An example for determining the position of critical stress: SEM image of nominal 70 nm feature width line pair arrays used to identify the critical S_{1c} space. The numbers on the top of array represent the space widths between two small lines (S_1).

Resist Processing The resist process consisted of spin coating of the resist films (2000 rpm, 60 sec; 97nm thick), softbaking the film at different baking conditions, e-beam exposure, post-exposure baking of the film (110°C, 1 min), development (AZ300, 30 sec), rinsing of the structures in deionized water, and finally drying of the patterned film with nitrogen stream.

8.3 Pattern Collapse Modeling

Adhesion Model In this model, resist lines are considered as rigid beams without any bending or breaking type of deformation. Pattern beams are only failed by the loss of adhesion between the resist and substrate. Two rotation moments are involved in this system, shown in Figure 8.2. One is the moment produced by capillary force (F_{cap}) and the other is the moment produced by Van der Waals forces (F_{vdw}) at the resist-substrate interface. When the capillary moment overcomes the adhesion moment, the pattern will begin to peel off from the substrate and it is considered that collapse occurs completely and instantaneously. Equation (8.2) denotes this adhesion-based failure mode collapse criteria. The left side on the equation (8.2) is the rotation moment produced by Van der Waals forces and the right side is the rotation moment caused by capillary force. Rearranging equation (8.2), it is possible to solve for the critical inner space width (S_{1c}) for which these two moments are equally balanced as shown in equation (8.3). For any inner space width smaller than S_{1c}, it is expected that pattern collapse by adhesion failure will occur.

$$\frac{ADW}{6\pi h_0^{\ 3}} \leq 2\gamma DH\cos\theta\left(\frac{1}{S_1}-\frac{1}{S_2}\right) \tag{8.2}$$

$$S_{1c} = \frac{12\pi h_0^{\ 3} H\gamma\cos\theta \cdot S_2}{AWS_2 + 12\pi h_0^{\ 3} H\gamma\cos\theta} \tag{8.3}$$

Here A is the Hamaker constant that describes the resist-substrate interaction, D is the resist line length, W is the resist line width, H is the resist height, h_o is the Lennard-Jones distance for describing the interaction of the resist with the substrate, γ is the surface tension of rinse liquid, and θ is the contact angle of the rinse liquid on the resist feature sidewall. Hamaker constant (A=0.8x10^{-20} J) and Lennard-Jones distance (h_0= 8Å) were obtained from literature[17].

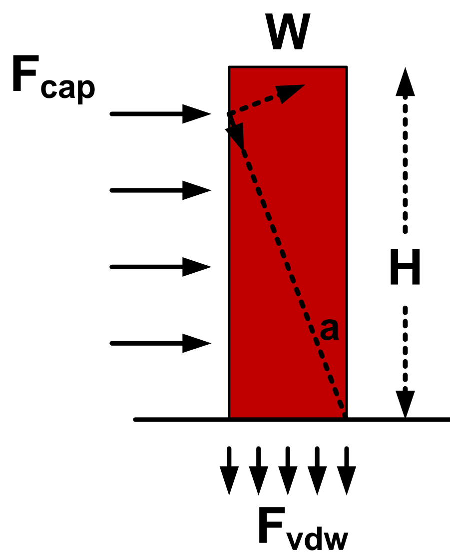

Figure 8.2 Schematic of the two important moments involved in the adhesion failure of a resist line from the substrate.

Elastic Model In our test patterns, the resist beams of are surrounded by inner S_1 space and outer S_2 space. After development, the surface of the rinse liquid between resist beams becomes concave due to the hydrophilic surface, as illustrated in Figure 8.1B. The capillary forces present during the drying process can be estimated by the Young-Laplace equation as shown in equation (8.4).

$$P = \gamma\left(\frac{1}{R^{'}} - \frac{1}{R^{''}}\right) \tag{8.4}$$

where γ is surface tension. R' and R'' are the principal radii of curvature of meniscus perpendicular and parallel to the beams, respectively. When the resist line length D is much longer than space between the resist line features (e.g. in our pattern design, D= 5μm, S_2= 200nm, and S_1 varies from 200nm to 10nm), the radius of curvature of the meniscus parallel to the beams (R'') can be approximated to be infinity. However, while it may be tempting to treat R' as a constant for a particular pattern geometry, in reality this value can change as the resist feature bends or deforms, as shown in Figure 8.1B. The displacement on the top of the beam (δ) and the angle of deflection of structure (φ) can be introduced to calculate the radius of curvature of the liquid meniscus for the structure as it is deforming. The radii of curvature (R_1) of the rinse liquid in the inner space S_1 and outer space S_2 (R_2) are given in equations (8.5) and (8.6), respectively.

$$R_1 = \frac{S_1 - 2\delta}{2\cos(\theta - \varphi)} \tag{8.5}$$

$$R_2 = \frac{S_2 + \delta}{2\cos(\theta + \varphi)} \tag{8.6}$$

The total pressure (P) generated by the surface tension of the rinse liquid from inner space and outer space is expressed as

$$P = P_1 - P_2 = \frac{2\gamma\cos(\theta - \varphi)}{S_1 - 2\delta} - \frac{2\gamma\cos(\theta + \varphi)}{S_2 + \delta} \tag{8.7}$$

Here θ is the contact angle. So the net capillary force (ω) acting on small resist beams is

$$\omega = PD = \left[\frac{2\gamma \cos(\theta - \varphi)}{S_1 - 2\delta} - \frac{2\gamma \cos(\theta + \varphi)}{S_2 + \delta} \right] \cdot D \tag{8.8}$$

In this model, the resist beam is regarded as an elastic body and pattern line is considered as a beam supported at one end with the substrate (adhesion failure is ignored). The displacement on the top of resist corner is expressed as[9]

$$\delta = \frac{\omega H^4}{8EI} \tag{8.9}$$

and φ is given by[18]

$$\tan \varphi = \frac{\omega H^3}{6EI} \tag{8.10}$$

where I is the moment of inertia. For the beam geometry, I is given by

$$I = \frac{DW^3}{12} \tag{8.11}$$

from the equations (8.5), (8.6), (8.7), and (8.8), the displacement δ can be arranged as

$$\delta = \frac{3H^4}{2EW^3} \left[\frac{2\gamma \cos\theta}{S_1 - 2\delta} + \frac{8\gamma \sin\theta \cdot \delta}{3H(S_1 - 2\delta)} - \frac{2\gamma \cos\theta}{S_2 + \delta} + \frac{8\gamma \sin\theta \cdot \delta}{3H(S_2 + \delta)} \right] \tag{8.12}$$

In our designed pattern array, the inner space S_1 between the two parallel resist lines decreased from left to right to simulate the increasing capillary stress. The critical space (S_{1c}) is determined by identifying the position in each test structure array where the smallest S_1 was observed between a pair of adjacent lines in the test structure that exhibited no sign of collapse or deformation. Therefore, the critical space can be calculated by requiring $d\delta/dS_1$ goes to infinity when the resist collapse occurs. The physical meaning of this collapse criterion is when $d\delta/dS_1$ goes to infinity, the elastic restoring force of resist beams can't afford the increasing capillary forces and the resist beams will continuously bend until two resist beams come into contact.

Elastoplastic Model In the elastoplastic model, the resist beams are considered to undergo the elastic and plastic mechanical behavior during the deformation. The stress-

strain curve of the resist nanostructure is idealized by the elastic-and-plastic model and illustrated as in Figure 8.3. The resist beam undergos the elastic behavior at low strains with a slope of Young's modulus (E) and plastic behavior at larger strains with a constant yield stress (σ_Y)[19]. If the capillary force exerted on the resist line is large enough to cause the stress at the bottom corners of the structure (i.e. the points of highest stress in the resist line structure) to equal the material's yield stress, the corners will begin to undergo plastic deformation. Thus, the onset of plastic deformation will be triggered when the capillary force is equal to a value shown in equation (8.13), and this line force is denoted as ω_e, derived in the previous literature[10].

$$\omega_e = \frac{\sigma_Y D W^2}{3H^2} \tag{8.13}$$

If the capillary force is increased beyond ω_e, the material across the entire resist line structure's base will eventually undergo plastic deformation. The minimum force (ω_p) to reach this level of complete plastic deformation of the resist structure can be computed as shown in equation (8.14), derived in the previous literature[10].

$$\omega_p = \frac{\sigma_Y D W^2}{2H^2} \tag{8.14}$$

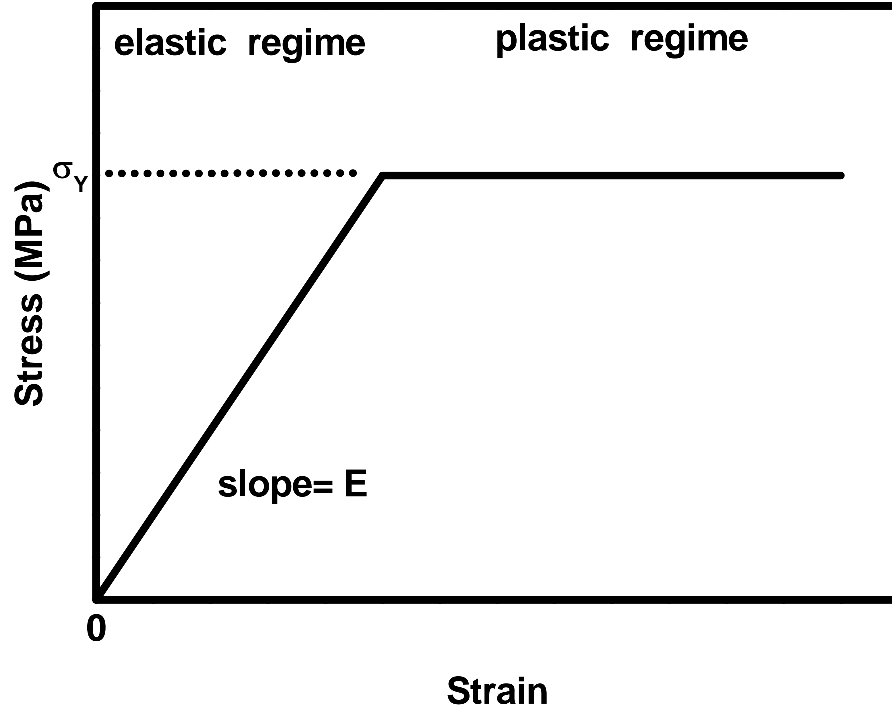

Figure 8.3 Schematic of the elastoplastic stress-strain curve assumed for the mechanical behavior of the polymeric photoresists studied in this work.

On the other hand, the curvature of the neutral surface in the plastic deformation region of the resist beam can be computed as shown in equation (8.15).

$$\frac{d^2y}{dx^2} = \frac{M}{EI} = -\frac{\sigma_Y}{Ey_Y} = -\frac{\sigma_Y}{E\sqrt{3\left(\frac{W^2}{4} - \frac{wx^2}{2\sigma_Y D}\right)}} \tag{8.15}$$

The curvature of the neutral surface in elastic deformation region of the resist line can be computed as shown in equation (8.16).

$$\frac{d^2y}{dx^2} = \frac{M}{EI} = -\frac{6wx^2}{EDW^3} \tag{8.16}$$

The curvature of neutral surfaces must satisfy the following boundary conditions: (i) no displacement (no slip) occurs at the base of the structure and (ii) continuity must be maintained between the elastic and plastic deformation regions of the resist structure. Application of these conditions allows for the calculation of the displacement (δ) and the angle of deflection (φ) at the top of the resist line structure as shown in equations (8.17) and (8.18).

$$\delta = \frac{\sigma_y^2 DW}{E\omega}\left\{\frac{1}{2} - \sqrt{\frac{1}{3}\left(1 - \frac{\omega}{\omega_p}\right)}\right\} \quad (8.17)$$

$$\tan\varphi = \frac{\sigma_Y}{E}\sqrt{\frac{2\sigma_Y D}{3\omega}}\left\{\frac{\sqrt{2}}{3} - \sin^{-1}\left(\sqrt{\frac{2}{3}}\right) + \sin^{-1}\left(\sqrt{\frac{\omega}{\omega_p}}\right)\right\} \quad (8.18)$$

Consequently, equations (8.8) and (8.13) through (8.18) can be solved simultaneously to determine capillary force ω, displacement δ, and the deflection angle φ for a resist feature as a function of the inner space S_1. Pattern collapse is assumed to occur when the rate of change of displacement at the top of the resist feature with respect to changing S_1, $d\delta/dS_1$, goes to infinity. At that point, the elastic restoring force of the beam is unable to balance further increases in the capillary force due to decreases in S_1 and the structures will spontaneously bend until the adjacent resist lines come into contact with one another.

8.4 Results and Discussion

In the literatures, most of collapse models have proposed so far to predict the pattern collapse behavior of resist structures have used the simple assumption that the bulk properties of the resist describe the mechanical behavior of the resist nanostructures as well. However, it has been reported over the last many years that a large number of

polymer film properties deviate from their bulk behavior when the film dimension becomes sufficiently small[11,20,21]. Therefore, in our pattern collapse work we were also interested to see to what degree such dimensionally dependent material properties might play a role in the pattern collapse behavior of photoresist nanostructures which by definition have large surface to volume ratios. Figure 8.4 shows the effective modulus of the ESCAP-1 model photoresist material as a function of the resist film thickness as measured by the thin film buckling experiments described earlier[13]. It is very clear that the resist modulus is dependent on the film thickness, becoming highly non-linear at small film thicknesses less than 100 nm due to confinement effect[11-12]. The modulus as a function of thickness can be modeled using a simplified two-layer model based on the volume ratio of each layer. In such a two-layer model, the polymer film can be thought of as consisting of a soft surface polymer layer and a robust bulk polymer region. The surface layer on the top of polymer film is very thin and encompasses the region that has a mass density much lower than that in the bulk. This lower-density property results in a higher mobility of polymer chains in this surface region and a lower mechanical modulus. In relatively thick films, this surface layer is only a small portion of the whole volume of the film. Therefore, the effect of soft surface layer on the effective modulus of the film is negligible and the effective modulus of polymer film is independent of the film thickness. For ultrathin films however, the ratio of the volume of this "soft" surface layer to more dense and rigid inner bulk-like volume of the polymer becomes significant, and the properties of this thin surface layer begin to strongly affect the overall effective properties of the film. The end result is the observed trend where the effective modulus of the film decreased rapidly with decreasing film thickness.

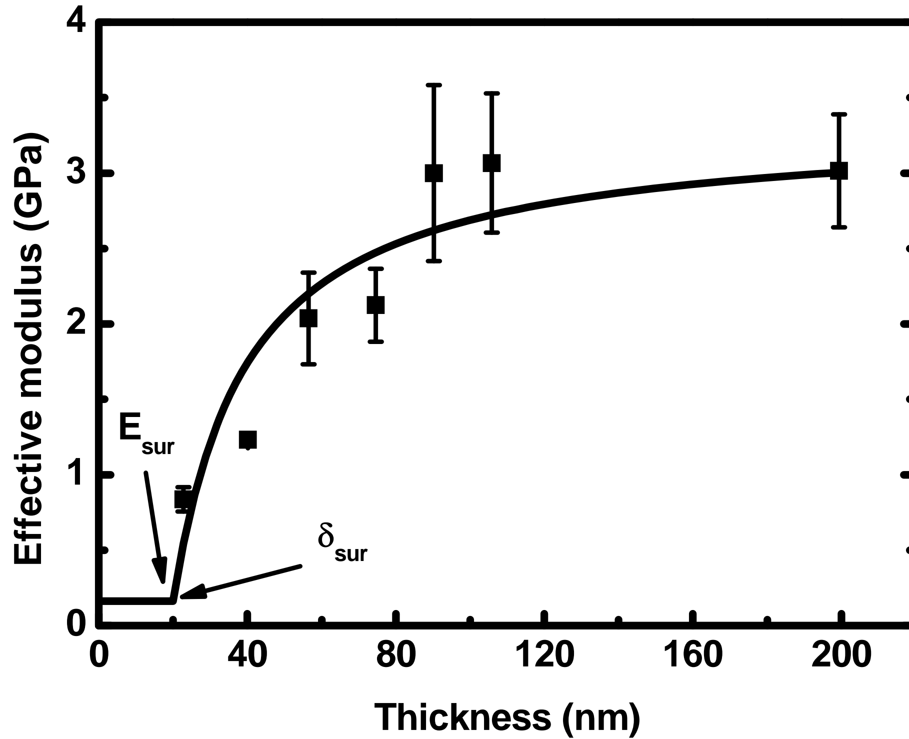

Figure 8.4 Effective moduli as a function of feature width measured by buckling metrology. Solid line represents the result of the simplified two-layer model.

To interpret the experimental resist modulus data and provide a functional form for the modulus behavior that could be used in further modeling, a simplified two-layer model as described in equation (8.19) and the solid curve in Figure 8.4 was proposed and fit to the data to find three parameters to describe the ESCAP-1 resist modulus: (1) the surface film thickness (δ_{sur}), (2) the surface modulus (E_{sur}), and (3) the bulk modulus (E_{bulk}). The best fit was obtained for δ_{sur}=20.0 nm, E_{sur}=0.162 GPa and E_{bulk}=3.32 GPa. After the film thickness shrank under surface layer thickness, the film modulus kept the same as the modulus of surface layer. To apply this dimensionally dependent modulus behavior as determined by 2-D film buckling in the mechanical response of three-

dimensional line structures, the resist effective modulus for 3-D line structures was also obtained using a simple volume weighted effective modulus model as shown in equation (8.20). This effective modulus model for the resist lines was incorporated into the elastoplastic pattern collapse models described earlier and used to predict the pattern collapse behavior of the ESCAP-1 model resist.

$$E_{eff} = E_{sur}(\frac{\delta_{sur}}{h_f}) + E_{bulk}(1 - \frac{\delta_{sur}}{h_f}) \tag{8.19}$$

$$E_{eff} = E_{sur}[1 - \frac{(H-\delta_{sur})(W-2\delta_{sur})}{HW}] + E_{bulk}[\frac{(H-\delta_{sur})(W-2\delta_{sur})}{HW}] \tag{8.20}$$

Figure 8.5 and 8.6 show a comprehensive comparison of four different pattern collapse models and a series of experimental pattern collapse data collected for the ESCAP-1 model resist used in this work. The black solid data points in each of the plots in Figure 8.5 and 8.6 represent experimental pattern collapse data collected for the ESCAP-1 model resist from high resolution pattern collapse test structures created using e-beam lithography for films of several different thicknesses ranging from ~100 nm thick to ~265 nm thick. In each plot in Figure 8.5 and 8.6, the lines represent the predictions from the various pattern collapse models. The red dash line shows the calculated critical inner space width (S_{1c}) from the adhesion model as a function of resist feature width. The adhesion model results were calculated using a combination of experimental parameters (γ=0.073 N/m, and θ=75 °) and literature reference data (A=0.8×10^{-20} J, and h_0=0.8 nm)[17]. The blue dot line in each plot represents the calculated critical inner space (S_{1c}) from the purely elastic deformation-based model. The orange dash-dot line in each plot shows the calculated critical inner space width (S_{1c}) from the elastoplastic deformation-based pattern collapse model for the case where the resist polymer modulus is assumed to be equal to the bulk resist polymer modulus as determined from the film buckling experiments (E_{bulk}=3.32 GPa). The green solid line in each plot shows the calculated critical inner space width (S_{1c}) from the elastoplastic deformation-based pattern collapse

model (called as modified elastoplastic model) for the case where the resist polymer modulus is assumed to be depedent on the feature size and described by the model shown in equation (8.20). The purely elastic model that considers the resist beams only undergo elastic deformation overestimated the collapse results, suggesting that the purely elastic model is an ideal condition and couldn't explain the practical resist collapse behavior. Furthermore, in the larger feature width regions, the adhesion-failure model best fits the best experimental collapse, suggesting that the adhesion strength between the resist pattern and the substrate is the main factor for pattern collapse in the larger feature width region in our test array. In the smaller feature width regions, the elastoplastic model using a constant bulk resist modulus (i.e. the dash-dot lines) did not match the experimental pattern collapse results for the various resist film thicknesses very well. In contrast, the modified elastoplastic model which treated the resist modulus as a function of the resist feature size (i.e. the green solid lines in figure 8.5 and 8.6) matched the experimental pattern collapse data quite well. This indicated that the dimensional dependent properties play a very important role in the complex resist behavior. The previous collapse models using the constant bulk properties in literatures have to be modified.

(A)

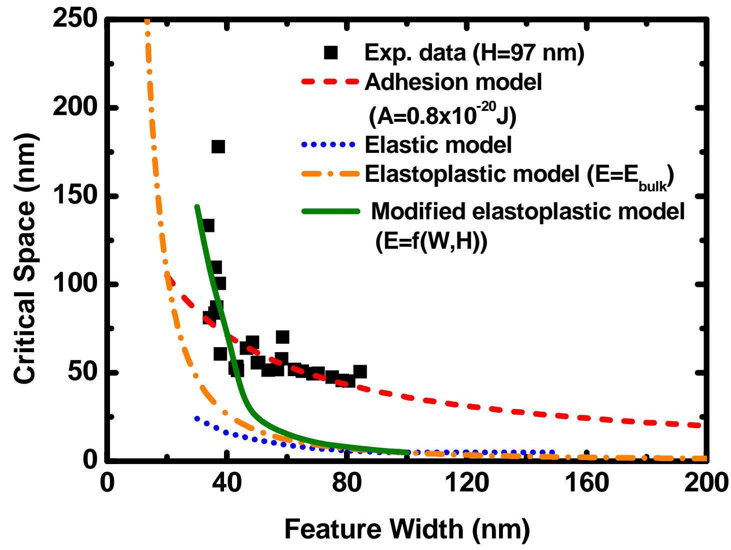

(B)

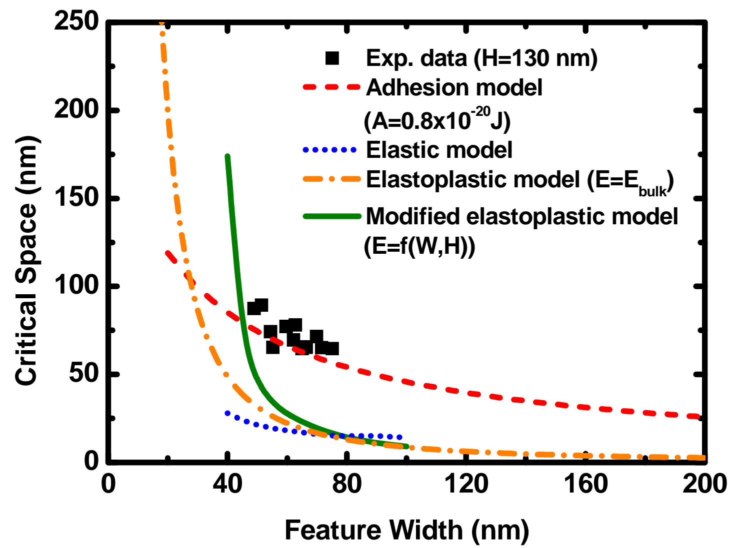

Figure 8.5 Comparison of critical spaces for adhesion model, elastic model, elastoplastic model using constant resist modulus, elastoplastic model considering resist modulus as a function of feature size. (A) 97 nm thick , (B) 130nm thick resist films.

(A)

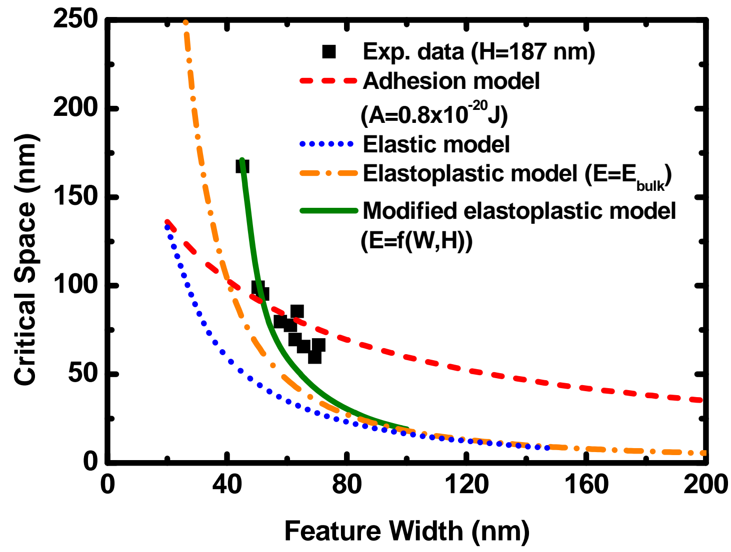

(B)

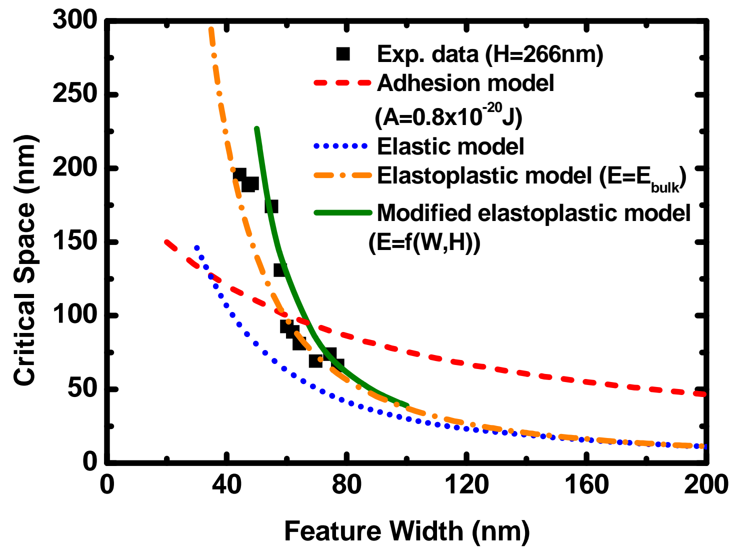

Figure 8.6 Comparison of critical spaces for adhesion model, elastic model, elastoplastic model using constant resist modulus, elastoplastic model considering resist modulus as a function of feature size. (A) 187nm thick and (B) 266nm thick resist films.

The pattern collapse test structure we designed is used to increase the capillary stress by controlling the inner space (S_1). The capillary stress increased from large inner space to small inner space (from top to bottom in the figure 8.5 and 8.6). For the resist pattern with larger feature width, the trend of increasing capillary stress (i.e. decreasing critical space) intersected the curve of adhesion-failure model before intersecting the elastoplastic model and purely elastic model, indicating that the resist beams fail by the loss of adhesion strength prior to the elastoplastic failure when the inner space is decreased. The experimental data match the result of adhesion-failure model indicating that the resist lines were collapsed by adhesion failure in the larger feature width region. For the resist pattern with smaller feature width, the increasing capillary stress hits the modified elastoplastic model curve before the adhesion model curve, elastic model curve, and elastoplastic model curve. This indicated that resist beams with smaller feature width collapse first by the weak mechanical properties (elastoplastic deformation) before the resist beams are failed by adhesion strength. The modified elastoplastic model is consistent with the experimental data. Therefore, in our test pattern structure, the collapse failure of resist patterns with larger feature width is controlled by the adhesion strength between the resist and the substrate. For the resist pattern with smaller feature width, the pattern collapse is mainly caused by the mechanical properties of resist itself. The experimental data showed that the collapse failure mode shifted from adhesion failure region to elastoplastic failure region as the resist thickness increased. It also suggested that the resist pattern with high aspect ratio fails by elastoplastic deformation before loss of adhesion.

Figure 8.7 shows the failure prediction as the function of features and resist height. The data points were calculated from the intersection of adhesion model and modified elastoplastic model in the different resist thickness. A relatively straight line dividing into two failure regions was obtained and it can be used to predict the failure condition. Below this transition line, the elastoplastic behavior dominates the collapse performance. In this

region, resist pattern fails by the weak mechanical properties. So the effective way to mitigate pattern collapse occurring in this region is to enhance the mechanical properties of patterns. On the other hand, above this transition line, the resist line collapse is mainly caused by adhesion failure. To mitigate pattern collapse in this region, one can apply the adhesion promoters on the resist-substrate interface to increase the adhesion strength. This phase-diagram like result can also provide us to insight to pattern behavior and help us look for efficient ways to improve pattern collapse issues.

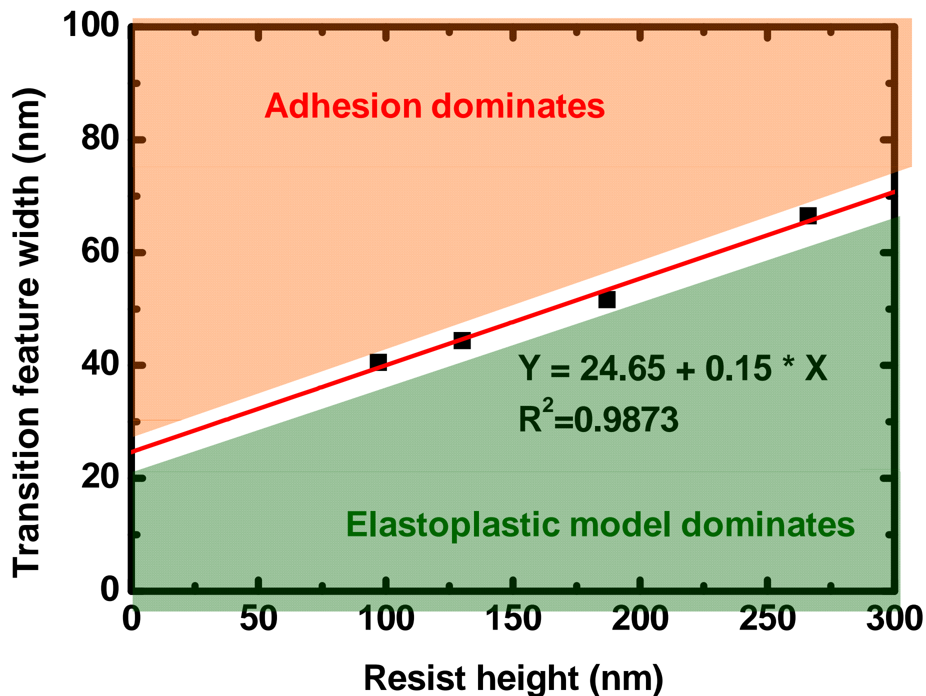

Figure 8.7 Resist collapse diagram predicted by our adhesion failure and elastoplastic failure model.

For the another case, two parallel resist structure of width *W* are separated by a narrow space (S_l) that is filled with rinse liquid. It is assumed that there is no rinse liquid on the outside of the resist beams. Figure 8.8 shows the predicted critical height as a function of feature width for the width-space ratio of 1:5 using our adhesion-failure and

modified elastoplastic-failure based collapse modeling. One inflection point can be observed in the modified elastoplastic model curve because the soft surface layer begins to dominate the whole film mechanical properties as the feature width shrinks. For the larger feature width, the critical height predicted from the modified elastoplastic model is less than adhesion-failure model, which suggests that the resist pattern is limited by mechanical properties of resists and resist beams collapse by weak mechanical properties first before patterns fail by the adhesion. For sub-25 nm patterning, the modified elastoplastic curve and adhesion curve almost overlap, suggesting that both adhesion and elastoplastic failure are occurring at nearly the same condition and we must fix both modes at the same time in order to improve collapse issue for sub-25 nm patterns.

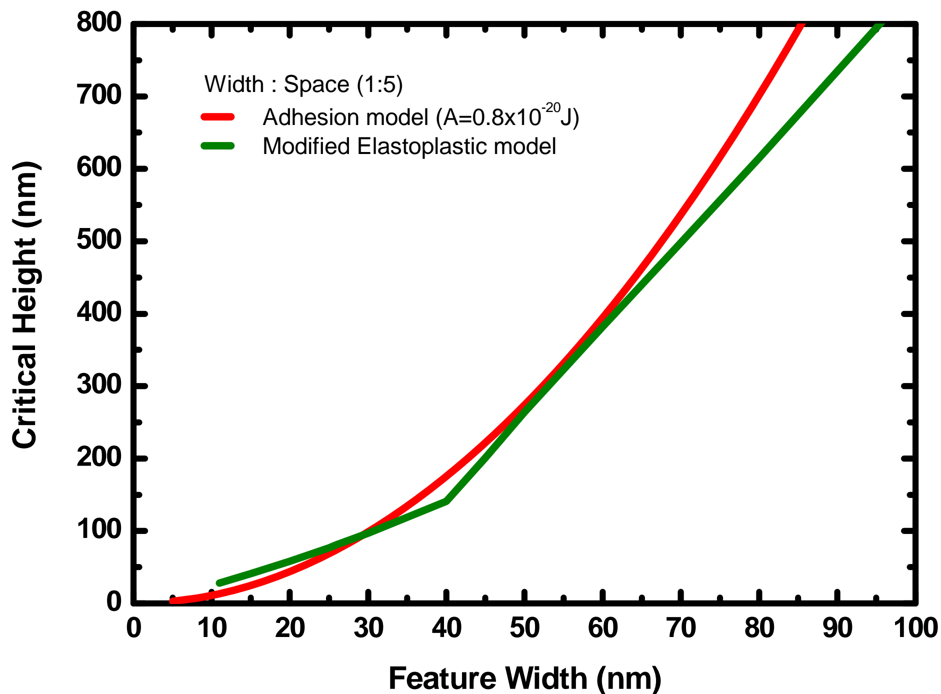

Figure 8.8 Predicted critical height as a function of feature width for 1:5 space/width ratio.

Figure 8.9 shows the critical aspect ratio prediction of pattern collapse behavior using our adhesion-failure and modified elastoplastic-failure based pattern collapse modeling. The dash line represents resist behavior expected if resist maintained bulk modulus and collapse mode switched from adhesion failure to elastoplastic failure. For sub-50 nm feature widths at relaxed pitches (e.g. 1:5 etc.), the failure mode becomes elastoplastic deformation and lower than expected critical aspect ratios are observed due to high surface to volume ratio and non-bulk modulus in the resist.

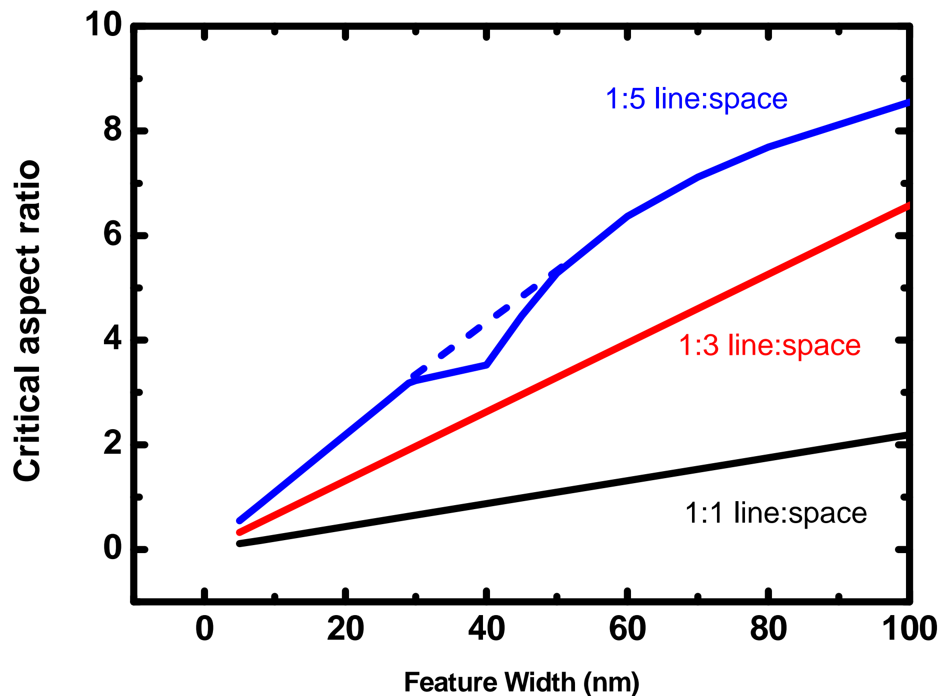

Figure 8.9 Predicted critical aspect ratios as a function of feature width for various line/space ratios. Dashed line represents behavior expected if resist maintained bulk modulus.

Pattern collapse model predictions have been made using only resist material and resist-substrate-rinse liquid material properties measured or estimated from other simple experiments. This ability to provide such an excellent prediction of the experimental data supports the idea that this level of combined adhesion-failure and elastoplastic-failure based pattern collapse modeling where one explicitly considers the dimensionally dependent mechanical properties of the resist can be quantitatively predictive and useful for understanding the pattern collapse behavior of polymeric nanostructures.

8.5 Conclusions

Microstructures and nanostructures of photoresists are deformed and collapsed during the lithographic drying process. A comprehensive pattern collapse model that accounts for both adhesion-based pattern failure and elastoplastic deformation-based failure has been presented which explicitly accounts for the dimensionally-dependent resist modulus properties. It has been shown that this model is quantitatively predictive for a model chemically amplified resist. It has also been shown that explicitly treating the dimensionally-dependent mechanical properties of the resist is important for obtaining such quantitative predictions and understanding the behavior of polymeric resist nanostructures.

8.6 References

1. Helbert, J. N.; Saha, N., Application of Silanes for Promoting Resist Patterning Layer Adhesion in Semiconductor Manufacturing. *J Adhes Sci Technol* **1991,** *5* (10), 905-925.

2. Kawai, A.; Moriuchi, T.; Niiyama, T.; Kishioka, T.; Maruyama, D.; Sakaida, Y.; Matsumoto, T., Adhesion improvement of ArF resist pattern depending on BARC material. *Microelectron Eng* **2006,** *83* (4-9), 659-662.

3. Guerrero, D. J.; Xu, H.; Mercado, R.; Blackwell, J., Underlayer Designs to Enhance EUV Resist Performance. *J Photopolym Sci Tec* **2009,** *22* (1), 117-122.

4. Takei, S.; Ogawa, T.; Willson, C. G., Study of fluorinated silicon-based resist material and photoreactive underlayer for defect reduction in step and repeat ultraviolet nanoimprint lithography. *Micro Nano Lett* **2011,** *6* (6), 422-424.

5. Kotera, M.; Ochiai, N., Three-dimensional simulation of resist pattern deformation by surface tension at the drying process. *Microelectron Eng* **2005,** *78-79*, 515-520.

6. Drechsler, A.; Petong, N.; Bellmann, C.; Busch, P.; Stamm, M.; Grundke, K.; Wunnicke, O.; Reichelt, J., The effect of adsorbed cationic surfactant on the pattern collapse of photoresist lines in photolithographic processes. *Prog Coll Pol Sci S* **2006,** *132*, 82-94.

7. Alvine, K. J.; Ding, Y. F.; Douglas, J. F.; Ro, H. W.; Okerberg, B. C.; Karim, A.; Lavery, K. A.; Lin-Gibson, S.; Soles, C. L., Effect of Fluorosurfactant on Capillary Instabilities in Nanoimprinted Polymer Patterns. *J Polym Sci Pol Phys* **2009,** *47* (24), 2591-2600.

8. Namatsu, H.; Kurihara, K.; Nagase, M.; Iwadate, K.; Murase, K., Dimensional Limitations of Silicon Nanolines Resulting from Pattern Distortion Due to Surface-Tension of Rinse Water. *Appl Phys Lett* **1995,** *66* (20), 2655-2657.

9. Tanaka, T.; Morigami, M.; Atoda, N., Mechanism of Resist Pattern Collapse during Development Process. *Jpn J Appl Phys 1* **1993,** *32* (12B), 6059-6064.

10. Yoshimoto, K.; Stoykovich, M. P.; Cao, H. B.; de Pablo, J. J.; Nealey, P. F.; Drugan, W. J., A two-dimensional model of the deformation of photoresist structures using elastoplastic polymer properties. *J Appl Phys* **2004,** *96* (4), 1857-1865.

11. Singh, L.; Ludovice, P. J.; Henderson, C. L., Influence of molecular weight and film thickness on the glass transition temperature and coefficient of thermal expansion of supported ultrathin polymer films. *Thin Solid Films* **2004,** *449* (1-2), 231-241.

12. Stafford, C. M.; Harrison, C.; Beers, K. L.; Karim, A.; Amis, E. J.; Vanlandingham, M. R.; Kim, H. C.; Volksen, W.; Miller, R. D.; Simonyi, E. E., A buckling-based metrology for measuring the elastic moduli of polymeric thin films. *Nat Mater* **2004,** *3* (8), 545-550.

13. Yeh, W.-M.; Noga, D. E.; Lawson, R. A.; Tolbert, L. M.; Henderson, C. L., Thin film buckling as a method to explore the effect of reactive rinse treatments on the mechanical properties of resist thin films. *Proc. SPIE* **2010,** *7639*, 76391I-6.

14. Jouve, A.; Simon, J.; Foucher, J.; David, T.; Tortai, J. H.; Solak, H., Overcoming pattern collapse of ultra high resolution dense lines obtained with EUV resists. **2005**, 720-731.

15. Jouve, A.; Simon, J.; Pikon, A.; Solak, H.; Vannuffel, C.; Tortai, J. H., Overcoming pattern collapse on e-beam and EUV lithography. **2006**, 61531C-61531C.

16. Yeh, W. M.; Noga, D. E.; Lawson, R. A.; Tolbert, L. M.; Henderson, C. L., Comparison of positive tone versus negative tone resist pattern collapse bahavior. *J Vac Sci Technol B* **2010,** *28* (6), C6s6-C6s11.

17. Prausnitz, J. M.; Lichtenthaler, R. N.; Azevedo, E. G. d., *Molecular Thermodynamics of Fluid-Phase Equilibria (3rd Edition)*. Pearson Education: 1998.

18. Hearn, E. J., *Mechanics of materials : an introduction to the mechanics of elastic and plastic deformation of solids and structural materials* 3rd ed.; Oxford ; Boston : Butterworth-Heinemann, 1997.: 1997.

19. Beer, F.; Johnston, J. E. R.; DeWolf, J.; Mazurek, D., *Mechanics of materials, 5th ed.* McGraw-Hill Higher Education: New York, 2009.

20. Stafford, C. M.; Vogt, B. D.; Harrison, C.; Julthongpiput, D.; Huang, R., Elastic moduli of ultrathin amorphous polymer films. *Macromolecules* **2006,** *39* (15), 5095-5099.

21. Chung, J. Y.; Nolte, A. J.; Stafford, C. M., Surface Wrinkling: A Versatile Platform for Measuring Thin-Film Properties. *Adv Mater* **2011,** *23* (3), 349-368.

CHAPTER 9

CONCLUSIONS AND RECOMMENDATIONS

9.1 Conclusions

The need for sub-20 nm imaging is critical for the continued scaling of semiconductor devices to smaller and smaller geometries. One of the challenging issues is pattern collapse caused by unbalanced capillary forces during the final rinse and drying process. The use of surfactants offers a convenient method to reduce capillary forces. An important issue is that the surfactant may diffuse into the resist structure and result in another deformation issue. In this work, we focused on the alternative approaches that are compatible with lithographic process to mitigate the pattern collapse. In general, two primary forces can overcome the capillary forces: mechanical restoring force and adhesion force. First, an e-beam lithography pattern with a series of varying line and space widths has been specifically designed in order to quantitatively study pattern collapse behavior. This pattern generates increasing stress in the pairs of resist lines as one moves across the pattern array from left to right and eventually a sufficiently small space value (critical space, S_{1c}) was reached in each array such that the stress applied to the resist exceeded the critical stress (σ_c) required for pattern bending and subsequently feature deformation and collapse. The patterns we designed allowed us to qualitatively and quantitatively study pattern collapse and obtain consistent, reproducible results.

For the approaches to reinforce the mechanical restoring forces of resist structures, we have developed a quick surface crosslink (called as reactive rinse) that involves the actual strengthening of the resist using the crosslink reaction via carbodiimide chemistry while the resist structures are still in their wet state. The mechanism of reactive rinse includes that carboxyl groups are activated with *N*-ethyl-*N*′-(3-dimethylaminopropyl)

carbodiimide hydrochloride (EDC) in the presence of *N*-hydroxysuccinimide (NHS) and form NHS esters. The NHS esters then can react with necleophiles, such as primary amine groups to form stable amide bonds[1,2] or hydroxyl groups to form ester bonds[3]. Based on the types of functional group on the resist surface, the complementary linkers can be chosen for the reactive rinse approach and enhance the mechanical strength of resist structures. The surface contact angle and grazing angle IR results have indicated that the reactive rinse method is able to covalently crosslink the functional groups and form ester liners on the resist surfaces. The buckling metrology by using our design strain stage has also confirmed that the use of reactive rinse in post-development process results in a significant enhancement of the mechanical properties of resist films. The results of critical stress analysis and SEM studies of the resulting patterns confirm that the use of reactive rinse can significantly enhance the mechanical properties of the resist and dramatically mitigate pattern collapse. Another advantage of this reactive rinse is that an aqueous-based process allows for the compatibility with high volume, track-based lithographic processes.

For the approaches to increase the adhesion strength at the interfacial surface of resist and substrates, we have successfully synthesized a triethoxysilane compound, vinyl ether silane (VE) which can be used to modify the silicon or silicon nitride substrates and form covalent bonding with the resist film, instead of changing the surface energies by using common HMDS. Compared to traditional HMDS vapor primed surfaces, the implementation of the VE adhesion promoter provids a significant improvement in the adhesion-based failure in small sub-60 nm resist features. Additionally, Soft bake conditions have also been discussed. The lower baking temperature for vinyl ether modified samples can enhance the pattern adhesion and resist lines can stand in higher capillary stress.

Relatively little attention has been paid to other process-dependent factors which may also significantly impact such collapse behavior. We have also probed the extent to

which the time during which a resist structure is subjected to capillary force-induced loads affects the pattern collapse behavior of such structures. This focus is on modulating drying rate of the final rinse liquid (water) and quantifying the observed changes in pattern collapse. The different methods used in this work are: (1) drying slowly by normal evaporation in stagnant room air, (2) drying in a vacuum oven, (3) drying in a flowing nitrogen stream, and (4) spin-drying. The effect of these different drying methods on the resulting pattern collapse behavior has been quantified by measuring the change in the critical stress at the point of pattern collapse using simple parallel line resist test structures subjected to the different drying conditions. SEM analysis and critical stress results showed that fast drying rates appear to reduce the resist collapse and the line pair orientations in each pattern array with respect to the wafer radius revealed an apparent effect of fluid flow/centrifugal forces on collapse.

Most collapse models in literatures have been proposed to predict the resist collapse behavior considering the constant bulk properties of resist film. However, dimensionally dependent material property effects are important for collapse of small feature width resist structures, which has been confirmed on our buckling technology. Finally, a comprehensive pattern collapse model that incorporates both adhesion based pattern failure and elastoplastic deformation-based failure, and dimensionally dependent resist modulus properties has been developed. This model is able to provide such an excellent prediction of the experimental data. It supports the idea that this level of combined adhesion-failure and elastoplastic-failure based pattern collapse modeling where one explicitly considers the dimensionally dependent mechanical properties of the resist can be quantitatively predictive and useful for understanding the pattern collapse behavior of polymeric nanostructures.

9.2 Recommendations for Future Work

For the resist surface crosslinking, reactive rinse method via carbodiimide chemistry shows superior improvement on the resist collapse. In addition, the ionic bonding on the resist surface with two functional quaternary ammoniums has been also studied. Hexamethonium bromide (HMBr) salt with two quaternary ammonium cations was applied as a reactive linker for ionic bonding with the caroxylate anions on the resist surface and enhancesd the resist mechanical properties, shown in Figure 9.1. The mechanical property data are also consistent with the critical stress results that surface rinse can enhance the resist collapse resistance to capillary stress. The critical stress results also showed that the efficiency of HMBr ionic rinse provides significant improvement on resist collapse issue as the covalent reactive rinse. It is an aqueous process and very compatible with high volume, track-based lithographic processes. In addition, EDC/NHS chemistry is not needed anymore for the surface reaction. Total rinse process contains only one step rinse and complete in two minutes. Furthermore, the developer for almost all modern photoresists is tetramethylammonium hydroxide (TMAH), a quaternary ammonium base. It will be a great breakthrough if we can find an ionic linker with the combination of at least two quaternary ammonium cations and function as a developer for resist. Based on this case, hexamethonium hydroxide may be one of potential candidates for such 'bi-functional' linkers.

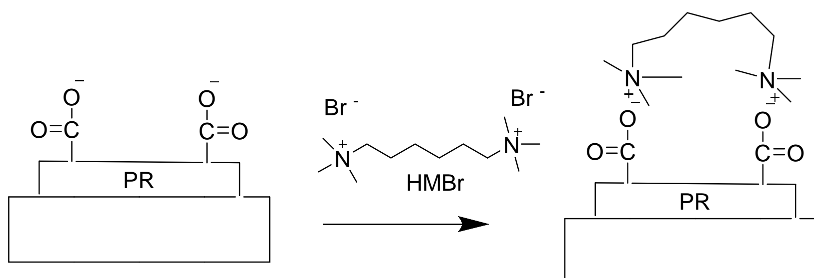

Figure 9.1 Schematic illustration of the HMBr rinse process.

For adhesion promoters, vinyl ether functionalized silane (VE) is capable of covalently attaching phenolic resists to the substrate surface during the post-apply bake process and provides a significant improvement in the adhesion-based failure in small sub-60 nm resist features. The next step is to pursue an adhesion promoter that can not only covalently attach specific positive-tone resists but also negative-tone resists to the substrate surface. Figure 9.2 represents the schematic surface process of proposed benzophenone dimethylchlorosilane for negative-tone resists. Dimethylchlorosilane groups provide the ability to covalently attach on the substrate and photoreactive benzophenone groups are well-known to attach to C-H bonds in a wide range of different chemical environment[4,5]. The crosslink reaction occurs in the region exposed to e-beam or UV source for enhancing substrate adhesion, which is well-suited for negative-tone system.

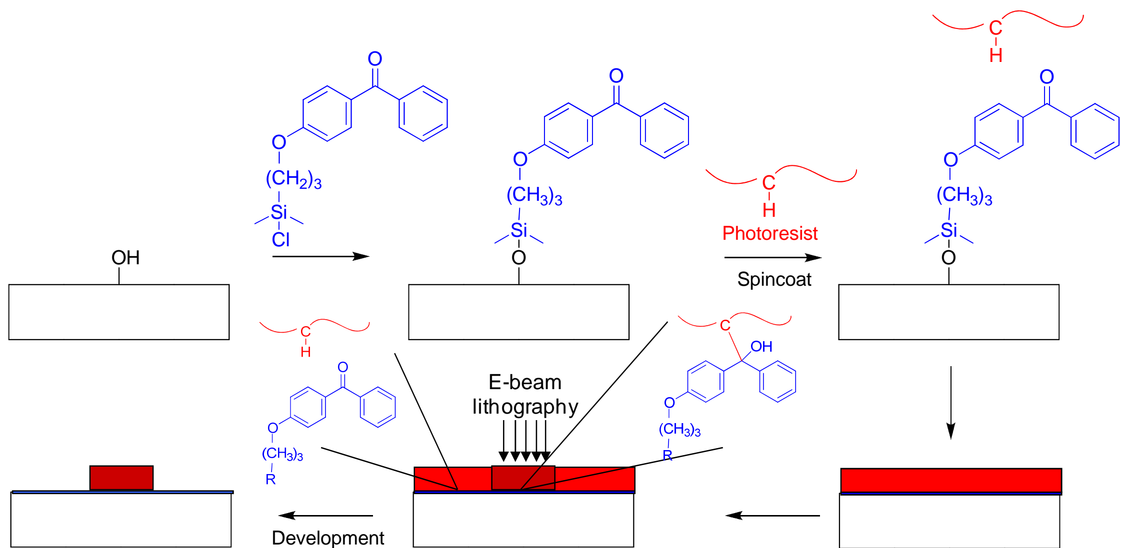

Figure 9.2 Schematic representation of the photoreactive surface modification technique for increasing adhesion strength using benzophenone dimethylchlorosilane.

9.3 References

1. Powell, H. M.; Boyce, S. T., EDC cross-linking improves skin substitute strength and stability. *Biomaterials* **2006,** *27* (34), 5821-5827.

2. Updegrove, T. B.; Correia, J. J.; Chen, Y. F.; Terry, C.; Wartell, R. M., The stoichiometry of the Escherichia coli Hfq protein bound to RNA. *Rna* **2011,** *17* (3), 489-500.

3. Everaerts, F.; Torrianni, M.; Hendriks, M.; Feijen, J., Biomechanical properties of carbodiimide crosslinked collagen: Influence of the formation of ester crosslinks. *J Biomed Mater Res A* **2008,** *85A* (2), 547-555.

4. Dorman, G.; Prestwich, G. D., Benzophenone Photophores in Biochemistry. *Biochemistry-Us* **1994,** *33* (19), 5661-5673.

5. Prucker, O.; Naumann, C. A.; Ruhe, J.; Knoll, W.; Frank, C. W., Photochemical attachment of polymer films to solid surfaces via monolayers of benzophenone derivatives. *J Am Chem Soc* **1999,** *121* (38), 8766-8770.